Title
The Dynamics and Components of Intracellular Lipid Inclusion Formation in Mycobacteria

Author
Fines, Daniel

Publication Date
2023

Peer reviewed|Thesis/dissertation

The Dynamics and Components of Intracellular Lipid Inclusion Formation in Mycobacteria

By

Daniel Fines

A dissertation submitted in partial satisfaction of the

requirements of the degree of

Doctor of Philosophy

in

Molecular and Cell Biology

in the

Graduate Division

of the

University of California, Berkeley

Committee in charge:

Professor Sarah A Stanley, Chair
Professor Arash Komeili
Professor Daniel Portnoy
Professor Kathleen Ryan

Summer 2023

Abstract

The Dynamics and Components of Intracellular Lipid Inclusion Formation in Mycobacteria

by

Daniel Fines

Doctor of Philosophy in Molecular and Cell Biology

University of California, Berkeley

Professor Sarah A Stanley, Chair

Mycobacterium tuberculosis is an airborne bacterial pathogen responsible for the infectious disease tuberculosis. Tuberculosis is the second leading infectious killer after COVID-19 and was responsible for over 1.6 million deaths in 2021. Astoundingly, a quarter of the world is thought to have been infected by *M. tuberculosis.* If left untreated, TB has a high mortality rate of up to 50%. While a strict regime of antibiotics can treat the disease, the rise of multidrug resistant clinical *M. tuberculosis* strains threatens the world. Typically, a majority of the population can quell the disease into a latent TB infection (LTBI), although in 5-10% of cases, an infected individual is unable to prevent disease progression and the active bacteria can start their infection anew. These harrowing statistics demand the need to understand the biology of *M. tuberculosis* and the development of model systems to study the bacterium and its pathogenesis.

Intracellular lipid inclusions (ILI), receptacles of concentrated lipids, have long been perceived as hallmarks of non-replicating persistent bacteria found in LTBI. These organelles are thought to provide fuel for basal metabolic processes while the dormant bacteria withstand the immunological and chemical artillery launched by host immune cells. Understanding how and why ILI are formed would promote identification of tactical therapeutic targets against dormant bacilli and allow for sustained prevention and control of TB. Here, we provide surprising evidence that refutes this longstanding belief and suggests that ILI can be formed in actively replicating *Mycobacterium marinum.* We find this discovery is corroborated in several clinical *M. tuberculosis* strains and through next generation RNA sequencing we uncover some key differences in the transcriptional landscape of ILI producing and ILI barren bacteria, allowing us to decouple non-replicating persistence from ILI formation. Separately, we utilize an arrayed transposon mutagenesis library in *M. marinum* to identify four genes involved in the ILI formation pathway. *M. marinum* mutant strains with disruptions in these genes were used to study the role of ILI, allowing us to add mounting evidence to the importance of ILI in mycobacterial infection. Together, these findings suggest an alternative function of ILI in replicating *M. marinum* and *M. tuberculosis*, as well as provide novel models to study the purpose of ILI in *M. tuberculosis* pathogenesis.

Dedication

This work is dedicated to my family, Alexandre Fines, Yoko Fines, and Simon Fines, and to my partner, Amanda Su. Thank you all for your support every step of the way.

Table of Contents

List of Figures and Tables

Chapter Two

Chapter Three

Acknowledgements

First and foremost, I would like to thank my mentor, Sarah Stanley. You have provided unwavering support, fostered intellectual growth, and guided me to be a better person and scientist. To this day I am still unsure what you saw in a young naïve first year stumbling through his pursuit of a scientific career, but I feel incredibly blessed you took the chance on me and guided me to become a still young but slightly less naïve scientist.

To my parents, your constant encouragement was felt across the country. Je suis redevable à vous deux, merci beaucoup. いつもおうえんしてくれてほんとうにありがとう。Simon, our weekly gaming sessions kept me sane throughout this program, I always looked forward to somehow getting absolutely nothing done in our campaigns every time. Thank you so much for your love and being there for me.

To Amanda, I am so grateful to have you in my life. I truly do not think I would be here if not for your laughter and love these past 5 years. You were with me every step of the day, from interview weekend, throughout long stressful days, and to the end of our time here. I can't wait to continue our life together in Boston.

To my friends, thank you for continuing to be integral parts of my life. Whether it be absolutely smoking you in Smash, absolutely smoking you in Mario Party, absolutely smoking you in Apex, absolutely smoking you in tennis, absolutely smoking you in 7 Wonders, absolutely smoking you in hiking, or anything else, I appreciate you throwing to boost my self-esteem. I somehow convinced some of you to move over here, and as my time here ends, I look forward to recruiting many of you back over to the east coast and reuniting with old friends.

To all of those in the Stanley lab past and present, thank you for providing a welcoming environment for me. You all have been such wonderful colleagues and friends and I wish you all the best.

Finally, thank you to my thesis committee for your support. Your input and critical perspectives proved invaluable in my development as a scientist.

Chapter 1: *Mycobacterium tuberculosis* Pathogenesis and Lipid Bodies

M. tuberculosis pathogenesis

Mycobacteria are a genus of bacteria comprised of over 150 species, among which many are human pathogens [1]. The most prominent species is *Mycobacterium tuberculosis* (Mtb), the causative agent of the deadly infectious disease tuberculosis (TB). If left untreated TB has a high fatality rate of 50%, though through an extensive antibiotic regimen of 4 to 6 months of treatment with multiple antibiotics, about 85% of patients can be cured [2]. TB is the 13th leading cause of death worldwide and had been the leading cause of death by a single infectious disease agent for decades until the recent Coronavirus disease 2019 (COVID-19) epidemic [3]. The recency and unprecedented challenges of the COVID-19 pandemic proved difficult for medical staff to discern between COVID-19 and TB symptoms, leading to undiagnosed and untreated cases masking true TB counts in 2020 and 2021. Worldwide casualties by TB in 2021 are estimated to be over 1.5 million, double the number of HIV/AIDs casualties; troublingly, a drastic consequence of misdiagnosed/missed TB cases due to COVID-19 is a predicted dramatic spike in TB cases and deaths in the future [3]. Although it is hard to diagnose a singular explanation for this uncontrolled worldwide dissemination there are a few possibilities. The first is the lack of a reliable and potent vaccine. In many countries with prevalent rates of TB children are vaccinated with bacille Calmette-Guérin (BCG), a live attenuated form of *Mycobacterium bovis*. Since its first prescribed dose in 1921, BCG has been used to prevent childhood extrapulmonary presentations of the disease, with some studies showcasing high efficacy against disseminated forms of TB such as military TB or meningitis, as well as against leprosy, caused by another member of the *Mycobacteria* genus *Mycobacterium leprae* [8], [9]. The efficacy however has also been shown to vary dramatically, and studies estimate that the protection provided by BCG, the sole vaccine against TB, falls anywhere from 0-80% [10], [11]. The vaccine also drastically drops in protection as the patient ages, further highlighting the necessity of more potent preventative measures against the disease. The efforts made towards antitubercular vaccine development and the intricacies behind the interplay of host immune response and bacterial pathogenesis will not be covered further here; comprehensive commentary on these subject matters can be found elsewhere [12].

A second possibility for the global spread of TB is the unique pathogenesis of Mtb. Mtb is an airborne pathogen, spread from person to person in aerosolized droplets often as a result of coughing or talking. The inhaled bacteria traverse the nasal cavity and reach the alveoli in the lungs where it reaches its first potential host: the alveolar macrophage [13], [14]. Macrophages are cells that ingest foreign substrates and are normally thought to eliminate invading microbes, yet in the war between host and pathogen things are not always as they seem. Indeed, Mtb has co-evolved with humans, its only known reservoir, for tens of thousands of years [15], [16]. It is only natural that through these lifetimes Mtb has evolved some mechanisms of protection against host defenses. For example, a macrophage typically will engulf an invading microbe, a process called phagocytosis. After the microbe is phagocytosed, the bacilli containing phagosome

undergoes a maturation process that results in the degradation of the microbe. This process entails the fusion of the phagosome with an endosome which triggers the accumulation of vacuolar ATPase molecules on the membrane of the vesicle. The V-ATPase pumps H^+ protons into the microbe encapsulating vacuole to decrease the pH of the structure and acidify the bacterial environment. The maturation of the phagosome is complete when it ultimately fuses with the lysosome to form the phagolysosome. This structure maintains the acidic (pH 4.5) environment of the late-stage phagosome and also allows for the treatment of the microbe with reactive oxygen species (ROS) [16]. ROS production is initiated by NADPH complexes associated with phagolysosomes and are often extremely potent antibacterial molecules. The phagosome also contains lytic enzymes such as proteases, lysozymes, and cathepsins that degrade microbes [12], [17]–[19]. Clearly, the phagosome typically serves as a surefire means of eliminating invasive pathogens. In the case of Mtb however many of the steps leading to phagosome maturation are inhibited. In fact, Mtb infected macrophages are often arrested at the early phagosome stages [20]–[22]. The intricacies of the mechanism behind this arrested development have yet to be fully understood, though some key players have been implicated in this arrest. Discovered in 2003 the type VII secretion system ESX-1 is thought to play a role in delayed phagosomal maturation [20]–[22]. Indeed, macrophages infected with ESX-1 Mtb mutants were able to achieve phagosomal maturation; these ESX-1 mutants are incredibly attenuated *in vivo* [12], [23]. ESX-1 has been characterized in mycobacteria to perforate host membrane, allowing for cytosolic access by Mtb, or even actin-based motility escape from the phagosome into the cytosol by *Mycobacterium marinum* [22]–[26]. This access to host cytosol drastically alters the bacterial environment and is thought to be the reason for the unrestricted bacterial replication in what should be a bactericidal prison. Nevertheless, the success of both host and pathogen varies from interaction to interaction, but in most immunocompetent humans Mtb is eventually sequestered into large multicellular structures in the lungs called granulomas. Granulomas are a classical histopathological markers of TB disease and are large lesions composed of macrophages, foamy macrophages, multinucleated macrophages, and dendritic cells, as well as adaptive immune cells such as CD4 and CD8 T cells [12], [27]. These structures are thought to be the final line of defense against Mtb dissemination. Indeed, the siege of host cells attacking the bacteria through acidic and ROS warfare, as well as the modulation of the environment into an oxygen deplete hypoxic surrounding would eradicate many common microbes [28], [29]. In many cases, this proves sufficient in controlling Mtb, forcing it into a state of non-replicating persistence (NRP) and TB latency. In fact, an astounding 25-30% of the world is infected with Mtb, but a majority of these cases are cases of latent TB infection (LTBI) [30], [31]. However, in 5-10% of cases immunity wanes, especially in elderly or immunocompromised individuals, and the NRP Mtb, having prevailed in its war of attrition against the host, undergoes a metabolic renaissance and rapidly replicates to infect a new host.

Non-replicating persistence. Despite such a high prevalence of cases, there is still much that remains unknown about LTBI. Studies on LTBI date back to as early as the 1950s when researchers examined tuberculous lesions in patients and stained tissue samples for bacilli. They reported a variance in the number of replicating bacteria and

hypothesized that the replicative status of the bacilli could be dependent on its availability to acquire oxygen and nutrients [32]. Later works supported this finding when researchers identified non-replicating bacteria in “blocked” (hypoxic) lesions but were able to cultivate these bacteria in culture [33], [34]. These two works provided some of the first evidence that non-replicating bacteria from hypoxic lesions were in a state of non-replicating persistence (NRP) and could be resurrected. This sparked the necessity of *in vitro* hypoxia models to study NRP bacteria outside of lesions, leading to what is now perhaps the most commonly used hypoxia model: the Wayne model [35], [36]. The sealing of bacterial cultures in airtight containers coupled with a gentle stir leads to a gradual depletion of oxygen, allowing for a homogenous metabolic shift at the population level from an aerobic to anaerobic state [36]. The establishment of the Wayne model and other models of NRP advanced the field’s understanding of NRP related phenotypes significantly. Morphologically, dormant Mtb exhibit a thickened cellular envelope [38]–[40]. Moreover, NRP induced by hypoxia or acid stress results in increased antibiotic resistance to many first line antitubercular drugs such as isoniazid, rifampin, and ethambutol [41], [42]. Subsequent works suggest that hypoxia-induced NRP Mtb exhibit increased resistance to rifampin as a result of the thicker cellular envelope [43]. The thickened membrane is not exclusive to hypoxia however, as nutrient-deprivation based models of NRP have shown evidence of a remodeled cell envelope [44]. This theory, however, has yet to be fully explored. In addition, while the mechanism behind NRP dependent antibiotic resistance has yet to be fully understood, it is now widely recognized that NRP leads to an altered metabolic program in Mtb. Since the advent of the Wayne model of NRP, the metabolic transitions to and out of NRP have been well characterized, leading to a greater understanding of Mtb metabolism.

M. tuberculosis metabolism

Central carbon metabolism. A traditional central carbon metabolism delineates the journey of carbon as it becomes enzymatically altered via the processes of glycolysis, the tricarboxylic acid (TCA) cycle, gluconeogenesis, and the pentose phosphate pathway. Carbon in the form of glucose is converted to pyruvate via glycolysis. From there, a pyruvate dehydrogenase oxidizes the terminal product of glycolysis into CO_2 and acetyl-CoA, the precursor to the TCA cycle. The TCA cycle is critical for aerobic respiration and for the production of molecules needed for the biosynthesis of amino acids and nucleotides [45], [46]. Many bacteria are diauxic and preferentially metabolize a single carbon source to support their growth [47]. Upon depletion of this carbon source, the cell can shift to its next preferred source, continuing the cycle until the depletion of carbon sources that the bacteria can metabolize. Mtb on the other hand can co-catabolize carbon sources and interweaves a classically defined central carbon metabolism (CCM) with fatty acid metabolism pathways [47]–[52]. Even chain fatty acids are β-oxidized to acetyl-CoA which can feed into the TCA cycle directly or via the glyoxylate shunt, an alternative route in the TCA cycle that bypasses the carbon dioxide producing steps in the TCA cycle to allow for continued metabolism without excessive loss of carbons [53]. If needed, the enzyme phosphoenolpyruvate carboxykinase PEPCK, encoded by *pckA,* channels these fatty acid derived carbon sources through a

reversal of glycolysis to form glucose in a process called gluconeogenesis [54]. Odd chain fatty acids and cholesterol on the other hand can be catabolized to propionyl-CoA as a precursor to the methylcitrate cycle, whose terminal products pyruvate and succinate feed into the TCA cycle [55], [56]. Both the glyoxylate shunt and methycitrate cycle involve the enzyme isocitrate lyase *icl.* Research examining the virulence of *icl* and *pckA* mutant Mtb strains in mice found these strains to be highly attenuated *in vivo*, adding to mounting evidence that fatty acids are a major carbon source utilized by Mtb in mice [54], [57], [58]. Moreover, *pckA* mutant strains exhibited no growth defects when grown in media containing glucose, yet experienced an arrested development when fatty acids were provided as a sole carbon source [57]. This work coupled with the displayed attenuation of *pckA* mutant Mtb in mice suggests a sequestering of glucose away from Mtb by infected host cells and highlights the necessity of non-sugar-based carbon sources for successful and sustained infection of the host by Mtb. This notion that Mtb preferentially utilized fatty acids as a carbon source in infection dates back to the 1950s. When bacilli taken from infected patients' lungs were cultured on various carbon sources, researchers found elevated respiration rates by the bacteria in the presence of fatty acids [59]. The predominant utilization of fatty acids by mycobacteria in retrospect is to be expected; sequencing of the Mtb genome decades later revealed that the genetic blueprint of Mtb houses approximately 250 distinct fatty acid metabolism enzymes, a seemingly superfluous quantity when compared to the 50 fatty acid related enzymes encoded by the similarly genomic sized *Escherichia coli* [60], [61]. Studies examining the transcriptional changes of Mtb in infectious models revealed the upregulation of fatty acid associated genes [62]–[68]. Transcriptomics and metabolomics have shed some light into the assimilation of sugar and lipid-based carbon sources into the CCM while simultaneously revealing critical information about alternative fatty acid utilization pathways in the bacteria.

Fatty acid metabolism. Aside from their integration into the CCM, free fatty acids are also incorporated into key lipids in the mycobacterial membrane. The process by which extracellular lipids are converted to the bacterial biophysical mass, however, is relatively poorly understood. First, exogenous fatty acids must have a means of entering the cell. Mycobacterium have a uniquely complex membrane architecture: a classical phospholipid bilayer in the inner membrane covalently bound to an arabinogalactan-peptidoglycan layer constituting the aqueous periplasmic space is ultimately encompassed by an impermeable and asymmetrical outer membrane comprised of the aptly named mycolic acids [69], [70]. As one might expect, this membrane would require a shuttle protein or hydrophobic channel to mediate active transport of fatty acids into the cell across this intricate cellular envelope. This key protein eluded the field for several years until the characterization of the Mce1/LucA complex [71]. Through a forward genetic screen originally planned to identify cholesterol utilization genes, the researchers identified *Rv3723/lucA,* a gene predicted to encode a membrane protein. Surprisingly, this protein was not only involved in cholesterol metabolism but impacted fatty acid metabolism as well. Analysis of the *lucA* mutant transcriptional landscape identified *mce1* among the differentially expressed genes, and further investigation into *mce1* implicated a role in the accumulation of fatty acids in the bacteria. Ultimately, LucA was characterized to interact with both the Mce4 (cholesterol import) and Mce1

(fatty acid import) proteins, and radiolabeled and fluorescent lipid uptake assays cemented Mce1 as a long chain fatty acid (LCFA) importer [71], [72]. Thus, *lucA* and the *mce1* loci work in tandem to transport LCFA through the mycobacterium cell envelope. From there long chain or other length free fatty acids follow one of two paths: degradation or synthesis. β-oxidation is a critical mechanism by which Mtb derives energy, made abundantly clear by the over 100 β-oxidation annotated genes [72]. Through β-oxidation LCFA are broken down to produce FADH2 and NADH, as well as acetyl-coA which is assimilated into the TCA cycle [73]. Fatty acids, however, can also undergo biosynthesis in the form of elongation or polymerization. Shorter free fatty acids can be elongated to $C_{16\text{-}24}$ via the type I fatty acid synthase (FAS-I) enzyme or elongated further to $C_{20\text{-}62}$ mycolic acids [74], [75]. In certain circumstances, free fatty acids can be esterified to glycerol to form diacylglycerol (DAG) and triacylglycerol (TAG). 15 putative triacylglycerol synthase (*tgs*) genes have been identified, and several have been shown to be essential for growth *in vivo*, highlighting the importance of TAGs for proper mycobacterium cellular growth [76], [77]. Once incorporated into TAGs, the lipids are thought to localize to the outer membrane of mycobacterium or to cellular lipid bodies [78]–[81].

Lipid bodies

Lipid body structure. Lipid bodies are conserved organelles present across all facets of the kingdom of life [82]. Liposomes, as lipid droplets were originally named, were first described in the late 19th century [83]. Since then some semblance of lipid bodies have been found in countless species; indeed, lipid bodies are ubiquitous in eukaryotes and are found in select prokaryotes including actinobacteria, cyanobacteria, and some archaea [83]–[86]. Despite the wide breadth of species that can form lipid droplets, the structure of this organelle remains structurally analogous across the organisms. Cryogenic electron microscopy (Cryo-EM), an electron microscopy technique used in conjunction with cryogenic capture of cells to determine structural biological information, allowed researchers in 2002 to visualize and identify the lipid droplet structure as a phospholipid monolayer encapsulating a neutral lipid rich core [87]. In eukaryotic cells, the neutral lipid core is predominantly TAG and cholesterol ester filled. While the biological and physical properties that dictate lipid droplet formation have yet to be fully characterized, a few components in the biogenesis of lipid bodies are understood. First, triacylglycerol synthases found along the endoplasmic reticulum (ER) synthesize TAGs within the lipid bilayer. TAG initially disperse between the two phospholipid layers of the ER; however, as TAGs approach a critical concentration of 5-10% in the ER bilayer, they begin to amalgamate and form a lens-like structure [88]–[90]. The observed budding of lipid droplets in model membrane systems is a seemingly spontaneous nascence with no proteins required to initiate lipid droplet budding. Indeed, work done in *Saccharomyces cerevisiae* and artificial lipid droplets have implicated membrane composition as a key determinant of lipid body formation; phospholipid species and composition affect surface tension which in turn determines whether a lipid droplet will bud [91]–[94]. While no proteins have directly been implicated as catalysts of lipid droplet formation, there nevertheless has been evidence that fat storage inducing transmembrane (FIT) proteins, seipins, and perilipins are involved in regulating lipid

droplet homeostasis, with some evidence implicating their involvement in the budding process [95]–[99]. After the budding of lipid droplets, both lipid droplet fusion and fission can occur: fusion is initiated by membrane contact cites with some evidence of protein mediated tethering while the process of lipid droplet fission is not yet understood [100], [101]. Other proteins have been identified to be lipid droplet associated, though their function has yet to be established. In fact, highly sensitive proximity based proteomic labeling has identified anywhere from 30 to over 150 lipid droplet associated proteins [102], [103]. The presumed lipid droplet proteome includes lipid metabolism proteins and perilipins, but also includes membrane trafficking and degradation related proteins. The lipid body associated proteins proved critical in the understanding of the cellular function of lipid droplets.

Eukaryotic lipid droplet function. For many years, cellular lipid bodies had been perceived as mere storage depots of fatty acids, ready at a moments' notice to provide energy in a β-oxidation dependent manner. Monumental advancement in the eukaryotic field has since established these structures as having roles far beyond a repository of molecular fuel and solidified them as bona fide multifunctional organelles. For instance, at the cellular level it was discovered that key enzymes involved in the synthesis of phosphatidylcholine (PC), a major phospholipid in eukaryotic cells, were lipid droplet bound. Further investigation revealed that lipid droplets function as a site of PC synthesis and thus functioned as a secondary site (aside from the ER) of phospholipid biogenesis [104]. Lipid droplets have also been implicated in protection again ER and mitochondrial stress. For example, studies found that disrupted lipid droplet formation led to increased expression of the unfolded protein response (UPR), a cellular adaptive response implemented to re-establish ER homeostasis, as a result of excess lipid signaling molecules prolonging UPR activation [84], [105]. It is believed that redundant free fatty acids not compartmentalized in lipid bodies had a toxic effect on the cells and resulted in ER stress. In a similar vein, proper lipid droplet formation is essential to prevent lipotoxic damage to mitochondria by free fatty acids [84], [106]. Lipid droplets have also been documented in plants and display features similar to eukaryotic lipid bodies with the characteristic TAG filled organelle encompassed by a phospholipid monolayer [106]. Studies of plant lipid structures likewise have suggested alternate roles of lipid droplets. When oleosin, a lipid droplet binding protein, was knocked out in soybean plants, researchers found a marked perturbation in lipid droplet formation wherein 50 nm micro-droplets were formed instead of the plant's typical 1 μm droplets. This disruption led to decreased viability of the seeds, suggesting a link between lipid droplet homeostasis and proper development in plants [107].

Lipid bodies have also been implicated in the immune response by host cells. Indeed, these organelles have been well documented as sites of eicosanoid synthesis. Eicosanoids are lipid-based signaling molecules that regulate pro-inflammatory responses, and eicosanoids species have been shown to localize to lipid droplets, such as the case of prostaglandin E_2 (PGE_2) in macrophages or leukotriene in neutrophils and eosinophils [108]–[110]. On top of being a site of eicosanoid synthesis, lipid droplets have yet another role in response to infections as sites of protein sequestration [111]. Specifically, viperin, an antiviral protein induced during hepatitis C infection, has

been shown to localize to lipid droplets [112], [113]. While a lipid droplet defective model has yet to be used in the context of infection, lipid droplets certainly seem to be centralized structures that play a critical role in the immune system as sites of critical molecule and protein localization. Aside from direct associations with the immunological response of host immune cells in infection, lipid droplets have also been implicated in protecting organisms from disease. For example, when adipose tissue cells are unable to properly esterify free fatty acids into TAGs, an accumulation of excess fatty acids runs rampant and leads to lipotoxicity in the body, resulting in dire consequences such as type 2 diabetes [114]. Dysregulated lipid droplet homeostasis has also been implicated in liver disease and cardiovascular disease [115]. The association of proper lipid droplet balance and disease has been further studied in the context of neurodegenerative diseases. Indeed, mice lacking DDH2, a brain TAG hydrolase, displayed a marked increase in TAG accumulation in the brain and lipid droplet aggregation in neurons. The disruption of proper lipid homeostasis led to these DDH2 knockout mice to display behaviors of the neurological disease hereditary spastic paraplegia [116].

Prokaryotic intracellular lipid inclusion function. While widely studied in the eukaryotic fields, their presence and significance has only recently gained traction in the prokaryotic field, perhaps due to their relative scarcity in prokaryotic species. Intracellular lipid inclusions (ILI), nomenclature reserved for lipid bodies found in prokaryotic cells, are structurally similar to eukaryotic lipid droplets with a phospholipid monolayer encapsulating a neutral lipid rich core. The neutral lipid species that constitute the ILI differs from species to species, with a majority of prokaryotes forming polyhydroxyalkanoate (PHA) rich ILI. Select prokaryotes, typically of the phylum *Actinobacteria*, differ from the PHA producing genera and instead accumulate TAG or wax ester rich organelles [85]. The drivers and mechanisms of ILI formation however are yet to be fully characterized. In terms of stimuli, environmental stressors seem to play a key part in ILI formation. For example, in *Rhodococcus opacus* a low nitrogen to carbon ratio environment results in ILI rich bacteria [117]. With regards to the physical processes behind ILI formation, the machinery behind the biogenesis of ILI is yet to be uncovered. It is believed that much like eukaryotic lipid droplets TAG synthesis proteins catalyze the biosynthetic reaction to incorporate free fatty acids and glycerol into TAGs at the lipid bilayer. From there however, no proteins have directly been implicated in the budding or nascency of ILI. In fact, very few proteins in general have been characterized as components of the ILI formation pathway. TadA, the product of *tadA* (TAG accumulation deficiency) in *R. opacus*, was shown to be involved in ILI aggregation, with *tadA* knockout strains having a 30-40% reduction in TAG accumulation [118]. The limitations in the understanding of genes involved in the physical formation of ILI result in restricted genetic ILI knockout models, thus making it difficult to study the role of ILI in prokaryotes. Nevertheless, some work has been conducted to elucidate environmental conditions that prompt ILI formation and on the role that ILI may play in bacteria. For example, there are lines of indirect evidence that the effects of toxic fatty acids can be insulated by ILI. The TAG synthesizing *Nocardia globerula*, a gram-positive rod-shaped bacterium, was able to be cultivated with pristane as a carbon source. This growth condition is known to inhibit β-oxidation mediated

growth in other bacteria. Lipid analysis of the TAG synthesized by *N. globerula* revealed the ability of this bacteria to sequester the oxidation-derived intermediates that were a result of pristane metabolism into its ILI, suggesting the role of its ILI in protection from and growth on an otherwise toxic medium [119]. A recent study in *Rhodococcus jostii* demonstrated that ILI colocalize to DNA via an intermediary protein microorganism lipid droplet small (MLDS). When MLDS is knocked out, ILI no longer bind to DNA. The mutant bacteria suffer greater DNA damage when exposed to UV light, suggesting ILI play a role of protection from genotoxic stress [120].

Mycobacterial intracellular lipid inclusions. Recent work in *Mycobacteria*, members of the *Actinobacteria* phylum, has further expanded the field's understanding of ILI. First identified in 1946, ILI in mycobacteria have since been a point of interest for many scientists due to their correlation with the difficult to treat state of NRP [78], [121]–[125]. Mtb isolated from human sputum have been found to contain ILI, and work on lab strains of Mtb has identified ILI to be predominantly TAG filled, suggesting that Mtb accumulates these structures while growing in lipid rich environments [123], [124]. Work on these laboratory strains of Mtb has elucidated key genes correlated to the presence of ILI and shed light on environmental factors that stimulate ILI formation. As previously mentioned, Mtb can utilize host lipids to seemingly sustain itself in the granuloma, sites of stressors including hypoxia, nutrient limitation, and nitric oxide (NO) stress [28], [54], [55], [57], [58], [126]. It is in these lesions that Mtb shifts to a state of NRP with characteristic arrested metabolism, increased antibiotic resistance, and bountiful ILI. Indeed, *in vivo* and *in vitro* works across mycobacteria have pinpointed how specific stressors induce ILI formation. First, hypoxia induces the dormancy survival regulator (DosR) regulon. The DosR regulon consists of approximately 48 genes, of which the TAG synthesizing *tgs1* gene is a part [127], [128]. As TAGs constitute the neutral lipid rich core of ILI in mycobacteria, it comes as no surprise that disruption of *tgs1*, the predominantly expressed *tgs*, leads to marked TAG reduction [129]. Nutrient limitation has also been implicated in the accumulation of TAG. Indeed, much like *R. opacus*, *Mycobacterium abscessus* and *Mycobacterium smegmatis* also become ILI rich in nitrogen low carbon high environments. *M. abscessus* stimulated to make ILI were found to be more virulent than non-ILI rich *M. abscessus*, implicating ILI and TAG accessibility as critical components of mycobacterial virulence [78], [130]. Iron depravation, though not as well studied, seems to also induce ILI formation in Mtb strain *H37Rv* [131]. Finally, NO stress, similar to hypoxia, leads to an upregulated DosR regulon and TAG accumulation, made evident by several microarray and radioactive fatty acid metabolomics studies in Mtb [76], [132], [133]. Interestingly, when grown in axenic culture devoid of external stressors, laboratory strains of Mtb lack ILI, hinting at key differences in metabolism and genetics between lab and clinical Mtb strains [131].

Aside from the environmental impetuses of ILI formation, several studies have identified ILI associated proteins. Recently, work in BCG implicated heparin-binding hemagglutinin adhesin (HBHA) in ILI formation, as illustrated by ILI barren *hbha* mutant strains [134]. Interestingly, HBHA is a homolog of the previously mentioned *R. opacus* ILI associated protein TadA, suggesting that HBHA shares similar ILI regulatory characteristics with TadA. In BCG however, *hbha* mediated ILI formation is only

manifested under NO stress [134]. Other researchers applied homology in a different direction when they screened the Mtb genome for amino acid sequence similarities to the mammalian lipid droplet associated protein perilipin. From this study they identified mycobacterial perilipin-1 (MPER1), the product of *ppe15/mper1*, which when knocked out in Mtb cultured in ILI inducing conditions led to ILI loss [136]. A plethora of other proteins have been implicated to be ILI associated. In 2018, researchers probed the ILI proteome in *M. smegmatis*. Researchers investigated the amphipathic helix motif found on phage shock protein A (PspA) in conjunction with liquid chromatography-tandem mass spectrometry (LC/MS) on purified ILI to identify proteins predicted to bind to ILI. Surprisingly, they uncovered over 400 ILI associated proteins in *M. smegmatis*, although the co-localization of these proteins to ILI and their roles has yet to be clearly determined [137].

M. marinum as a model to study *M. tuberculosis*

The global spread of TB and its difficulty to treat accentuate the necessity to study Mtb. This deadly pathogen, however, requires a biosafety level 3 containment laboratory for researchers to safely study it. Furthermore, the bacterium is an extremely slow growing organism with a doubling time of 18-24 hours [138]. These intricacies and complications warrant safer and easier to handle bacteria to serve as proxies to Mtb. *M. marinum* is one such species commonly used to study Mtb. *M. marinum,* a member of a nontuberculous class of mycobacterium called NTM, is an waterborne bacterium known as a natural pathogen of fish that can also cause skin and soft tissue infections in humans [139]. The first discovery of *M. marinum* dates back to 1926 when “spontaneous tuberculosis” was identified in saltwater fish at the Philadelphia Aquarium [139]. Since then it has been known to infect saltwater and freshwater fish, as well as many other aquatic creatures. Its spread to human is rare but has been documented, often due to unsanitary conditions of swimming pools or fish tanks leading to so called “fish tank granulomas,” granulomatous lesions on the skin [140]. What makes *M. marinum* a particularly alluring species to study is its relative ease of handling. As a less pathogenic organism, the regulations around safe handling of *M. marinum* are much less restrictive than with Mtb and only require a biosafety level 2 laboratory space. Moreover, *M. marinum* has a doubling time of 4-8 hours, making it a much more enticing bacterium to work with due to its relatively faster generation time [141]. But perhaps the most prominent reason for its interest in the field of mycobacteria is its genetic relatedness to Mtb. 16s, DNA-DNA hybridization, and fatty acid analysis have placed *M. marinum* as the closest relative to Mtb [142]–[144]. For these reasons, *M. marinum* has been used to infect zebrafish or the amoeba *Dictyostelium discoideum* to study host-pathogen interactions and provide a glimpse inside the black box of Mtb pathogenesis. Strikingly, *M. marinum* pathogenesis has remarkable parallels to Mtb pathogenesis, with the aggregation of infectious cells leading to granuloma formation in zebrafish [145], [146]. Mtb, as previously mentioned, resides in granulomas during TB infection. These granulomas are conglomerates of immune cells such as dendritic cells, CD4 and CD8 T cells, and foamy macrophages. Recent work has established the *D. discoideum-M. marinum* host-pathogen model as a model for mycobacterial infection of foamy macrophages [147]. In this model, researchers observe the accumulation of ILI

by *M. marinum* in a host lipid dependent manner [148]. Parallels to Mtb infection continue its ability to induce latent infection in zebrafish and the correlated hypoxia-induced dormancy regulon mirroring that of the Mtb NRP transcriptome changes [149], [150]. Finally, *M. marinum* also shares many key virulence genes with Mtb, such as the critical type VII secretion system ESX-1 necessary for secretion of virulence factors and perforation of phagosomes [20], [151], [152].

Despite these similarities, it should be noted that *M. marinum* is of course a species distinct from Mtb. Indeed, the 6.5 Mb genome of *M. marinum* is substantially larger than the 4.4 Mb genome of Mtb. Of the additional genes in the *M. marinum* genome are those involved in actin-based motility. Despite its immotility in axenic conditions, *M. marinum* with functional ESX-1 protein expression can access and hijack host proteins Arp2/3 and WASP to polymerize free host actin in the cytosol, ultimately leading to an escape from the phagosome and cell to cell dissemination [26], [153]. Other key differences in their genomes may contribute to the divergence in culture conditions. Reflective of its natural replicative niche of water dwelling creatures, *M. marinum* optimally grows at 30°C and, unlike Mtb, cannot withstand the 37°C internal temperatures of warm blooded organisms [153]. Despite these differences, this pathogen nevertheless remains a strong proxy for studying Mtb and is a widely recognized model of Mtb pathogenesis [154]. Comprehensive study of *M. marinum* will prove to be critical in the understanding the external impetuses governing transcriptomic and lipidomic remodeling in Mtb, deciphering the mechanisms of the molecular ordinances operated by both sides of a contentious host cell-pathogen interface, and containing the spread of a deadly infectious disease afflicting a quarter of the global population.

Chapter Two: Mycobacterial formation of intracellular lipid inclusions is a dynamic process associated with rapid replication

Fines DM, Schichnes D, Knight M, Anaya-Sanchez A, Thuong NTT, Cox J, Stanley SA

Abstract

Intracellular lipid inclusions (ILI) are triacylglyceride rich organelles produced by mycobacteria thought to serve as energy reservoirs. It is believed that ILI are formed as a result of a *dosR* mediated transition from replicative growth to non-replicating persistence (NRP). ILI rich *Mycobacterium tuberculosis* (Mtb) bacilli have been reported during infection and in sputum, establishing their importance in Mtb pathogenesis. Studies conducted in mycobacteria such as *Mycobacterium smegmatis, Mycobacterium abscessus,* or lab Mtb strains have demonstrated ILI formation in the presence of hypoxic, nitric oxide, nutrient limitation, or low nitrogen stress, conditions believed to emulate the host environment within which Mtb resides. Here, we show that *M. marinum* and clinical Mtb isolates make ILI during active replication in axenic culture independent of environmental stressors. By tracking ILI formation dynamics we demonstrate that ILI are quickly formed in the presence of fresh media or exogenous fatty acids but are rapidly depleted while bacteria are still actively replicating. We also show that the cell envelope is an alternate site for neutral lipid accumulation observed during stationary phase. In addition, we screen a panel of 60 clinical isolates and observe variation in ILI production during early log phase growth between and among Mtb lineages. Finally, we show that *dosR* expression level does not strictly correlate with ILI accumulation in fresh clinical isolates. Taken together, our data provide evidence of an active ILI formation pathway in replicating mycobacteria cultured in the absence of stressors, suggesting a decoupling of ILI formation from NRP.

Introduction

Mycobacteria are a genus of bacteria that contain numerous human pathogens, the most prominent being *Mycobacterium tuberculosis* (Mtb), a deadly pathogen that causes over 1.5 million deaths annually [3]. It is estimated that up to 25% of the global population has been infected by Mtb, with many infected individuals harboring latent disease [30]. A major replicative niche of Mtb are host macrophages, cells that normally function to eliminate invading microbes. Understanding how Mtb survives and grows within macrophages is key to understanding its success as a pathogen. Lipid metabolism is central to Mtb's ability to growth within macrophages [157]–[159]. Mce1, a transporter found in the cytoplasmic membrane of mycobacteria, is essential for importing long chain fatty acids from the environment, including fatty acids obtained from host macrophages during infection [71]. It is assumed that Mtb utilizes host lipids as a carbon source to fuel intracellular growth. Mtb is also thought to exploit lipids at late stages of infection in the lipid rich environment of host necrotic lesions [160]. Mce1 is essential for growth in macrophages and during murine infection, demonstrating that the capacity to import lipids is a critical component of Mtb pathogenesis [71], [157].

During macrophage infection Mtb accumulates cytosolic lipid bodies, organelles consisting of a triacyglyceride (TAG) rich core bounded by a phospholipid monolayer [72], [76], [87], [158]. Despite the presence of lipid bodies across the kingdoms of life they have been studied predominantly in eukaryotes, largely due to their perceived scarcity in prokaryotic species. Recent advances in eukaryotic lipid droplet biology have established that these structures are not simply inert storage depots, but actively participate in a wide variety of processes including cellular stress responses, protein storage, and energy homeostasis [106], [113], [159]–[161]. Studies of *Actinobacteria* and *Proteobacteria* have advanced the field's understanding of intracellular lipid inclusions (ILI), a term reserved for prokaryotic lipid bodies [162]–[164]. Work in these organisms has shed light on environmental stimuli that lead to ILI formation and suggest that ILI play a dynamic role in bacteria. For example, ILI may play a role as a site of toxic fatty acid sequestration. Lipid analysis of TAGs synthesized by *Nocardia globerula* grown on pristane, a carbon source known to inhibit β-oxidation and growth in other bacteria, revealed the ability of this bacteria to sequester toxic oxidization-derived intermediates into the TAGs [119]. Furthermore, work in *Rhodococcus jostii* demonstrated that ILI colocalize to DNA via an intermediary protein, microorganism lipid droplet small (MLDS). In mutants lacking MLDS, ILI no longer bind to DNA and bacteria suffer greater DNA damage when exposed to UV light, suggesting ILI have a role in protecting the bacilli from genotoxic stress [120].

Work in *Mycobacteria*, members of the *Actinobacteria* phylum, has further expanded the field's understanding of ILI. Mtb isolated from human sputum has been found to contain ILI, suggesting that ILI are a feature of Mtb during human infection [123], [124]. Interestingly, lab Mtb strains form ILI in axenic culture under conditions that induce a "dormancy" regulon mimicking non-replicating states that exist *in vivo* [167]. When subjected to hypoxia, nutrient starvation, or nitric oxide stress, conditions thought to emulate the phagosome or granulomas that Mtb resides in during infection, Mtb

accumulates ILI [76], [78], [132]–[134], [165]–[167]. Interestingly, several clinical isolates form ILI when growing in axenic culture without environmental stressors, while most laboratory strains of Mtb apparently lack ILI [131]. It is not clear whether laboratory strains have lost the ability to form ILI during axenic culture, or whether this phenotype is variable even among clinical isolates. It is also possible that specific culture conditions are required to observe ILI formation. For example, *Mycobacterium smegmatis* and *Mycobacterium abscessus*, members of nontuberculous mycobacteria (NTM), were demonstrated to form ILI when subjected to nitrogen starvation simultaneous with carbon excess [130]. It is now recognized that ILI-rich states are correlated with enhanced and sustained virulence in mycobacteria. Nitrogen deprived ILI-rich *M. abscessus* are significantly more virulent compared to ILI deplete *M. abscessus* in zebrafish embryos [130]. In addition, ILI rich states have also been linked to enhanced antibiotic resistance. Carbon metabolism studies have determined that TAG synthesis inhibits growth, and bacteria induced to form ILI exhibited heighted resistance to first line antitubercular antibiotics [174] .

The current consensus in the field is that Mtb forms ILI during states of non-replicating persistence (NRP) or during times of stress [78], [124], [125]. It is widely recognized that upon gradual oxygen depletion, Mtb transitions to NRP, a transition initiated by the dormancy survival regulator DosR. Approximately 48 genes constitute the DosR regulon [127]. Among these genes is *tgs1*, the predominant triacylglyceride synthase, whose disruption leads to significant reduction in TAG levels [129]. TAG accumulation and ILI formation initiated by the DosR regulon has hence been accepted as markers of successful transition to NRP [124], [125], [168]. Yet some lines of evidence suggest that ILI formation may also be associated with replicative states of the bacteria. We recently showed that Mtb forms ILI in resting macrophages that are permissive for bacterial growth, and not in IFN-γ activated macrophages that restrict bacterial replication [169]. This finding was surprising given that IFN-γ activated macrophages produce NO, a stressor known to promote ILI formation *in vitro* [132], [170]. Indeed, although there are numerous observations related to ILI formation in mycobacteria*,* we know very little about the conditions under which they form, the mechanism of formation, or their function. Further, although the formation of ILI in axenic culture is thought to be a feature of L2 strains of Mtb, it is unclear whether ILI formation is linked to the fitness or virulence of this lineage. Interestingly, although ILI are thought to be the primary storage depot for TAGs in bacteria, recent reports have suggested that under specific conditions, mycobacteria export TAG to their outer membrane, though the reason remains unknown [80], [171]. Thus there remains much concerning ILI formation specifically, and TAG biology more generally, that requires elucidation.

Here, we use a laboratory strain of *Mycobacterium marinum* and clinical isolates of *M. tuberculosis* to define conditions leading to ILI formation in mycobacteria. *M. marinum* is a close relative of Mtb as shown by 16S and fatty acid profiling and shares a significant percentage of essential genes with Mtb [171]. This waterborne pathogen is commonly studied in a host-pathogen model to infect the amoeba *Dictyostelium discoideum;* in these contexts, *M. marinum* has also been shown to use host lipids to generate ILI during infection [147]. Through imaging, genetic, and biochemical assays we

characterize the dynamics of *M. marinum* ILI formation in axenic broth as well as in the presence of environmental factors previously demonstrated to induce ILI formation in mycobacteria. To our surprise, we discover that *M. marinum,* unique from other NTM and lab strains of Mtb, robustly forms ILI in axenic culture. This phenomenon is independent of environmental stressors and NRP, challenging the prevailing notion in the field that ILI formation is distinctly correlated with NRP or a response to stress. We also show that *M. marinum* utilizes fatty acids from media to create ILI, and that both *M. marinum* and Mtb form ILI during early log phase and then deplete them at later stages of growth. Interestingly, using super resolution microscopy, we find that at later stages of growth both species appear to accumulate TAGs in the cell envelope, further highlighting that ILI formation is specifically associated with active replication. Finally, we show that ILI formation in stress-free axenic culture may be a feature of most clinical isolates that is lost upon laboratory cultivation. Interestingly strains of Mtb that do not produce ILI in early log phase growth appear to instead accumulate neutral lipids in their cell envelope. Gene expression analysis in ILI high and ILI low isolates demonstrated a lack of correlation between *dosR* expression level and ILI status, contrary to what was expected. Taken together, these findings demonstrate that neither NRP nor *dosR* expression are required for ILI formation in some clinical Mtb strains, suggesting that an alternative pathway may be responsible for ILI accumulation.

Materials and Methods

Bacteria and Media
M. marinum strain M was grown in $7H9^{ADS}$ media (Middlebrook 7H9 Broth supplemented with 0.2% Tween-80, 0.2% Glycerol, 0.5% BSA, 0.2% dextrose, 0.085% NaCl). For single carbon source assays *M. marinum* was cultured in minimal media (0.08% NaCl, 0.04% L-asparagine, 3.5% Na_2HPO_4, 1.48% KH_2PO_4, 0.04% 5M Ammonium Iron Citrate, 0.02% 1M $MgSO_4 7H_2O$, 0.05% 1mg/mL $CaCl_2$, 0.01% 0.1mg/mL $ZnSO_4$, 0.2% EtOH, 0.2% Tyloxapol) supplemented with either 30 mM glycerol, 30 mM sodium acetate, 200 µM stearic acid, or 200 µM oleic acid. Cultures were shaken at 100 rpm at 32°C. *M. tuberculosis* H37Rv and Erdman were grown in $7H9^{OADC}$ (Middlebrook 7H9 Broth supplemented with 0.04% Tween-80, 0.2% Glycerol, 10% Middlebrook OADC Enrichment). The L1 clinical isolate TB1401420 was generously provided by the Kato-Maeda lab at the University of California, San Francisco, and was cultured in $7H9^{OADC}$. The L2 clinical isolate was generously provided by the Darwin lab at New York University and cultured in $7H9^{OADC}$. All Mtb strains were cultured at 37°C and rolled at 5 rpm.

Generation of SSB-GFP M. marinum
SSB-GFP plasmid was generously provided by the Russell lab at Cornell University. Electroporation of donor plasmids was conducted in electrocompetent *M. marinum* as previously described [172]–[174]. Transformed colonies were selected on Middlebrook 7H10 agar plates with 50 µg/mL hygromycin and cultured in $7H9^{ADS}$ supplemented with 50 µg/mL hygromycin.

Fluorescent and Phase Microscopy
For imaging of bacteria in axenic culture, bacteria were cultured as described above. For fluorescent microscopy, cultures were sampled and fixed with equal amounts of 10% formalin at the noted time points. Samples were pelleted at 2850 *g* for 5 minutes, washed with equal volume 1x PBS, and resuspended with equal volume of 5uM BODIPY 493/503 in PBS for or 5 µM LipiBlue in PBS for 45-60 minutes. Samples were washed twice with 1x PBS and resuspended in a final volume of 200 µL 1x PBS before being transferred into Phenoplate 96 plates. For imaging of bacteria in host cells, samples were washed with 1x PBS and fixed in equal amounts of 10% formalin. Samples were then washed with 1x PBS and incubated with an equal volume of 5 µM BODIPY 493/503 and DAPI 1:10000 in PBS for 45-60 minutes, with a final wash in 1x PBS. All plates were imaged on an Opera Phenix High Content Screening System. Resulting images were analyzed using CellProfiler image analysis software. For live imaging, mCherry fluorescent *M. marinum* cultures were grown to OD_{600} 0.6 in $7H9^{ADS}$ and then back diluted to 0.05. 200 µL of back diluted cultures were loaded into CellASIC ONIX Microfluidic Plates which were then connected to a CellASIC flow chamber. Phase contrast images were taken on an AxioObserver Z1 inverted microscope at 15 minute intervals over the course of 17 hours. Super-Resolution Structured Illumination Microscopy images were obtained on a ZEISS Elyra 7 inverted microscope and 3D reconstruction modeling was performed on the Imaris Cell Imaging software.

Lipid Extraction
M. marinum cultures were grown in 7H9^{ADS} media as described above. At specific time points cultures were pelleted at 2850 *g* for 5 minutes and washed 2x with Optima water. Total lipids were extracted via a 1:2 MeOH:Chloroform solution. The cultures were left rocking at room temperature for 1 hour and then spun down at 2850 *g* for 10 minutes. After the upper organic layer was transferred to a fresh tube a fresh aliquot of 1:2 MeOH:Chloroform was added to the remaining pellet. The pellet was rocked for another hour, spun at 2850 *g* for 10 minutes, and the upper organic layer was transferred to the corresponding tube. The solvent was dried under a gentle stream of nitrogen. The resulting lipid residue was resuspended in 1:2 MeOH:Chloroform.

Thin Layer Chromatography
TLC was conducted on Hard Layer Silica Gel UNIPLATES. The solvent mixture used for the analysis of TAG was toluene:acetone 99:1 (v/v). Spots were visualized by Coomassie Blue (0.2% in 20% MeOH) for 20 minutes followed by a destaining in 20% MeOH for up to 1 hour. Imaged plates were analyzed using the FIJI imaging package.

Replenishment Assays and BODIPY FL C_{16}
M. marinum was cultured in 7H9^{ADS} media to mid log phase and back diluted to an OD_{600} of 0.05. The cultures were then grown for 6 hours, and then pelleted at 2850 *g* for 5 minutes. Replenished cultures were resuspended in fresh 7H9^{ADS} media while unreplenished cultures were resuspended in their original media. Samples were taken 18 hours post resuspension. For BODIPY FL C_{16} supplementation, *M. marinum* with a transposon insertion in *mce1* was cultured in 7H9^{ADS} media to mid log phase and back diluted to an OD_{600} of 0.05. The culture was grown for 48 hours. BODIPY FL C_{16} was added to a final concentration of 2.5 µM for 4 hours. The culture was washed 1x with PBS and fixed with 10% formalin. Samples were then washed 2x with PBS and imaged immediately.

Environmental Stress Conditions
M. marinum cultures were grown to an OD_{600} of 0.6. For hypoxia assays, cultures were back diluted to an OD_{600} of 0.2. 20 mL of back diluted culture were placed in airtight Nalgene inkwell bottles. Methelyne blue was supplemented to track oxygen loss as previously described [36]. For acid stress, mid log cultures were washed in acidified media (classical media acidified with HCl to pH 5.5), and back diluted to OD_{600} 0.05 in acidified media. For NO stress, mid log cultures were washed in acidified media, and back diluted to OD 0.05 in acidified media supplemented with $NaNO_2$ (final concentration 1.5 mM) as previously described [173]. For nitrogen limited stress, mid log cultures were washed in minimal mineral salt medium (2 g/L Na_2HPO_4, 1 g/L KH_2PO_4, 0.5 g/L NaCl, 0.2 g/L $MgSO_4$, 20 mg/L $CaCl_2$, and 1 g/L NH_4Cl) or mineral salt medium nitrogen limiting (2 g/L Na_2HPO_4, 1 g/L KH_2PO_4, 0.5 g/L NaCl, 0.2 g/L $MgSO_4$, 20 mg/L $CaCl_2$, and 0.05 g/L NH_4Cl), and back diluted to OD_{600} 0.05 in minimal mineral salt medium or mineral salt medium nitrogen limiting as previously described [130].

Bacterial Infections

Bone marrow derived macrophages (BMDM) from C57BL/6 mice were seeded at 5e4 cells/ well into PhenoPlate 96 well plates 48 hours prior to infection in cell culture media (DMEM supplemented with 10% FBS, 10% CSF, and 1% glutamax). BMDM were placed in 33 °C tissue culture incubators 1 hour prior to infection to acclimate the cells to the appropriate temperature. Prior to infection, *M. marinum* was cultured in classical media to an OD_{600} of ~0.6. Bacteria cultures were pelleted at 2850 *g* for 5 mins and washed twice with 1x PBS. A slow spin speed at 58 *g* was performed to pellet clumped bacteria. The supernatant was collected and diluted into phagocytosis media (DMEM supplemented with 5% horse serum and 5% FBS) to achieve a multiplicity of infection of 1. Bacterial suspensions were added onto cells and spun at 335 g for 10 minutes. Infected cells were washed with 1x PBS and incubated in cell culture media at 33 °C. When necessary, media changes were performed every 2 days.

Isolation of RNA and RNA Seq

M. tuberculosis strains were cultured to mid log phase and back diluted in 30 mL of $7H9^{OADC}$ to an OD_{600} of 0.05. After 24 hours the cultures were pelleted at 2850 *g* for 5 minutes and resuspended in 1 mL Trizol. Samples were transferred to an o-ring tube with RNase and DNase free glass beads and bead beat for 30 seconds 3 times. Samples were pelleted and the supernatant was transferred to a fresh tube with 200 µL chloroform. Samples were centrifuged at 12000 *g* for 10 minutes at 4°C. Resulting aqueous phase was transferred to a fresh tube. Equal volume of 70% RNase free EtOH was added. Total RNA extraction was performed via a Qiagen RNease Mini Kit. Prepped samples were submitted to Azenta Life Sciences for RNA Sequencing and analysis.

Screening of Clinical Isolates

Mtb strains were cultured in 10 mL of $7H9^{OADC}$ to mid log phase. Cultures were back diluted to an OD_{600} of 0.05 and grown for 24 hours. Samples were pelleted and fixed as described above. Fixed samples were stained with 5 µM BODIPY 493/503 and DAPI 1:10000 in PBS for 45-60 minutes, with a final wash in 1x PBS. Samples were imaged and analyzed as described above.

RT-qPCR

M. tuberculosis strains were cultured to mid log phase and back diluted in 30 mL of $7H9^{OADC}$ to an OD_{600} of 0.05. Samples were collected 24 hours after back dilution. RNA was isolated as described above. For qPCR, cDNA was generated from 1 µg of RNA using Superscript III (Invitrogen Life Technologies) and random hexamer primers. Genes were analyzed using KAPA SYBR FAST qPCR master mix (Roche Kapa Biosystems). Each sample was analyzed in at least duplicate on a CFX96 Real-time PCR detection system (Bio-Rad). C_Q values were normalized to values obtained for 16S and relative changes in gene expression were calculated using the $\Delta\Delta C_Q$ method.

Results

M. marinum **produces ILIs during macrophage infection**. We first tested whether *M. marinum,* like *M. tuberculosis,* forms ILI in resting macrophages. We infected murine C57BL/6 bone marrow derived macrophages (BMDM) with *M. marinum* and observed robust replication of the bacteria during infection (Fig. S1, Table S1). Despite being in an ILI depleted state immediately upon infection (Fig. 1A), WT bacteria formed ILI throughout the course of the 72-hour infection, accumulating increasing levels of ILI until the point of host cell rupture (Fig. 1B, 1C). The Mce1/LucA complex has been implicated in the import of palmitate and other long chain fatty acids, leading to the formation of ILI during host cell infection by Mtb [71], [72]. Similar to Mtb, formation of ILI formation was reduced in *mce1* mutant *M. marinum*during infection of macrophages, particularly at early timepoints (Fig. 1C, 1D). *Mce1* mutants were able to form substantial levels of ILI at later timepoints, suggesting the existence of alternate fatty acid import mechanisms or *de novo* fatty acid synthesis by *mce1* mutants (Fig. 1C). The ESX-1 type VII secretion system is required for phagosomal perforation and virulence in both *M. marinum* and *M. tuberculosis* [177]*.* In *M. marinum,* this perforation results in liberation of the bacteria into the cytosol and actin-based motility for a fraction of the bacteria [26], [153]. The ESX-1 secretion system is also required for phagosome maturation arrest, and ESX-1 mutants have increased lysosomal residence. We next tested whether ESX-1 mutants are impacted in their ability to form ILI. We found that the *M. marinum* region of difference 1 (RD1) ESX-1 mutant was attenuated for ILI formation in macrophages compared to WT *M. marinum* (Fig. 1C, 1E). The ESX-1 mutant had a greater than 60% reduction in ILI signal at 72 hours compared to WT, an attenuation similar to the fatty acid import deficient *mce1* mutant (Fig. 1C). These data demonstrate that *M. marinum* utilizes the ESX-1 secretion system and Mce1 lipid importer to acquire fatty acids from the host to form ILI. Furthermore, the fact that *M. marinum* forms ILI during active replication in host cells is counter to the prevailing hypothesis that bacteria form ILI during conditions associated with dormancy.

M. marinum **forms ILIs while replicating in axenic culture.** Dissecting inputs into ILI formation during infection of host cell present numerous challenges due to the complexity of the host environment, which is ill defined. We therefore tested whether *M. marinum* produces ILI during logarithmic growth in axenic culture. We grew mCherry-expressing *M. marinum* in liquid media and sampled the culture at various intervals throughout the course of bacterial growth to monitor the dynamics of ILI formation. Each sample was stained with BODIPY 493/503 to visualize neutral lipid rich puncta [71], [174]. At the time point of inoculation into a fresh culture (0h) bacterial cells lacked ILI (Fig. 1F), yet six hours post inoculation bacteria were ILI rich (Fig. 1G). ILI levels waned as the bacteria grew until a state of ILI depletion was observed at 24 hours post inoculation (Fig. 1H, 1I). Quantification of the results showed that the peak of ILI formation occurred during early log phase, and a decrease in ILI abundance correlated with a decrease in replication rate of the bacteria (Fig. 1J). By the time bacteria approached stationary phase ILI had disappeared (Fig. 1I). The fact that bacteria had low ILI levels prior to inoculation indicates that the ILI rich state at the early time points

was a result of rapid neutral lipid accumulation and ILI formation while the bacteria were actively replicating in early log phase culture.

ILI in mycobacteria are classically composed primarily of TAGs [175]–[177]. To confirm that the neutral lipid puncta stained by BODIPY 493/503 were indeed ILI, we isolated lipids from cultures grown for 6 hours and 48 hours and normalized the lipid content to cell mass by OD_{600} measurements. TLC of the extracted lipids indeed confirmed that freshly cultured WT *M. marinum* has a marked increase in TAGs compared to the WT *M. marinum* cultured to a higher OD (Fig. 1K, Fig. 1L). To confirm that ILI are observed in actively replicating bacteria, we used a fluorescent reporter of single strand binding protein (SSB) that has been demonstrated to reliably identify bacteria undergoing active replication in *M. smegmatis* and *Mtb* [178]. Replicating bacteria, indicated by the SSB-GFP foci, contained Lipi-Blue stained ILI, implying replicating bacteria indeed formed ILI (Fig. 1M). As a final confirmation that *M. marinum* produces ILI during early log phase while actively replicating, we made use of phase microscopy in conjunction with a microfluidic system to capture live cell microscopy data. Phase contrast microscopy has been utilized in previous works to visualize ILI and allowed us to capture a time lapse video of *M. marinum* cells replicating [179], [180] (Fig. S2, Supplemental Video 1). Bacteria rapidly formed structures resembling ILI (Fig. S2 arrows, Supplemental Video 1). These structures occupied a significant portion of the cellular space and were capable of fusing with one another, characteristics consistent with previous findings in other prokaryotes [85]. Together, these data clearly support the finding that *M. marinum* forms ILI while actively replicating in early log phase in axenic culture. Unexpectedly, the bacteria seem to make and then deplete ILI all before reaching stationary phase, despite the fact that the media contains sufficient sources of carbon to fuel extensive bacterial growth.

***M. marinum* formation of ILI in axenic culture requires exogenous lipids.** To test if the ILI-rich status of bacteria in early log-phase growth was reflective of environmental conditions or growth phase, we grew bacteria to a timepoint at which they had depleted ILI and then replenished the culture with fresh media. Media-replenished cultures exhibited a marked increase in ILI (Fig. 2A, 2C) compared to cultures resuspended in their spent media (Fig. 2B, 2C). This result indicated ILI formation in *M. marinum* is stimulated by a component of media and is independent of bacterial growth phase. Having established that ILI formation is most robust in the presence of fresh media we sought to understand what components in the media induce *M. marinum* ILI formation. Both Mtb and *M. marinum* are known to import fatty acids during infection of host cells. We hypothesized that *M. marinum* similarly uptakes fatty acids during axenic growth and uses them to form ILI. *M. marinum* was cultured in minimal media supplemented with the sole carbon sources glycerol, acetate, stearate, and oleate (Fig. 2D-H). ILI accumulation, indicated by BODIPY 493/503 staining, revealed that *M. marinum* requires the presence of long chain fatty acids in the extracellular environment to form ILI, and that abundant alternative carbon sources such as glycerol or acetate are insufficient. To test whether *mce1* is required for ILI formation, we compared WT with a *mce1* transposon mutant (Fig. S3A-C). When grown in axenic culture, the *mce1* mutant failed to produce ILI (Fig. S3B, S3C), suggesting that mce1 is a conserved component

of ILI formation among *M. marinum* and Mtb. To confirm this finding, we supplemented the media with the fluorescent fatty acid BODIPY FL C_{16}. The *mce1* mutant again failed to form ILI, confirming that similar to its role in Mtb, Mce1 in *M. marinum* is a critical component in the import of exogenous 16 carbon chain fatty acids (Fig. S3D-F). Thus, *M. marinum* represents a tractable system for studying ILI formation without the need for a host cell infection.

Characterization of environmental factors contributing to *M. marinum* ILI formation. Nitrogen limitation has been well characterized to lead to ILI formation in many species, including *Rhodococcus opacus*, and the NTM *M. smegmatis* and *M. abscessus* [117], [130]. To study the consequences of a nitrogen limited environment on *M. marinum*, we cultured the bacteria in Minimal Mineral Salt Medium with standard (MSM) or low (MSM NL) amounts of nitrogen as previously described [130]. Nitrogen limitation did not lead to ILI formation in either condition, suggesting that nitrogen deprivation does not lead to a transcriptional reprogramming to promote ILI biogenesis in *M. marinum* (Fig. 3A-D). We next tested whether *M. marinum* forms ILI in in axenic culture when subjected to stressors that emulate a host environment. Granulomas, a hallmark of infection of humans with Mtb and of zebrafish with *M. marinum*, can become hypoxic under certain conditions [28], [166], [181]. While changes in the transcriptomic landscape of *M. marinum* in hypoxic conditions has shown an increase in *tgs1* expression, it is unknown whether hypoxia stimulates ILI formation in *M. marinum* or merely TAG accumulation [128]. To examine ILI formation under hypoxic conditions, we cultured WT *M. marinum* in airtight sealed inkwell bottles supplemented with methylene blue to track oxygen depletion levels [36]. Once the cultures were confirmed to be hypoxic, we sampled the cultures and imaged ILI. We found that bacteria recovered from hypoxic cultures were highly lipid loaded, with levels four times that of a culture grown in $7H9^{ADS}$ for six hours (Fig. 3E-G). Other widely recognized host driven responses are the production of nitric oxide (NO) as well as the acid stress in the phagosome. Previous studies have demonstrated ILI formation, TAG accumulation, or *tgs1* expression in nitric oxide or acid stress in other mycobacteria [129], [132]–[134]. We subjected WT *M. marinum* to acid and NO stress, culturing the bacteria in $7H9^{ADS}$ acidified to pH 5.5 with and without 3mM $NaNO_2$ as previously described [173]. Analysis of confocal microscopy images revealed that a combination of NO and acid stress, but not acid stress alone, stimulated ILI production (Fig. 3H-K). Together, the data highlights that ILI formation is a conserved consequence of hypoxia and NO stress, while acid and nitrogen deprivation induced ILI formation is not a shared characteristic of all mycobacteria.

***M. marinum* and Mtb can store neutral lipids in ILI or in cell membranes.** To more closely examine neutral lipid staining in *M. marinum*, we turned to super resolution structured illumination microscopy (SR-SIM) [185]. Bacteria were sampled at two time points for imaging via SR-SIM. SR-SIM images revealed neutral lipid rich ILI in cultures grown for six hours, while highlighting the absence of ILI in the older cultures (Fig. 4A-F). At 48 hours we observed a shift in neutral lipid localization from ILI in the cytosolic space to the bacterial surface, suggesting that TAGs or other neutral lipids are predominantly found in the mycobacterial membrane in late log phase bacteria (Fig. 4D-

F). Interestingly, BODIPY stained structures observed between some ILI at 6 hours are reminiscent of membrane bridges seen in eukaryotic cells between the endoplasmic reticulum and lipid bodies [186] (Fig. 4A arrows). 3D reconstruction modeling of the SR-SIM images demonstrate that at 6 hours the BODIPY stains contoured globular structures typical of lipid bodies, while at 48 hours the BODIPY stained the perimeter of the cytosolic tdTomato signal, indicating localization to the cell membrane (Fig. 4G-H + Supplemental video 2, 3).

We next sought to examine ILI formation in Mtb. It has been reported that lineage 2 (L2) strains form ILI in axenic culture more readily than do other lineages [131]. Moreover, L2 strains have been associated with increased TAG accumulation [185], [186]. We compared a set of Mtb strains from lineage 4 (L4) laboratory strains (H37Rv and Erdman), as well as a L2 strain Beijing 29and a lineage 1 (L1) clinical isolate TN1401420. Cultures were back diluted to an OD_{600} of 0.05 and were sampled at 24 hours (early log) and 120 hours (late log). When stained for neutral lipids, the L2 Mtb strain showed distinct puncta associated with ILI at 24 hours, while the L1 clinical isolate and laboratory strains H37Rv and Erdman lacked these structures (Fig. 5A-D, 5F). In the L2 strain ILI were depleted by 120 hours, similar to what we observed in *M. marinum* (Fig. 5E-F). Moreover, visualization and quantification of TAG content via TLC in the strains at 24 hours revealed that the L2 strain had elevated TAG levels compared to the other strains, allowing us to confirm a link between elevated TAGs and the ILI observed by microscopy in the L2 strain (Fig. 5G, 5H). Interestingly, despite the imaging assays showing a lack of distinct ILI in the Erdman and L1 strains, we see that these strains had a significant amount of TAGs relative to H37Rv. To investigate the subcellular localization of TAGs in these strains we imaged the bacteria using SR-SIM. H37Rv showed minimal neutral lipid staining while the Erdman and L1 strains had membrane associated or discrete, amorphous staining (Fig. 5I, 5J, 5L). The L2 strain exhibited BODIPY-stained puncta as expected (Fig. 5L). 3D reconstruction modeling of the images allowed us to better visualize the lipid localization. Through this modeling we can clearly see the spherical ILI present in the L2 strain as well as the membrane associated or discrete neutral lipid localization in the other strains (Fig. 5M-P, Supplemental video 4-7). This suggests that the L2 isolate is capable of shunting synthesized TAGs into ILI while the Erdman and L1 strains, which still accumulate quantifiable TAGs, are unable to do so.

RNA Seq reveals transcriptional differences between ILI-producing and ILI-deficient Mtb strains. We next used RNA Seq to identify transcriptional differences that might explain the observed differences in TAG abundance and ILI formation across the Mtb strains. We compared the transcriptional signatures of the strains after 24 hours of growth post dilution. PCA analysis revealed the distinct RNA landscape of the L2 strain from the other strains as well as the clustering of the L4 lab strains H37Rv and Erdman (Fig. 6A). Differential RNA expression of genes expressed in the ILI-producing L2 strain compared to the ILI-deficient H37Rv, Erdman, and L1 strains revealed several significantly differentially expressed genes (DEGs) (Fig. 6B). Of note, the L2 strain had a significantly upregulated DosR regulon, in line with what previous groups have reported [185], [186] (Fig. 6B, Table 1, Supplementary Data 1). Indeed, GO analysis of

genes upregulated in the ILI forming L2 strain compared to the other ILI deplete strains reveals significantly upregulated genes involved in response to hypoxia, oxygen levels, and stress (Table 1). The L2 strains grew similarly to the other strains, suggesting that despite the upregulated expression of stress response genes, the bacteria were not in hypoxic or stressed conditions (Fig. S4). KEGG analysis further supports these findings by clustering significantly upregulated DEGs into metabolic pathways, carbon metabolism, fatty acid metabolism, and two-component system associated pathways (Table 2). The top 20 significantly upregulated genes included several transmembrane-encoding proteins, including the membrane associated lipid transporter mycobacterial membrane protein large 4 (*mmpL4*) and its closely associated accessory protein mycobacterial membrane protein small 4 (*mmpS4*), which were not previously published to be associated with the DevR/DosR dormancy regulon [127] (Table 3). Not included in the top 20 but still significantly upregulated were the fatty acid biosynthesis associated genes *tgs1* and *tgs3* (Supplemental Data 1), which further corroborates the finding that the L2 strain had TAG rich ILI at this time point in axenic culture. Of note, a key gene involved in the Mtb NRP transcriptional landscape, isocitrate lyase *icl,* was significantly downregulated in the L2 strain. *Icl*, critical to the methylcitrate cycle and the glyoxylate shunt in Mtb, has been well characterized to be required for growth on fatty acids and survival in latent models of TB [55], [57], [58]. Furthermore, several lipases *lipC, lipF,* and *lipX* were also downregulated (Supplemental Data 1). The downregulation of these genes suggests that at 24 hours, the L2 strain forms ILIs but does not initiate the hydrolysis of TAGs or β-oxidation of fatty acids for growth.

Upregulated *dosR* is not required for ILI formation in Mtb. Given the differences in ILI signal between the L1 and L2 strains, we sought to investigate if ILI variance was an inter or intra lineage trait. We thus screened 60 clinical isolates comprised of L1, L2, and L4 strains to look for any correlates of ILI signal. To our surprise, we observed both inter and intra lineage variance in neutral lipid accumulation (Fig. 6C). Even among the L2 lineages, a lineage known to accumulate TAG and producing ILI, we identified low (TN044) and high (TN079, TN087, TN088) ILI producers (Fig. 6C, black and red arrows, respectively). We can thus deduce that ILI formation may not be a trait unique to L2 strains, but rather a shared albeit variable characteristic among recent clinical isolates. The DosR regulon has been implicated to be an upstream regulator of ILI formation and has been shown to be upregulated in L2 lineages. This led us to question if there was a link between *dosR* expression and ILI formation. We turned to qPCR to examine *dosR* expression of the previously mentioned low and high ILI producers. To our surprise, we saw no correlation between *dosR* expression and ILI formation (Fig. 6D). TN044, which exhibited quite low ILI signal, had *dosR* expression similar to the Beijing 29 and TN079 isolates. Even more surprising however was the muted expression of *dosR* in TN087 and TN088. These two isolates exhibited the highest ILI signal amongst our screened isolates yet had lower *dosR* expression than that of H37Rv. These data suggest that elevated *dosR* regulon expression is not required for ILI accumulation, separating ILI formation from a hypoxia driven dormancy regulon and hinting at another regulator or pathway distinct from dormancy regulon that drives lipid body formation.

Discussion

ILI have long been regarded as hallmarks of NRP [124], [125], [168]. The metabolic shift that accompanies the transition from active to dormant Mtb in hypoxia is accompanied by the accumulation of lipid bodies throughout the cellular space of the bacteria. Prior to this study, the consensus in the field has been that mycobacteria such as *M. smegmatis*, *M. abscessus*, or lab Mtb strains only accumulated TAG in the presence of hypoxia, acid stress, nutrient limitation, NO, or low nitrogen stress [76], [78], [129], [132]–[134], [165]–[167]. While only some of these conditions have been examined by microscopy for ILI formation, it nevertheless was widely accepted that ILI and a DosR mediated TAG accumulation are hallmarks of NRP in mycobacteria [76], [78], [124], [125]. Some works however have reported findings that challenge this belief. For example, transmission electron microscopy showed that some L1 and L2 strains, but not H37Rv, formed ILI in mid log phase without the need for external stressors [131]. Furthermore, radiolabeled fatty acid-based lipid analysis showed that L2 strains accumulated TAG [185]. These reports corroborate our findings that *M. marinum* as well as Mtb clinical isolates form ILI while actively replicating independent of environmental stressors. Moreover, we made the surprising observation that ILI are formed in early log phase and are depleted as the bacteria grow. The incorporation of free fatty acids into TAG is an energetically costly process—it is difficult to imagine the benefit of TAG synthesis when the fatty acids could directly be β-oxidized to fuel cellular growth. One possiblity is that ILI serve as a means of detoxifying cytotoxic free fatty acids. Eukaryotic lipid droplets are thought to prevent lipotoxicity by integrating free fatty acids into neutral lipids such as TAGs [84]. This belief is mirrored in mycobacteria where it is speculated that fatty acid metabolism counteracts the accumulation of cholesterol and methylcitrate cycle derived cytotoxic molecules by neutralizing and rerouting these molecules into TAGs [52]. Here, we observe the accumulation of ILI and TAG in mycobacteria upon fresh media replenishment at early log or exogenous fatty acid supplementation (Fig. 2). SR-SIM and 3D reconstructive modeling of *M. marinum* highlight the accumulation of TAG in spherical ILI at the early timepoints, yet these puncta disappear at later stages and are either less prevalent or localize to the membrane (Fig. 4). In line with our observations, previous work has suggested TAG accumulates in the mycomembrane as well as at the cytoplasmic membrane[80], [171]. The initial accumulation of TAG in ILI could be a means of protection against lipotoxic stress by the bacteria wherein superfluous free fatty acids that cannot be neutralized into TAGs to be compartmentalized in the lipid bilayer are instead sequestered into ILI. At later timepoints, when excess fatty acids have been depleted from the media, there is no longer a need for upregulated TAG synthesis, and thus basal TAG levels allow for neutral lipid distribution throughout the membrane. We thus speculate that ILI accumulation is a direct consequence of fatty acid availability. This idea is further supported by our replenishment assay (Fig. 2A-C) where cultures resuspended in fresh media formed ILI while those in the spent media did not. The uncoupling of ILI formation and growth phase shown in this assay suggests that ILI formation is merely a response to exogenous free fatty acid and not necessarily due to a specific growth phase.

There remains the outstanding question of what drives the differences in ILI formation between clinical isolates. Indeed, the previously mentioned studies observed ILI in

some, but not all, tested L1 and L2 strains [131]. This finding was somewhat contrary to what had been previously reported wherein TAG accumulation was found in only L2, and not L1 and L4, isolates [185]. The observed lack of TAG in L1 strains by the latter report is surprising, as our results show elevated TAG levels in an L1 strain compared to H37Rv as well as some quantifiable ILI accumulation in many L1 clinical isolates (Fig. 5G-H, Fig. 6C). The discrepancy between the findings could be explained by differences in culture conditions and captured time points. Nevertheless, the collective studies on the variance in ILI aggregation between lineages do raise the question of the genetic drivers of ILI formation. The DosR regulon regulates the transcription of many key genes in response to gradual oxygen deprivation and is thought to be the stress response pathway upstream of ILI formation [124]. Indeed, *tgs1*, the predominant triacylglycerol synthase, is one such gene whose induction is downstream of *dosR* [127]. In our study we make a surprising observation that decouples *dosR* expression from ILI formation and implicates the existence of a yet to be characterized ILI synthesis pathway. We observed that the ILI high TN087 and TN088 clinical isolates had significantly reduced *dosR* expression. In contrast, the ILI low strain TN044 had elevated *dosR* expression on par with the ILI high TN079 (Fig. 6D). Further work is being done to identify enriched SNPs associated with high ILI accumulation, as well as transcriptional profiling across a larger number of isolates to determine any genetic expression correlates to ILI level. It would be interesting to see if these investigations result in the identification of key genes directly involved in the ILI formation pathway. It is worth noting however that ILI formation in the absence of any facilitator proteins has been speculated. The composition of the lipid membrane has been theorized to be a driving force involved in the biogenesis of lipid bodies, with works on the ER membrane and in artificial lipid bodies demonstrating that dysregulated phospholipid composition and membrane surface tension alters lipid body aggregation [91]–[94], [187]. It would be exciting to see if any of the mycobacterial differentially expressed genes or enriched SNPs were involved in membrane composition homeostasis.

Our study also highlights that although we observed ILI formation in axenic culture absent of external stressors, we found that some conditions, such as hypoxia and NO stress, led to TAG accumulation as previously reported [78], [134]. However, we failed to see ILI in *M. marinum* cultured in nitrogen limited conditions (Fig. 3A-D). It is unclear how a low nitrogen/carbon ratio environment differentially affects *M. marinum*. Unlike *M. abscessus* or *M. smegmatis*, *M. marinum* has a wide range of hosts that can serve as a replicative niche for this environmental waterborne bacterium [139], [147]. The ability to infect freshwater and marine fish, amoeba, and humans necessitates flexible adaptation to diverse environments. It is plausible that the nitrogen/carbon ratios tested in this study, despite being harsh enough to stimulate ILI formation in *M. abscessus* and *M. smegmatis*, may not have been extreme enough for *M. marinum*. The effects of an altered nitrogen/carbon ratio have yet to be tested on lab and clinical Mtb strains—these findings may provide a hint about the differences between species' response to nitrogen deprivation. The discrepancy in response to stressors leads to speculation about the role of ILI. It has previously been thought that ILI are formed as a response to stress such as those found in the granuloma [76], [124]. Yet, as our findings show, *M. marinum* only forms ILI in some but not all previously identified stressors. Moreover, *M. marinum* and clinical Mtb isolates readily form ILI without these stressors (Fig. 1, Fig. 6C). It thus

proves difficult to ascertain if ILI have a role in response to or protection from stressors. Numerous studies have attempted to link ILI formation with response to stress. For example, *tgs1* has been shown to be one of the 48 genes in the hypoxia induced DosR regulon [127]. Furthermore, several reports have demonstrated the necessity of functional *tgs* and *mce1* expression *in vivo*, suggesting ILI are critical for sustained virulence in the host [71], [157], [188]. However, while these models result in ILI loss, they also lead to a dysregulated central metabolism. Metabolomics have delineated the incorporation of fatty acids into the central carbon metabolism [53], [189]. Furthermore, studies on *icl* knockout strains have found these mutants to be attenuated *in vivo*, highlighting the importance of fatty acid catabolism [55], [58], [190]. Mtb strains with disrupted *tgs* or *mce1* expression would impact fatty acid import and TAG accumulation, resulting in a severely imbalanced central carbon flux and cause possible misinterpretations of the role of ILI. While some evidence does suggest ILI can play a role beyond the compartmentalization of energy, it is currently impossible to decouple ILI from fatty acid metabolism. It would be interesting to probe the ILI formation pathway for proteins that mediate the construction of the physical ILI structure without a major disruption of TAG synthesis or fatty acid availability.

This study also captured ILI dynamics in a previously unstudied infectious setting. Although prior work had characterized ILI in the context of *D. discoideum* infection, the culture conditions of *D. discoideum* require the bacteria to be subjected to suboptimal temperatures. We wondered if the kinetics of ILI generation and degradation seen in this host-pathogen model were representative of clinical cases, where *M. marinum* infects patient extremities at a temperature closer to its' optimal replicative climate of 30-33°C. Interestingly, we found that BMDM infecting *M. marinum* accumulated ILI throughout the infection, unlike the accumulation and subsequent depletion of ILIs in axenic culture (Fig. 1). These ILI dynamics of ILIs in macrophage infections mirror that of *M. marinum* in *D. discodeum*, suggesting the cooler infectious climates do not seem to strongly impact ILI accumulation in *M. marinum* [147]. We saw that neither the ESX-1 mutant nor *mce1 M. marinum* mutants were able to accumulate ILI to the same degree as the WT strain. Of note, although the ESX-1 and *mce1* mutants exhibited ILI formation deficiencies, they were still able to form quantifiable amounts of ILI. Mycobacteria in the absence of LCFA are able to biosynthesize *de novo* fatty acids through *fas*, which encodes a fatty acid synthase. It is likely that despite a nutrient limited environment caused by the ESX-1 and *mce1* mutants, mutant *M. marinum* biosynthesizes free fatty acids to incorporate into TAG.

Many facets of ILI in mycobacteria remain unexplored: the specific transcriptomic and proteinaceous drivers of ILI formation, the means of nutrient acquisition by the bacteria in host cells, and the role of ILI in pathogenesis are all critical components of ILI biology that require further study. Here, we highlight that *M. marinum*, unique to other NTM, forms ILI while replicating in axenic culture. This trait is shared across L1, L2, and L4 lineages and not among lab strains of Mtb, demonstrating the importance and relevancy of using *M. marinum* as a proxy to study ILI in the clinical context. Our RNASeq results identified many potential targets for future investigation of ILI associated genes; further characterization these genes as well as examination of the differences in the membrane mosaic of mycobacteria could provide insight into the molecular machinery that dictates

ILI formation. Finally, an examination of *dosR* expression and ILI accumulation highlighted a remarkable finding that ILI formation is independent of *dosR* expression. Together, our findings reveal that neither a non-replicating state nor an upregulated DosR regulon are required for ILI formation in *M. marinum* and clinical Mtb isolates. Continued characterization of this finding as well as other aspects of ILI formation are critical to understanding the Mtb dormancy state and will identify promising therapeutic targets against LTBI infection and the global TB pandemic.

Acknowledgements

The authors thank David Russell for the gift of the SSB-GFP plasmid; Midori Kato-Maeda for the gift of the L1 strain; William Jacobs for the gift of the L2 strain Beijing 29; Mary West at the UC Berkeley QB3 facility for assistance with confocal imaging; Azenta Life Sciences for RNA Sequencing and Analysis. We thank the members of the Stanley, Cox and Vance labs for helpful discussions, and Heran Darwin and Daisy Ji for reading a draft version of this manuscript. This work was supported by NIH grant AI113270 to SAS. DMF was supported in part by a Public Health Service Institutional Research Training Award NIH T32 GM007232.

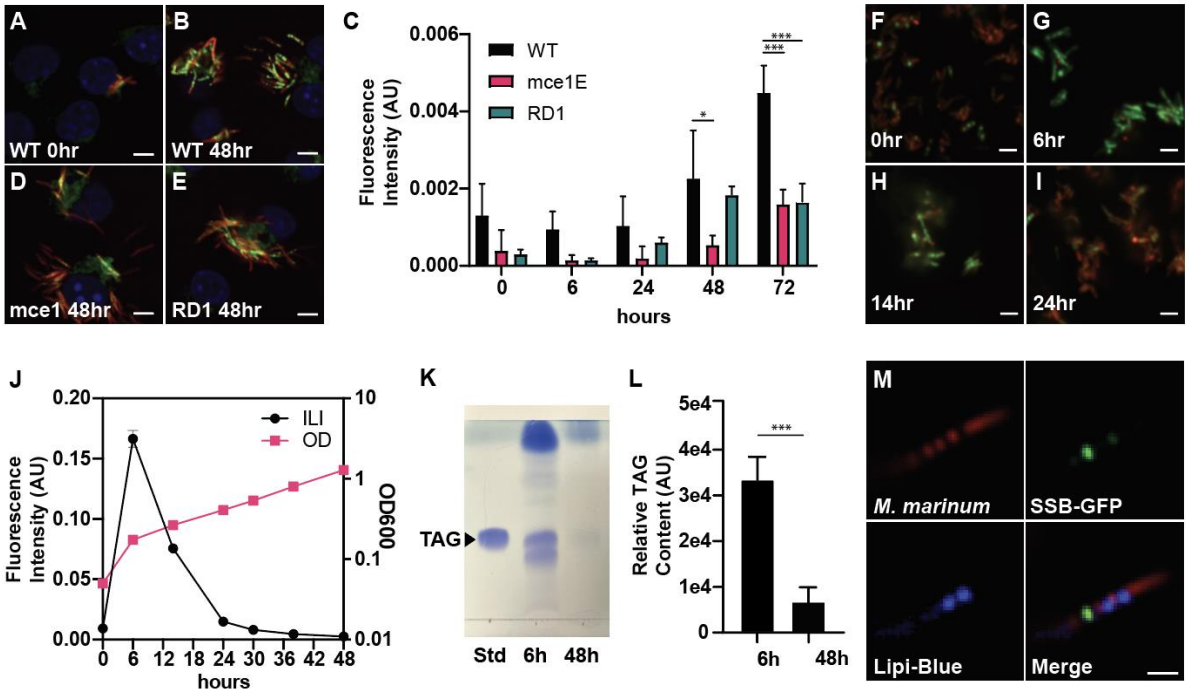

Figure 1. *M. marinum* forms ILIs while replicating in axenic culture. A-E. Confocal images of BMDM (A) immediately after infection by mCherry fluorescent WT *M. marinum* or 48 hours post infection by mCherry fluorescent (B) WT *M. marinum*, (D) *mce1* mutant *M. marinum*, or (E) *RD1* mutant *M. marinum.* Samples were stained for neutral lipids with BODIPY 493/503. Infections were at MOI=1. Scale bars represent 5 µm. (C) The integrated BODIPY 493/503 signal per bacteria was calculated with CellProfiler. Data are means ±SD (n=4). Fluorescence intensities were compared using a Student's t-test *p<0.05, ***p<0.001. **F-J.** Mcherry fluorescent WT *M. marinum* was cultured in $7H9^{ADS}$ and sampled at (F) 0 hours, (G) 6 hours, (H) 14 hours, and (I) 24 hours. (J) Samples collected at indicated timepoints were sampled for OD_{600} and stained for neutral lipids with BODIPY 493/503. Scale bars represent 5 µm. The integrated BODIPY 493/503 signal per bacteria was calculated with CellProfiler. Data are means ±SD (N=3). **K-L.** WT *M. marinum* was cultured in $7H9^{ADS}$ for 6 hours and 48 hours. Samples were visualized by (K) TLC and (L) analyzed for relative TAG abundance. Data are means ±SD (N=2). TAG band intensities were compared using a Student's t-test ***p<0.001. **M.** SSB-GFP expressing mCherry fluorescent WT *M. marinum* was cultured for 6 hours and stained for neutral lipids with Lipi-Blue. Scale bar represents 2 µm.

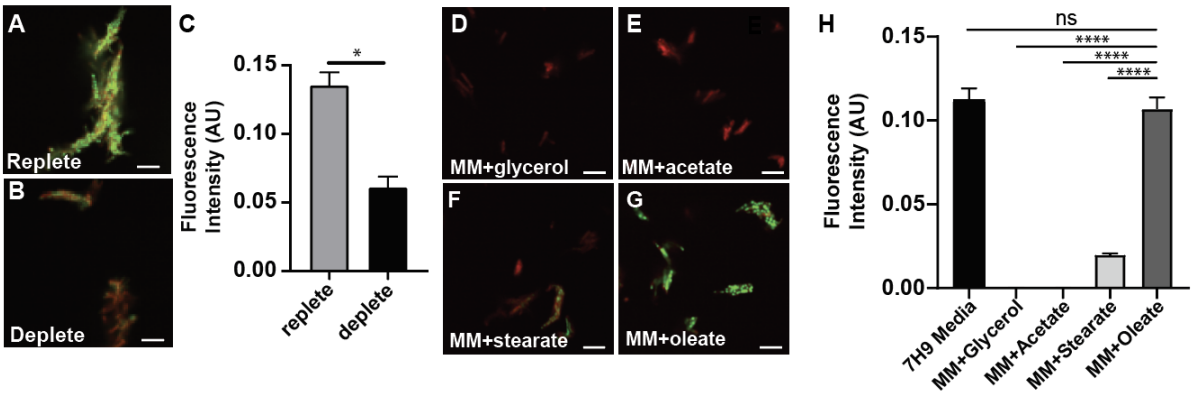

Figure 2. *M. marinum* formation of ILI in axenic culture requires exogenous lipids. **A-C.** mCherry fluorescent WT *M. marinum* was cultured for 6 hours and resuspended in (A) fresh, nutrient replete media or (B) the same, nutrient deplete media. Samples were collected 18 hours post resuspension and stained for neutral lipids with BODIPY 493/503. Scale bars represent 5 µm. (C) The integrated BODIPY 493/503 signal per bacteria was calculated with CellProfiler. Data are means ± SD (N=2). **D-I.** Fluorescence intensity was compared using a Student's t-test *p<0.05. mCherry fluorescent WT *M. marinum* as cultured in (D) 7H9^{ADS} or Minimal Media supplemented with (E) glycerol, (F) acetate, (G) stearate, or (H) oleate and stained for neutral lipids with BODIPY 493/503. Scale bars represent 5 µm. (I) Integrated BODIPY 493/503 per bacteria was quantified with CellProfiler. Data are means ±SD (n=3). Fluorescence intensity was compared using a Student's t-test ****p<0.0001.

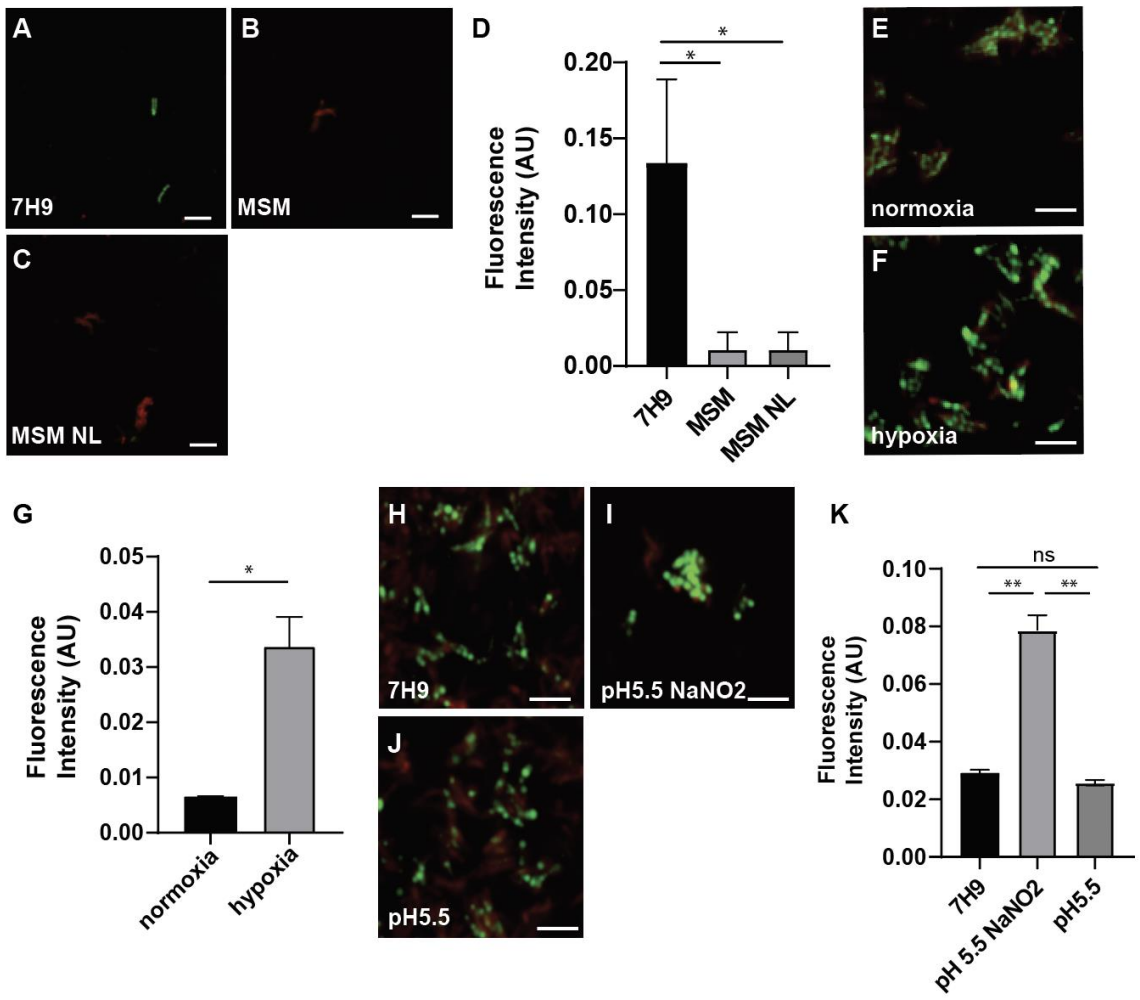

Figure 3. Characterization of environmental factors contributing to *M. marinum* ILI formation. **A-D.** mCherry fluorescent WT *M. marinum* strain was cultured in (A) 7H9^{ADS}, (B) MSM, or (C) MSM NL media and stained with BODIPY 493/503. Scale bars represent 5 µm. (D) Integrated BODIPY 493/503 signal per bacteria was quantified with CellProfiler. Data represent means ±SD (N=3). Fluorescence intensity was compared using a Student's t-test *p<0.05. **E-G.** mCherry fluorescent WT *M. marinum* strains were cultured in 7H9^{ADS} (E) in shaking flasks or (F) in airtight sealed inkwells. Samples were collected after (E) 6 hours or (F) hypoxic conditions were reached as indicated by methylene blue and stained with BODIPY 493/503. Scale bars represent 5 µm. (G) Integrated BODIPY 493/503 signal per bacteria was quantified with CellProfiler. Data represent means ±SD (N=2). Fluorescence intensity was compared using a Student's t-test *p<0.05. **H-K.** mCherry fluorescent WT *M. marinum* strains were cultured in (H) 7H9^{ADS}, (I) 7H9^{ADS} acidified to pH 5.5 and supplemented with 1.5mM $NaNO_2$, or (J) 7H9^{ADS} acidified to pH 5.5 and stained with BODIPY 493/503. Scale bars represent 5 µm. (K) Integrated BODIPY 493/503 signal per bacteria was quantified with CellProfiler. Data represent means ±SD (N=2). Fluorescence intensity was compared using a Student's t-test **p<0.01.

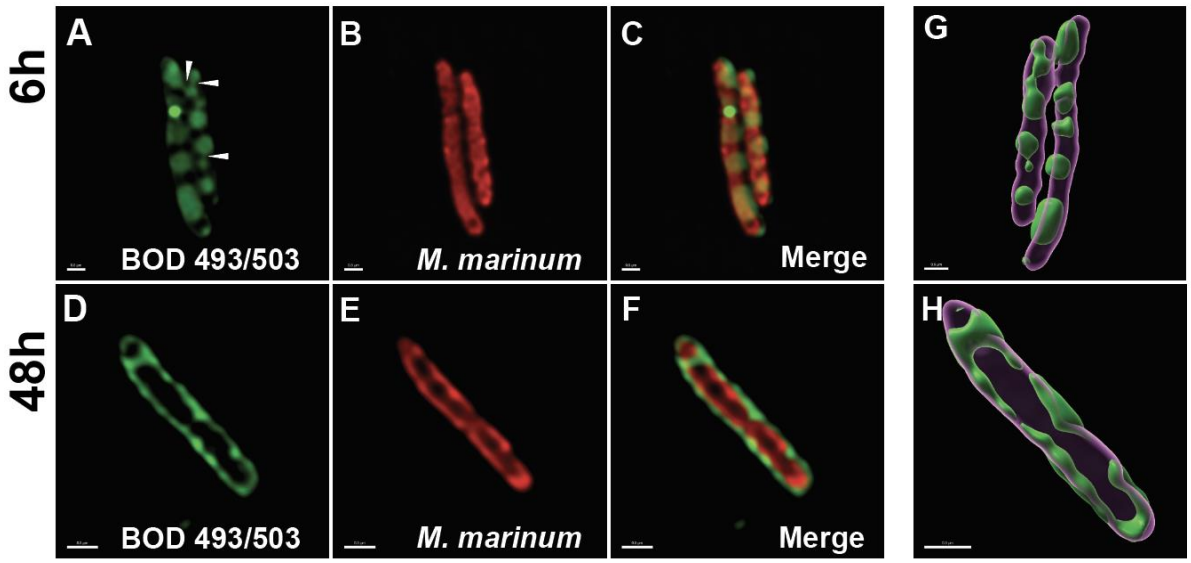

Figure 4. *M. marinum* can store neutral lipids in ILI or in cell membranes. A-F. mCherry fluorescent WT *M. marinum* strains were cultured in 7H9^{ADS} for (A-C) 6 hours or (D-F) 48 hours stained with BODIPY 493/503 and imaged via SR-SIM. White arrows in (A) indicate membrane bridge-like structures. Scale bars represent 0.5 µm. **G-H.** SR-SIM images of mCherry fluorescent WT *M. marinum* strains cultured for (G) 6 hours or (H) 48 hours were 3D modeled using Imaris. Scale bars represent 0.5 µm.

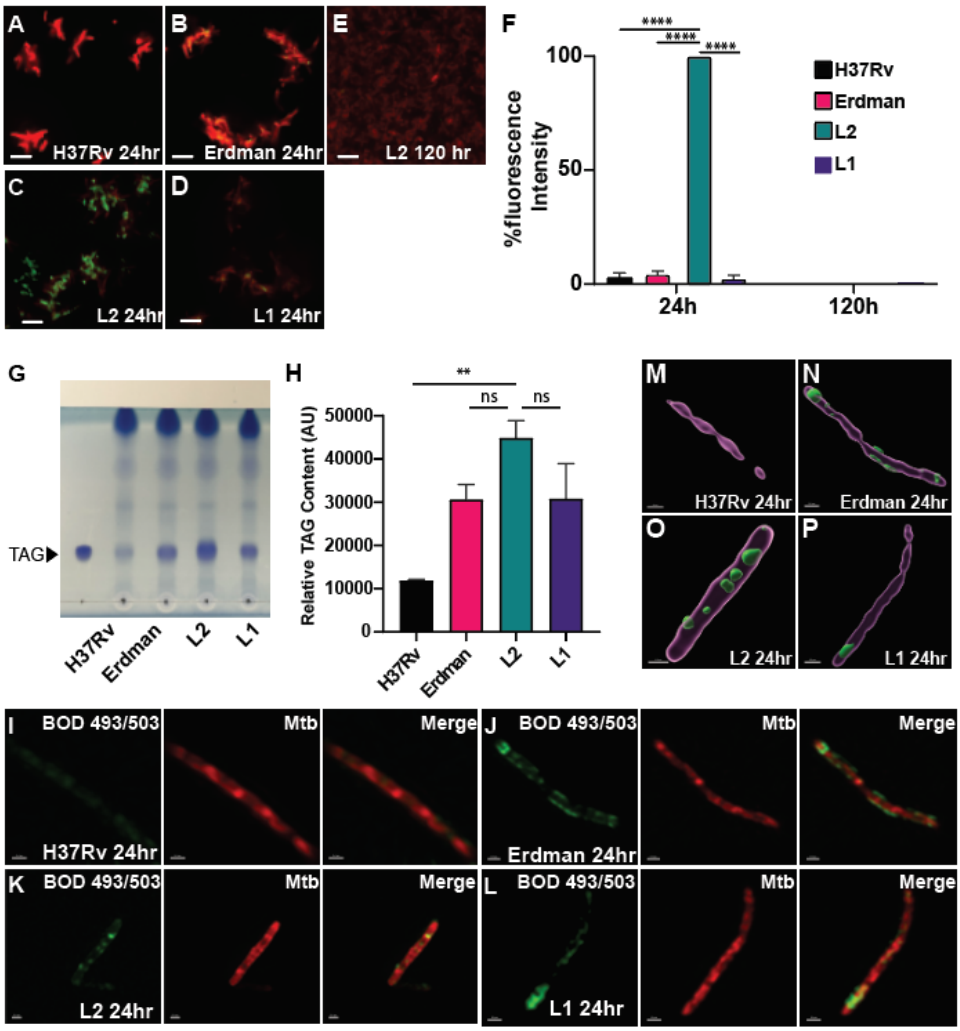

Figure 5. Mtb can store neutral lipids in ILI or in cell membranes. A-F. Tdtomato fluorescent (A) H37Rv, (B) Erdman, (C) L2, and (D) L1 strains were cultured in 7H9^{OADC} for 24 hours or (E) 120 hours and stained with BODIPY 493/503. Scale bars represent 5 µm. (F) Integrated BODIPY 493/503 signal per bacteria was quantified with CellProfiler. Data represent means ±SD (N=3). Fluorescence intensity was compared using a Student's t-test ****p<0.0001. **G-H.** H37Rv, Erdman, L2, and L1 strains were cultured for 24 hours and sampled for lipid analysis. Samples were visualized by (G) TLC and (H) analyzed for relative TAG abundance. Data are means ±SD (N=3). TAG band intensities were compared using a Student's t-test **p<0.01. **I-L.** Tdtomato fluorescent (I) H37Rv, (J) Erdman, (K) L2, and (L) L1 strains were cultured for 24 hours, stained with BODIPY 493/503, and imaged via SR-SIM. Scale bars in (I) represent 0.4 µm and (J-L) 0.5 µm. **M-P.** SR-SIM images of Tdtomato fluorescent (M) H37Rv, (N) Erdman, (O) L2, and (P) L1 strains were 3D modeled using Imaris. Scale bars represent 0.5 µm.

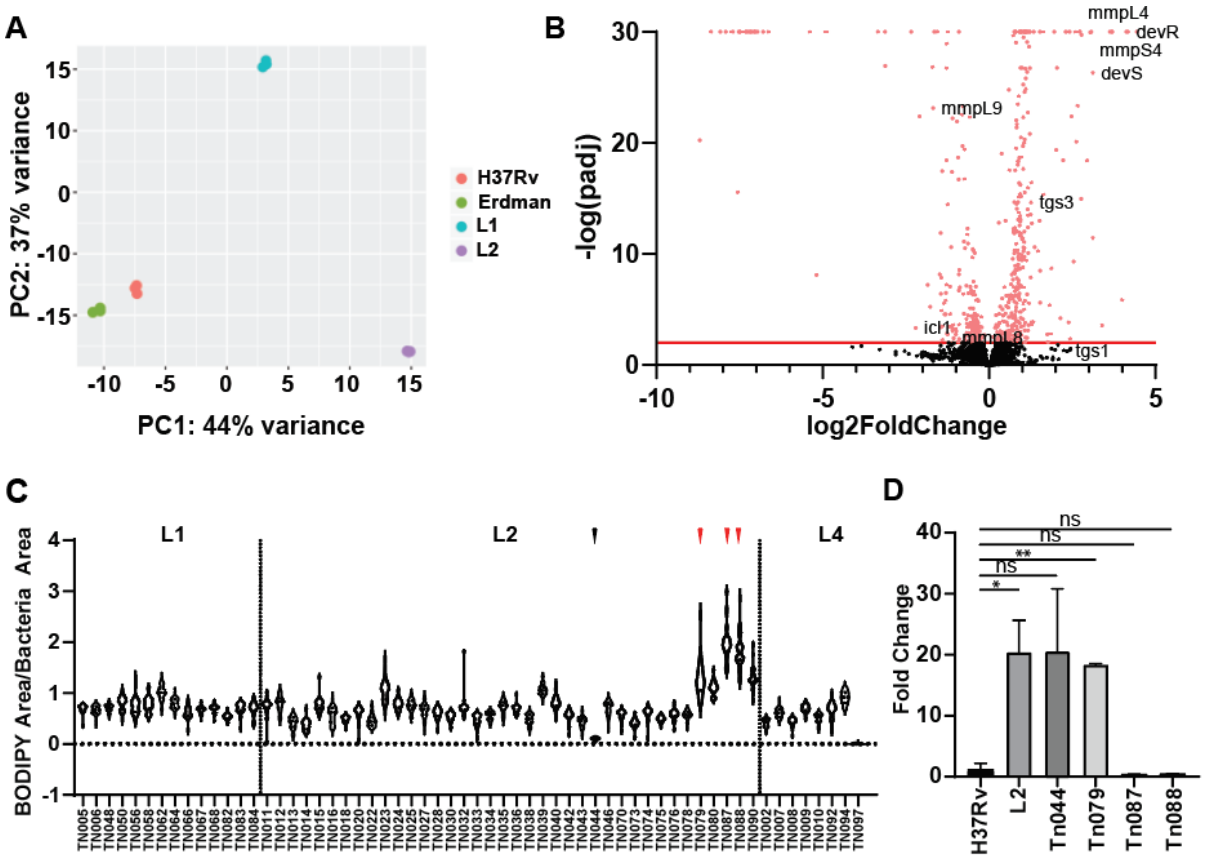

Figure 6. Upregulated *dosR* is not required for ILI formation in Mtb. A. H37Rv, Erdman, L2, and L1 strains were cultured for 24 hours and sampled RNASeq analysis. PCA analysis of the RNASeq is reflective of three biological replicates. **B.** Volcano plot of RNASeq analysis. The red line indicates padj (p value) = 0.05. Analysis was performed from three biological replicates. **C.** Clinical isolates were cultured for 24 hours and screened for ILI formation via BODIPY 493/503 staining. Violin plot of the integrated BODIPY 493/503 signal per bacteria is reflective of three technical replicates. Dotted lines indicate separation between the lineages. The black arrow indicates ILI low isolate TN044. Red arrows indicate ILI high isolates TN079, TN087, and TN088. **D.** Lab and clinical isolates were cultured for 24 hours and sampled for RT-qPCR analysis of *dosR* expression. Quantification was performed in reference to 16S and then normalized to H37Rv levels. Data are means ±SD (N=3). Fold change was compared using Student's t-test *p<0.05, **p<0.01.

GO Name	GO ID	P-value
GO:0009628	response to abiotic stimulus	1.78E-04
GO:0006950	response to stress	3.91E-04
GO:0001666	response to hypoxia	4.18E-04
GO:0036293	response to decreased oxygen levels	5.70E-04
GO:0070482	response to oxygen levels	6.94E-04
GO:0000103	sulfate assimilation	1.63E-03
GO:0010134	sulfate assimilation via adenylyl sulfate reduction	4.57E-03
GO:0010438	cellular response to sulfur starvation	4.57E-03
GO:0031667	response to nutrient levels	7.42E-03
GO:0070814	hydrogen sulfide biosynthetic process	7.48E-03
GO:0070813	hydrogen sulfide metabolic process	7.48E-03
GO:0019419	sulfate reduction	7.48E-03
GO:0034605	cellular response to heat	7.48E-03
GO:0016043	cellular component organization	9.64E-03
GO:0007154	cell communication	1.18E-02
GO:0071840	cellular component organization or biogenesis	1.39E-02
GO:0009408	response to heat	1.53E-02
GO:0009267	cellular response to starvation	1.77E-02
GO:0031669	cellular response to nutrient levels	1.77E-02
GO:0009991	response to extracellular stimulus	2.00E-02
GO:0000160	phosphorelay signal transduction system	2.13E-02
GO:0042594	response to starvation	2.13E-02
GO:0071704	organic substance metabolic process	2.37E-02
GO:0050896	response to stimulus	2.41E-02
GO:0009266	response to temperature stimulus	2.57E-02
GO:0006979	response to oxidative stress	2.74E-02
GO:0043412	macromolecule modification	2.94E-02
GO:1901658	glycosyl compound catabolic process	3.07E-02
GO:0022611	dormancy process	3.07E-02
GO:0006400	tRNA modification	3.21E-02
GO:0032502	developmental process	3.68E-02
GO:0044238	primary metabolic process	4.33E-02
GO:0071496	cellular response to external stimulus	4.53E-02
GO:0031668	cellular response to extracellular stimulus	4.53E-02
GO:0032259	methylation	4.85E-02
GO:0016310	phosphorylation	4.85E-02

Table 1. GO analysis of significantly upregulated DEGs in the L2 strain compared to H37Rv, Erdman, and L1 strains.

KEGG ID	KEGG Pathway
mtu01100	Metabolic pathways - Mycobacterium tuberculosis H37Rv (12)
mtu01110	Biosynthesis of secondary metabolites - Mycobacterium tuberculosis H37Rv (5)
mtu00230	Purine metabolism - Mycobacterium tuberculosis H37Rv (4)
mtu01120	Microbial metabolism in diverse environments - Mycobacterium tuberculosis H37Rv (4)
mtu02020	Two-component system - Mycobacterium tuberculosis H37Rv (3)
mtu00920	Sulfur metabolism - Mycobacterium tuberculosis H37Rv (3)
mtu01232	Nucleotide metabolism - Mycobacterium tuberculosis H37Rv (3)
mtu00910	Nitrogen metabolism - Mycobacterium tuberculosis H37Rv (2)
mtu00450	Selenocompound metabolism - Mycobacterium tuberculosis H37Rv (2)
mtu00261	Monobactam biosynthesis - Mycobacterium tuberculosis H37Rv (2)
mtu00561	Glycerolipid metabolism - Mycobacterium tuberculosis H37Rv (1)
mtu03018	RNA degradation - Mycobacterium tuberculosis H37Rv (1)
mtu00052	Galactose metabolism - Mycobacterium tuberculosis H37Rv (1)
mtu00521	Streptomycin biosynthesis - Mycobacterium tuberculosis H37Rv (1)
mtu00680	Methane metabolism - Mycobacterium tuberculosis H37Rv (1)
mtu00983	Drug metabolism - other enzymes - Mycobacterium tuberculosis H37Rv (1)
mtu00500	Starch and sucrose metabolism - Mycobacterium tuberculosis H37Rv (1)
mtu01200	Carbon metabolism - Mycobacterium tuberculosis H37Rv (1)
mtu01502	Vancomycin resistance - Mycobacterium tuberculosis H37Rv (1)
mtu00470	D-Amino acid metabolism - Mycobacterium tuberculosis H37Rv (1)
mtu00520	Amino sugar and nucleotide sugar metabolism - Mycobacterium tuberculosis H37Rv (1)
mtu00240	Pyrimidine metabolism - Mycobacterium tuberculosis H37Rv (1)
mtu00061	Fatty acid biosynthesis - Mycobacterium tuberculosis H37Rv (1)
mtu01212	Fatty acid metabolism - Mycobacterium tuberculosis H37Rv (1)
mtu01250	Biosynthesis of nucleotide sugars - Mycobacterium tuberculosis H37Rv (1)
mtu01240	Biosynthesis of cofactors - Mycobacterium tuberculosis H37Rv (1)
mtu00010	Glycolysis / Gluconeogenesis - Mycobacterium tuberculosis H37Rv (1)
mtu00190	Oxidative phosphorylation - Mycobacterium tuberculosis H37Rv (1)

Table 2. KEGG analysis of significantly upregulated DEGs in the L2 strain compared to H37Rv, Erdman, and L1 strains.

Gen ID	Gene Description	padj
Rv0450c	mmpL4	7.78E-294
Rv3182	Conserved hypothetical protein	1.60E-261
Rv0451c	mmpS4	1.20E-233
Rv3309c	upp	2.30E-168
Rv3366	spoU	1.58E-107
Rv0449c	Conserved hypothetical protein	1.96E-95
Rv3273	Probable transmembrane carbonic anhydrase (carbonate dehydratase)	1.33E-84
Rv3427c	Possible transposase	5.08E-81
Rv3133c	devR	7.07E-78
Rv3367	PE_PGRS51	9.49E-76
Rv3238c	Probable conserved integral membrane protein	5.25E-67
Rv3221a	rshA	7.34E-64
Rv3393	iunH	6.15E-60
Rv3396c	guaA	1.97E-56
Rv2660c	Hypothetical protein	5.95E-56
Rv3239c	Probable conserved transmembrane transport protein	8.73E-50
Rv2662	Hypothetical protein	2.32E-49
Rv3179	Conserved protein	1.56E-46
Rv2107	PE22	4.40E-46
Rv3081	Conserved hypothetical protein	1.57E-44

Table 3. Top 20 significantly upregulated DEGs in the L2 strain compared to H37Rv, Erdman, and L1 strains.

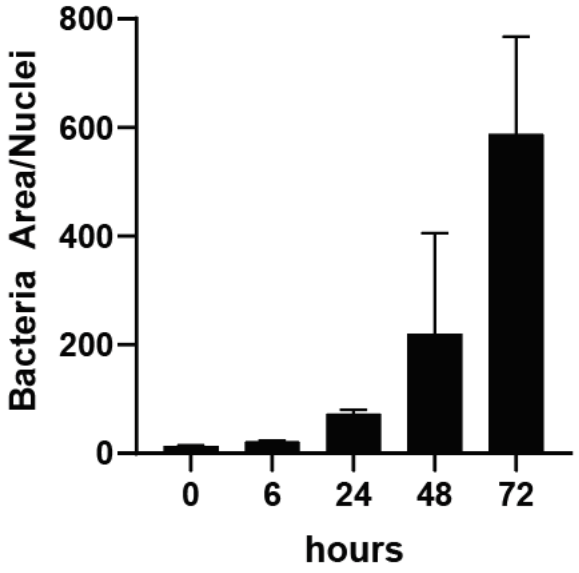

Figure S1. Quantified WT *M. marinum* growth in BMDM. BMDM were infected with mCherry fluorescent WT *M. marinum* at MOI=1. Samples were taken at indicated timepoints and stained with DAPI. Mcherry signal per macrophage nucleus was quantified using CellProfiler. Data represent means ±SD (n=4).

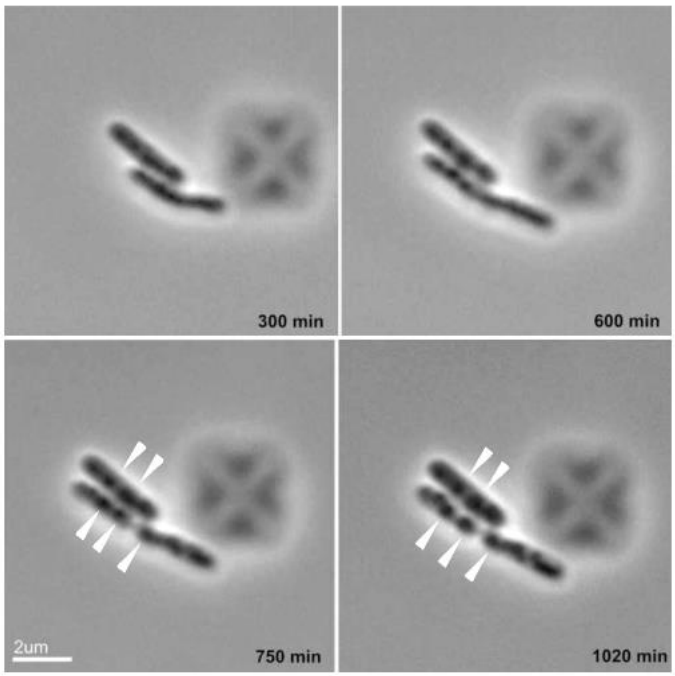

Figure S2. Live imaging of *M. marinum* cultured in CellASIC flow chamber. Mcherry fluorescent WT *M. marinum* was cultured in a CellASIC flow chamber with 7H9^{ADS} media flowing through the system. Phase contrast images were taken every 15 minutes over the course of 17 hours. Images capture a replicating *M. marinum* bacterium with ILI (white arrows). Scale bar represents 2 µm.

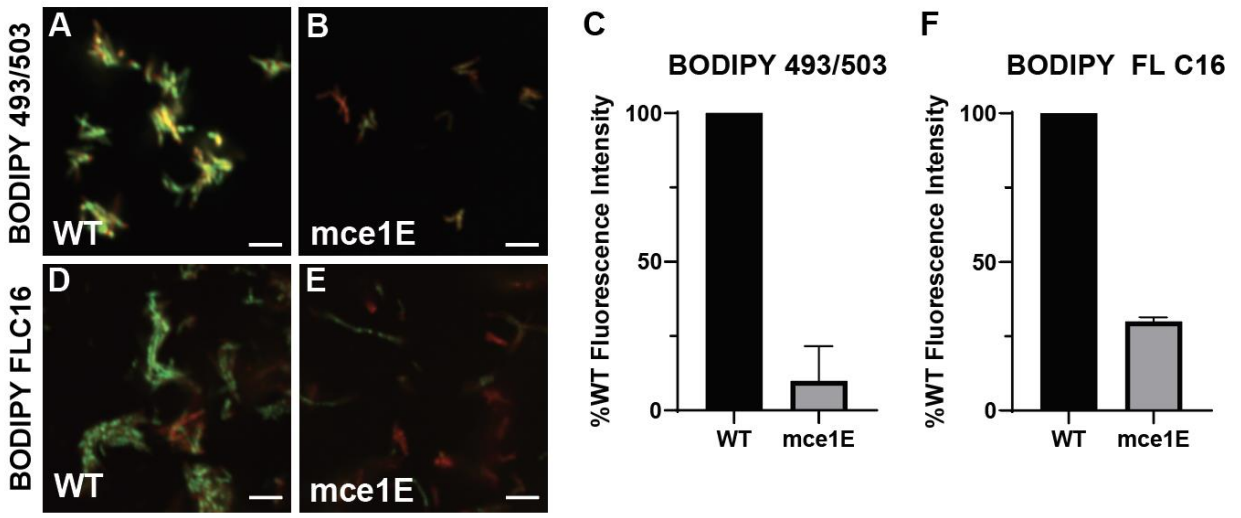

Figure S3. *Mce1 M. marinum* mutants are deficient for ILI formation and fatty acid import. A-C. Mcherry fluorescent (A) WT *M. marinum* and (B) *mce1* mutant *M. marinum* were cultured for 6 hours in $7H9^{ADS}$ and stained with BODIPY 493/503. (C) Integrated BODIPY 493/503 signal per bacteria was quantified with CellProfiler and normalized to WT *M. marinum* signal. Data represent means ±SD (N=3). **D-F.** Mcherry fluorescent (D) WT *M. marinum* and (E) *mce1* mutant *M. marinum* were cultured for 48 hours in $7H9^{ADS}$ and pulsed with 2.5 µM BODIPY FL C_{16} for 4 hours. Data represent means ±SD (N=2).

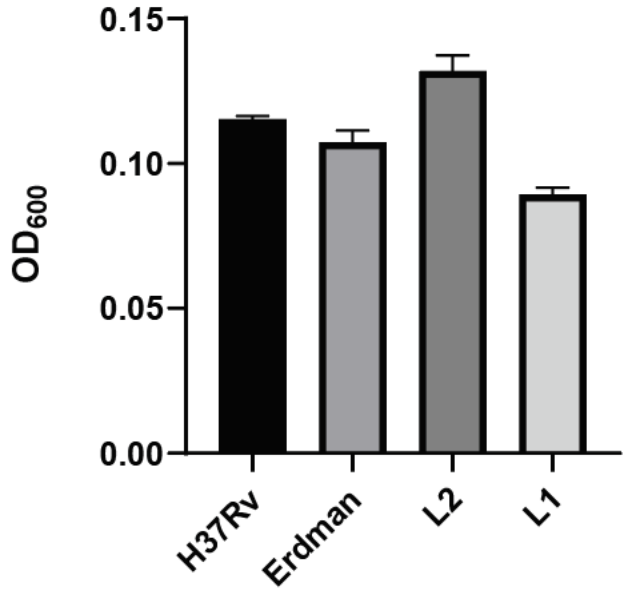

Figure S4. OD_{600} of Mtb cultures at time of sampling. H37Rv, Erdman, L2, and L1 strains were cultured in $7H9^{OADC}$ and back diluted to OD_{600} 0.05. Cultures were sampled for OD_{600} readings 24 hours post inoculation. Data represent means $\pm$SD (N=3).

Chapter Three: Identification of novel genes involved in intracellular lipid inclusion formation in *Mycobacterium marinum*

Fines DM, Knight M, Dinshaw KM, Stanley SA

Introduction

The unique ability of *Mycobacterium tuberculosis* (Mtb) to shield itself against the onslaught of immunological warfare by host cells is nothing short of remarkable. From withstanding the acidic phagosome and deadly reactive oxygen species in macrophages to holding out against a siege of immune cells cutting off the supply of oxygen in the hypoxic structure known as the granuloma, Mtb has used its defense mechanisms to coexist with its human host for thousands of years [191], [192]. Indeed, estimates place the worldwide prevalence of latent tuberculosis infection (LTBI) at 25-30%, highlighting Mtb's superb resilience [30], [31]. Yet despite such a high prevalence, there is still much that remains unknown about LTBI. Work has been done to show that bacteria in LTBI cases are in states of non-replicating persistence (NRP). NRP is commonly defined by a transcriptomic and metabolic reprogramming of an active bacteria into a dormant one, often induced as a result of a transition from an aerobic environment, such as the alveolar architecture in our lungs, to an oxygen deplete environment, such as the granuloma. This dormant, NRP state is associated with increased resistance to many first line antitubercular drugs as well as a shift towards a lipid loaded bacterial cell. Indeed, lipid bodies in mycobacterium have long been regarded as a hallmark of NRP and a sure sign of a successful transition from an active to a dormant state [78].

For many years, cellular lipid bodies have been perceived simply as containers of fatty acids. These structures can be hydrolyzed and subsequently β-oxidized to fuel cellular metabolism. Monumental advancement in the eukaryotic field has since redefined these structures with roles far beyond a repository of molecular fuel and solidified them as bona fide organelles involved in protection against ER and lipotoxic stress as well as a mechanism for protein scaffolding. Significant work has been done to uncover seipins, perilipins, and fat storage inducing transmembrane (FIT) proteins as key proteins involved in the formation of lipid droplets [190]. While widely studied in the eukaryotic fields, their presence and importance has only recently gained traction in the prokaryotic field, perhaps due to their relative scarcity in prokaryotic species. Intracellular lipid inclusions (ILI), a term reserved for lipid bodies found in prokaryotic cells, are structurally defined by a phospholipid monolayer encapsulating the batteries of the cell: neutral lipids. While the specific species of neutral lipid can vary from organism to organism, in the genus *Mycobacterium* triacylglycerol (TAG) constitutes the neutral lipid rich core [76], [191]. Despite their discovery dating back to the 1940s and their correlation with the difficult to treat state of NRP, mycobacterial ILI remain poorly understood [192]. Studies on laboratory strains of Mtb have guided the field to uncover some key genes correlated to the presence of ILI, such as the hypoxia response regulator *DevR/DosR*, the triacylglycerol synthase *tgs1*, and the fatty acid import associated genes *mce1* and *LucA* [71], [76], [127]. Proteomics have been conducted on

Mycobacterium smegmatis to identify predicted ILI associated proteins, revealing a sizable repository of uncharacterized proteins, though their co-localization to ILI has yet to be definitively demonstrated [194], [195]. Other genes have been implicated in ILI formation, though work remains to be done to fully characterize their role. These genes include the heparin-binding hemagglutinin adhesin *hbha*, which when knocked out in nitric oxide (NO) stressed *Mycobacterium bovis* BCG led to ILI loss, and mycobacterial perilipin-1 *mper1/ppe15,* which when knocked out in acid, nutrient, and hypoxic stressed Mtb led to ILI loss [134], [135]. The product of *mper1* MPER1 was interestingly discovered due to its, albeit weak, sequence similarity to the mammalian perilipin proteins. Perilipins are among the few eukaryotic proteins, alongside seipins and fat storage inducing transmembrane (FIT) proteins shown to impact ILI formation [93], [98].

The scarcity of known proteins involved in ILI formation in mycobacteria led us to screen for genes along the ILI genesis pathway in *Mycobacterium marinum*, a close relative of Mtb [194]. Here, we use a fluorescence microscopy based high throughput screen on a transposon mutagenesis library in *M. marinum* to identify over 100 mutants deficient in ILI. We go on to triage these mutants by filtering them through a secondary screen in macrophages to identify top hits in the context of infection. We identify 4 highly impacted *M. marinum* strains and begin to characterize how the mutated genes are involved in ILI formation.

Materials and Methods

Bacteria and media
M. marinum strain M was grown in 7H9 media (Middlebrook 7H9 Broth supplemented with 0.2% Tween-80, 0.2% Glycerol, 0.5% BSA, 0.2% dextrose, 0.085% NaCl). For carbon starvation conditions *M. marinum* was cultured in minimal media (0.08% NaCl, 0.04% L-asparagine, 3.5% Na_2HPO_4, 1.48% KH_2PO_4, 0.04% 5M Ammonium Iron Citrate, 0.02% 1M $MgSO_4 7H_2O$, 0.05% 1mg/mL $CaCl_2$, 0.01% 0.1mg/mL $ZnSO_4$, 0.2% EtOH, 0.2% Tyloxapol). Cultures were shaken at 100 rpm at 32°C.

Transposon screen
M. marinum transposon mutagenesis library was generously provided by the Welch lab at UC Berkeley. 5 µL was taken from the library to inoculate 95 µL of 7H9 media in 96 well microplates. After a 48 hours incubation at 32°C, 100 µL of 5 µM BODIPY FL C_{16} in 7H9 was added onto the wells. Samples incubated with the BODIPY FL C_{16} for 4 hours and subsequently pelleted at 2850 *g* for 5 minutes before being washed 1x with PBS, fixed in 10% formalin, washed 2x with PBS, and transferred to Phenoplate 96 well plates. All plates were imaged on an Opera Phenix High Content Screening System. Resulting images were analyzed using the CellProfiler image analysis software. A composite z-score was calculated for each mutant based on two replicates.

DNA isolation
10 mL of *M. marinum* was cultured in 7H9 Media to OD_{600} 0.4-0.8. Culture was pelleted 2850 *g* for 5 minutes and resuspended in 500 µL RB Buffer (25 mM Tris-HCl pH 7.9, 10 mM EDTA, and 50 mM glucose) with 50 µL 10 mg/mL lysozyme. Following an overnight incubation at 32°C, 100 µL of 10% sodium dodecyl sulfate and 50 µL 10 mg/mL proteinase K was added prior to an incubation at 55°C for 30 minutes. 200 µL of 5M sodium chloride was then added followed by 150 µL Cetrimide Saline Solution (10 g hexadecyltrimethylammonium bromide, 4.1 g sodium chloride in 90 mL water). Samples were incubated at 65°C for 10 minutes. An equal volume of chloroform:isoamyl alcohol (24:1) was added, after which samples were centrifuged for 10 minutes at 10000 *g*. The aqueous layer was transferred to a fresh tube and 0.7x volume of isopropanol was added. Samples were centrifuged again for 10 minutes at 10000 *g*. The supernatant from each sample was decanted and the remaining pellets were washed with 70% alcohol and air dried before a final resuspension in water.

Sequencing of transposon insertion site
M. marinum transposon mutagenesis mutant DNA was sequenced via sequential arbitrary PCRs. The initial PCR was performed using primers 5'- GGC CAC GCG TCG ACT AGT ACN NNN NNN NNN GAG GG -3' and 5'-CGC TTC CTC GTG CTT TAC GGT ATC G-3', followed by a second PCR using primers 5'-GCC TTC TTG ACG AGT TCT TCT GAG-3' and 5'-GGC CAC GCG TCG ACT AGT AC-3'.

Complementation of M. marinum mutants
WT *M. marinum* M (NCBI Reference Sequence: NC_010612.1) DNA was isolated and select regions were amplified for insertion into pMV306zeo under the GroEL2 promoter

for constitutive expression of the gene. Amplified regions for complementation of *M. marinum* mutants: *MMAR_0250* (nts 282337-283161), *MMAR_2242* (nts 2695706-269864), *MMAR_3091* (nts 3742222-3744051), *MMAR_4531* (nts 5559038-5560750). Electrocompetent *M. marinum* were transfected and plated on Middlebrook 7H10 Agar plates supplemented with 0.5% BSA, 0.2% dextrose, 0.085% NaCl, 0.05% Tween-80, and 50 µg/mL zeocin.

Cell culture
Murine bone marrow derived macrophages (BMDM) were isolated from C57BL/6 mouse femur and tibia bone marrow. Cells were cultured in DMEM with 10% FBS, 1% glutamax and 10% supernatant from 3T3-M-CSF cells for 6 days with media addition on day 3.

Macrophage infections
C57BL/6 BMDM were seeded at 5e4 cells/ well into PhenoPlate 96 well plates 48 hours prior to infection in cell culture media (DMEM supplemented with 10% FBS, 10% CSF, and 1% glutamax). BMDM were placed in 33 °C tissue culture incubators 1 hour prior to infection to acclimate the cells to the appropriate temperature. Prior to infection, *M. marinum* was cultured in 7H9 media to an OD_{600} of 0.5-0.8. Bacteria cultures were pelleted at 2850 *g* for 5 mins and washed twice with 1x PBS. A slow spin speed at 58 *g* was performed to pellet clumped bacteria. The supernatant was collected and diluted into phagocytosis media (DMEM supplemented with 5% horse serum and 5% FBS) to achieve a multiplicity of infection of 1. Bacterial suspensions were added onto cells and spun at 335 *g* for 10 minutes. Infected cells were washed with 1x PBS and incubated in cell culture media at 33 °C in tissue culture incubators. At the indicated timepoints, samples were washed 1x with PBS, fixed with 10% formalin, and then stained with 5 µM BODIPY 493/503 and 1:1000 DAPI for 45-60 minutes. Samples were then washed 2x with PBS and immediately imaged on the Opera Phenix. All images were analyzed using the CellProfiler image analysis software. For CFU experiments infected cells were lysed with 0.5% Triton X-100 in water for 10 minutes at 33 °C. Serial dilutions in PBS + 0.05% Tween-80 were plated on Middlebrook 7H10 Agar plates supplemented with 0.5% BSA, 0.2% dextrose, and 0.085% NaCl.

Replenishment assays
M. marinum was cultured in 7H9 media to mid-log phase and back diluted to an OD_{600} of 0.05. At indicated time points, replenished cultures were resuspended in fresh 7H9 media while unreplenished cultures were resuspended in their original media. Samples were taken for OD_{600} measurements and imaging via BODIPY 493/503 on a confocal microscope as described above.

Lipid uptake assays
M. marinum strains were cultured in 10 mL 7H9 Media to OD_{600} 0.4-0.8 in 30 mL Nalgene inkwells. 0.2 µCi of ^{14}C oleic acid was added to each inkwell and incubated at 32°C for 2 hours. 1.5 mL of the bacterial culture was then collected and pelleted at 2850 *g* for 5 mins. Samples were then washed 3x in cold wash buffer (0.1% Fatty acid free-

BSA and 0.1% Triton X-100 in PBS). Samples were then fixed in 10% formalin. Radioactivity was quantified by scintillation counting.

Results

Primary screen for ILI formation genes in *M. marinum* transposon mutagenesis mutants identifies 100 ILI deficient mutants. To design the fluorescent based imaging screen, we had to first establish a proof of concept for our assay. Work described in Chapter 2 demonstrated the ability of *M. marinum* to import the exogenous long chain fatty acid oleate in axenic culture to form ILI. This led us to question if we could make use of a fatty acid import assay to screen for transposon mutagenesis mutants with an impacted ILI formation pathway. Previous work in our lab, as well as work in other labs, have shown that Mtb readily uptakes BODIPY FL C_{16}, a molecular construct comprised of a green fluorescent BODIPY (4,4-difluoro-3a,4adiaza-s-indacene) conjugated to a 16 carbon chain fatty acid [71], [169]. Furthermore, lipidomic analysis of RAW 264.7 macrophages has illustrated that palmitate constitutes a significant portion of free fatty acids in macrophages, making fluorescent palmitate a prime candidate compound for our screen [197]. To investigate the kinetics of ILI formation in *M. marinum,* we cultured WT *M. marinum* expressing the mCherry fluorescent protein for 48 hours, a time point we had previously shown in Chapter 2 to result in ILI depleted bacteria. BODIPY FL C_{16} was pulsed into the bacterial culture and time points were taken at 2-hour intervals to identify the length of time needed for the bacteria to incorporate the fatty acid. Confocal imaging determined that, similar to Mtb, *M. marinum* could import and incorporate BODIPY FL C_{16} into ILI (Fig. 1, right images). However, it was unclear whether there would be diffuse transport of the fluorescent fatty acid through the mycobacterial cellular envelope. To ascertain whether the mycomembrane was permeable to BODIPY FL C_{16}, we pulsed the fluorescent fatty acid into a bacteria culture grown in carbon-deplete minimal medium. When nutrient starved, *Mycobacteria* undergo a metabolic shift to dormancy, characterized by growth arrest. We reasoned that a metabolically inactive *M. marinum* would not uptake the fatty acid at the same rate as metabolically active *M. marinum*, allowing us to determine if BODIPY FL C_{16} diffused into the cytoplasm. Sampling at the previously assayed time points revealed that there did not seem to be any diffusion of the fluorescent fatty acid into the bacteria at the measured time points (Fig. 1, left images). Furthermore, 4 hours was determined to be a sufficient length of time to allow for fatty acid incorporation into ILI without signs of non-specific staining in the carbon starved controls.

Having established our controls, we next made use of a transposon mutagenesis library [198]–[200]. Briefly, mCherry expressing arrayed transposon mutants were seeded into 7H9 medium alongside mCherry fluorescent *M. marinum* in either 7H9 or carbon deplete medium. The bacteria were cultured for 2 days and pulsed with BODIPY FL C_{16} for 4 hours, after which they were fixed, imaged, and analyzed (Fig. 2A). Over 5500 transposon mutants were screened by microscopy on an Opera Phenix high-throughput confocal microscope. The integrated BODIPY signal was normalized to the mCherry signal area by CellProfiler to quantify the BODIPY FL C_{16} in the ILI puncta per bacteria. To select for the most significant mutants we pooled ILI signal from all mutants and assigned a z-score to each mutant to quantify the variance in ILI signal in an individual mutant compared to the others. From there, we selected a z-score threshold of -1.5, leaving us with approximately 350 mutants defective in ILI accumulation (Fig. 2B).

These mutants were again screened to verify their ILI phenotype, ultimately leaving us with 100 mutants highly impacted in ILI formation. The arrayed transposon library however was not sequenced. To triage the mutants and prioritize hits, we set out to design a secondary screen to select for the most impacted ILI deficient mutants.

Secondary screen in macrophages identifies 4 novel ILI deficient *M. marinum* mutants. To identify ILI formation genes in the context of infection, we designed a secondary screen in which the previously identified *M. marinum* mutants were used to infect C57BL/6 bone marrow derived macrophages (BMDM). *M. marinum* have access to actin-based motility upon phagosome perforation mediated by the ESX-1 type VII secretion system approximately 15 hours post internalization [26]. The access to the mammalian cytosolic space would result in a marked shift in the bacterial environment, and perforation attenuated *M. marinum* mutants had the possibility of displaying a false positive readout. To circumvent this issue the infected cells were fixed 6 hours post infection to capture a time point in which *M. marinum* could make ILI but prior to phagosomal escape (Fig. 3A). These samples were stained with BODIPY 493/503, a neutral lipid staining dye demonstrated to stain for lipid bodies [147], [169], [194]. From the previously triaged *M. marinum* mutants deficient in ILI formation in axenic culture we identified 5 highly ILI deficient mutants (Fig. 3B, 3C). Arbitrary PCR amplification of transposon insertion sites identified the mutants as *MMAR_0250, MMAR_0416 (mce1E), MMAR_2242 (gabT_1), MMAR_3091* (*mpa*), and *MMAR_4531* (Table 1). *Mce1E* encodes the Mce1E protein that has been previously implicated to be critical for the import of long chain fatty acids and ILI formation in Mtb [71]. This hit provided confidence that our other targets had a role in ILI formation. Indeed, genetic complementation of the strains confirmed that the transposon insertion in each of these genes was responsible for the ILI deficiency of the *M. marinum* mutants in BMDM infections. (Fig. 4A, 4B). As the images and subsequent analysis suggest, successful complementation of the transposon disrupted genes rescues ILI formation in the mutant bacteria. Unfortunately, the *M. marinum* genome is poorly annotated, leaving little known about our hits. *MMAR_0250* encodes an uncharacterized protein with no homologs in Mtb nor other mycobacterium and had no predicted protein domains by Pfam. *GabT_1*, predicted to encode the 4-aminobutyrate aminotransferase GabT, is interesting as it has no direct homolog to Mtb either. However, the *M. marinum* genome has a gene annotated as *gabT, MMAR_0166,* as well as one annotated as *gabT_2, MMAR_2118*. Interestingly, of the three *gabT* related genes, only *MMAR_0166/gabT* has a direct homolog to Mtb. The AlphaFold protein structure database allowed us to predict the structure of *MMAR_0250* and align it to *Rv2589*, the *gabT* annotated Mtb homolog of *MMAR_0166*. Surprisingly, MMAR_0250 (in red) appears to have significant structural identity to GabT (in blue) but seems to form what appears to be an almost trimeric structure (Fig. 5). Continuing with the hits, *mpa* has been extensively studied in Mtb and encodes the *Mycobacterium* proteasomal ATPase mpa, essential for proper degradation of targeted proteins and required for resistance against NO Stress [173], [195]. Finally, *MMAR_4531* encodes a conserved hypothetical protein with an Mtb homolog *Rv0976c*. Neither gene has been characterized although structural information collected from the Pfam database suggests the presence of an acyclic terpene utilization (AtuA) domain.

ILI deficient mutants exhibit growth delays. We next sought to characterize the mutants to better understand the impact of ILI loss on the bacteria. ILI formation in Mtb is often associated with an upregulated dormancy regulon leading to growth arrest. We examined if ILI deficiencies impacted growth by culturing the mutants in 7H9 broth. Compared to WT, ILI deficient mutants initially experienced a lag in growth which was restored by 48 hours (Fig. 6A). We had previously established that WT *M. marinum* quickly accumulates ILI over the course of 6 hours in fresh axenic culture and depletes them as they grow. The growth data suggests that a lack of ILI during a critical window immediately upon exposure to fresh media causes a developmental delay and impacts generation time. To determine if access to ILI inducing conditions expedited growth, we performed a media replenishment assay with WT *M. marinum*. Bacteria was initially cultured in 7H9 media to mid log phase and then back diluted to an OD_{600} of 0.05. Half of the cultures were left untreated while the remaining half were resuspended with fresh media to allow for sustained ILI formation. When provided with fresh media, the bacteria grew more than their non-replenished, spent media counterparts (Fig. 6B). To determine if the observed ILI deficiencies were a result of a dysfunctional import complex like in *mce1* mutants, we examined the ability of the mutants to uptake fatty acids. ^{14}C radiolabeled oleic acid was added to flasks culturing WT and mutant *M. marinum* strains. Radioactive counts per minute (cpm) of the bacteria revealed that unlike the *mce1* mutant, the other mutant strains did not have a deficiency in medium carbon chain fatty acid uptake (Fig. 7).

ILI deficient mutants are attenuated in macrophages. We next examined the impact of ILI loss on virulence. We infected C57BL/6 BMDMs with WT and mutant strains to ascertain the impact of ILI deficiency on bacterial growth over the course of infection. Colony forming unit (CFU) data demonstrated that compared to WT *M. marinum, MMAR_0250, MMAR_4531,* and *mce1E* mutants all displayed an attenuation in BMDM (Fig. 8A). Furthermore, in a separate microscopy-based approach, we used the mCherry signal to determine the amount of bacteria in each field of view. This experiment showed the attenuation of the *mpa* and *gabT_1* mutant strains in BMDM, as indicated by the substantially lower bacteria area (Fig. 8B). Taken together, we see an attenuation of all mutant strains in BMDMs across the various experiments, highlighting the importance of a functional ILI program in the pathogenesis of *M. marinum*.

Inconsistent results make it difficult to draw firm conclusions. The observed ILI deficiency in the identified mutants had been observed several times in both broth and macrophages. There were however instances where the phenotype was not as dramatic or was even absent in both broth and macrophage infections. Indeed, at times even the the *mce1E* mutant displayed an ILI signal on par with WT *M. marinum*, leading us to question if our WT *M. marinum* strain had waning or inconsistent ILI formation. We retroactively examined trends in ILI signal of the WT *M. marinum* from all prior experiments and found that the ILI signal had seemingly decreased over time. Interestingly, the WT *M. marinum* also seemed to have gotten clumpier. Of note, this was likely not due to repeated passaging of the bacteria as the cultures were grown from the same passage of frozen stocks. This suggested inconsistencies or changes in

the media or culture conditions rather than the bacteria itself. A series of assays testing specific media components such as bovine-serum-albumin (BSA) and Tween-80 sources, multiplicities of infection, downstream processing, flask manufacturer, and culture conditions were performed. Unfortunately, each assay led to continued inconsistencies with some mutants showing strong ILI deficiencies in some instances but not others. To address if the increased clumping of the bacteria was causative of altered ILI signal, we increased the Tween-80 concentration and tried other methods of declumping the bacteria. Unfortunately, these tactics did not lead to a restoration of the WT ILI signal. It is possible that mutations in phthiocerol dimycocerosate (PDIM), an outer membrane associated lipid, can lead to an increase in ILI formation. Our WT *M. marinum* however displayed typical PDIM levels, suggesting that the diminished ILI signal was not a result of differential PDIM expression. Further work will need to be done to understand the intricacies of why the WT *M. marinum* ILI signal waned and the cause of the variance in mutant ILI phenotypes. These inconsistencies suggest a yet to be discovered variable that, as shown by the variances in both mutant and WT ILI accumulation, may prove to be a major contributor or impetus of ILI formation. Of note, *MMAR_0250* was ILI deficient in a majority of the cases and its phenotype that was consistently rescued by its complementation construct. This suggests that *MMAR_0250* may be a bona fide gene involved in the regulation or formation of ILI.

Discussion

Lipid body formation remains poorly understood. In eukaryotic cells, extensive work in the field has established seipins, perilipins, and FIT proteins as key players of the lipid droplet formation pathway. The understanding of ILI formation in prokaryotic fields however still leaves much to be desired, with the identified proteins involved in fatty acid import or synthesis and not with the physical manifestation of globular lipid structures. To elucidate other proteins that may be involved in formation of ILI, we turned to a fluorescent lipid uptake screen in an arrayed transposon mutagenesis library in *M. marinum*. Over 5500 mutants were distilled down to 5 mutants highly defective in ILI accumulation in both axenic culture and in macrophage infections. These mutants displayed impaired lipid body generation when pulsed with an exogenous fluorescent fatty acid BODIPY FL C_{16} as well as when post stained with BODIPY 493/503 throughout the course of infection. One of our hits was a gene associated with the import of fatty acids *mce1E*, previously characterized to be a key component of the Mce1 complex and integral to ILI formation. This hit served as a positive validation of our screen and made our other hits very promising.

MMAR_0250 is a yet to be characterized hypothetical protein with no homologs in other bacteria. The knockout strain of this gene was attenuated in macrophage infections but did not seem to have a defect in fatty acid import. The lack of homology is quite interesting as this could shed light to a pathway unique to *M. marinum*. *M. marinum*, although the closest relative to Mtb, nevertheless differs from Mtb and other nontuberculous mycobacterium (NTM) in its pathogenesis. Indeed, a majority of NTMs are cultured at 37°C, a trait shared with Mtb. *M. marinum* on the other hand is frequently found in bodies of water and can be cultured at a range of temperatures, though its preferred climate is 30-33°C. This waterborne pathogen infects cold blooded creatures or in rare instances human extremities. Further characterization of *MMAR_0250* is required to understand if there is a link between the unique pathogenesis of *M. marinum* and this ILI formation associated gene. *GabT_1* was an interesting hit as although *M. marinum* does not have a direct homolog of this gene in other bacteria, it does contain three predicted *gabT* genes annotated *gabT_1, gabT_2,* and *gabT*, with the ultimate gene bearing homology in Mtb. The *M. marinum* genome however is poorly annotated, and the annotations are often a result of predicted function due to homology to other bacteria sequences or assumed from stress induced changes in large transcriptomic datasets. Thus, the validity of the *gabT_1* annotation was uncertain, especially given that *M. marinum* seemingly encoded for three 4-aminobutyrate aminotransferases when Mtb only encodes for one. Surprisingly, the predicted protein structure of GabT_1 had significant overlap with the Mtb GabT when aligned using the protein prediction software AlphaFold. Indeed, the entirety of the Mtb GabT aligned nearly perfectly with a portion of GabT_1, though GabT_1 appeared trimeric in nature. GabT in mycobacteria has been shown to be involved in the γ-aminobutyric acid (GABA) shunt, an alternative pathway within the TCA cycle [196]. Structural alignment of the Mtb GabT with *M. marinum* GabT_1 suggests GabT_1 may be able to serve a similar role to GabT in the GABA shunt while the extraneous domains hint at the possibility of a multifunctional protein. Indeed, there is evidence to suggest the role of GABA as a signaling molecule

in plants, as well as important for acid tolerance in several bacteria [197], [198]. It is exciting to consider that *gabT_1* may play a role tangential to acid tolerance in *M. marinum* and somehow influence ILI formation. Regarding the impact of *gabT_1* disruption, we observed that the *gabT_1* mutant strain was attenuated in macrophages, though it is unclear whether this attenuation is a consequence of a dysregulated GABA/TCA cycle or due to an ILI deficiency. Metabolomics will be required to decouple the influences of ILI loss from TCA dysfunction in the attenuation of *gabT_1* mutants. We were however able to determine that GabT_1 does not play a role in the import of fatty acids. Further characterization of *gabT_1* is required to uncover what secondary roles it may play, as well as uncovering why the *M. marinum* genome contains three GabT associated genes and their mechanistic involvement in ILI formation. A promising hit from our screen was *mpa. Mpa* is appreciated to be a core component of the mycobacterial proteasome and is involved in the degradation of targeted proteins [195]. We have two divergent hypotheses on the mechanism behind Mpa loss and ILI depletion. The first is that Mpa has a direct role in the formation of ILI and directly interacts with proteins or lipids to initiate or facilitate ILI biogenesis. This however seems unlikely given its well characterized role as a proteasome associated ATPase and lack of the ILI-binding amphipathic helix stucture. The second hypothesis involves the downstream targets of Mpa. In Mtb, certain proteins are targeted for degradation in a Pup (prokaryotic ubiquitin-like protein) dependent fashion. Roughly 750 proteins have been identified as pupylation targets [203]. First, pup attaches to lysine residues of the target substrates. From there, this pup-protein complex is shuttled to Mpa and translocated through the ATPase to be degraded [204]. It is enticing to consider that a target of Mpa-mediated degradation is a TAG hydrolase or perhaps a negative regulator of ILI formation. Following this line of logic, in *mpa* mutants these ILI inhibiting proteins would no longer be degraded, leading to excessive depletion of ILI in the cellular space and the displayed ILI deficient phenotype. Although the identity of pup-targeted substrate is unknown, it seems unlikely that the Mpa target is associated with lipid import or regulation of lipid import as the *mpa* mutant displayed WT levels of ^{14}C oleic acid import. Further investigation into the pupylation targets of the Mpa proteasome will be required to see if they are involved in stabilizing ILI levels in mycobacteria. Finally, MMAR_4531*.* Little is known about this conserved hypothetical protein though the gene does have homology to the Mtb gene *Rv0976c*, a gene found to be nonessential for growth in H37Rv [205]. Pfam analysis has identified an acyclic terpene utilization domain AtuA, a domain originally characterized in *Pseudomonas citronellolis*. Work in *P. citronellolis* suggests the role of *atuA* in the conversion of citronellol to 7-methyl-3-oxo-6-octenoyl-CoA, specifically in the generation of acetate along the pathway [209]. Interestingly, *P. citronellolis* is one of the few species documented capable of utilizing acyclic terpenes as a sole carbon source. While it has yet to be shown, and is perhaps unlikely, that *M. marinum* can utilize acyclic terpene, it would be interesting to investigate why *MMAR_4531* has an AtuA domain.

It is interesting to consider why the other mutants initially identified in the primary screen were not as impacted in their ability to form ILI in macrophages. One possibility is centered on the differences in the extracellular environment. In the initial screen the bacteria were seeded into 7H9 media in the absence of external stimuli that could spur

the accumulation of ILI. In mutants whose mutations dysregulated their metabolism, this environment may not necessitate the formation of ILI, leading to a surplus of mutants with an ILI-low phenotype. The macrophage environment however is very different, and bacteria experience stressors that typically lead to ILI formation in other mycobacteria [206]. It is possible that under these circumstances the mutant strains must prioritize sustainability and viability in the form of ILI formation to withstand the stressors imparted by the macrophages, leading to many of the previously ILI-low strains to display a normal ILI phenotype. While not the targets of our current study, further characterization of the mutants identified in the primary screen could reveal genes involved in the central carbon metabolism so critical that *M. marinum* is required to shunt carbons away from TAGs and ILI and into maintaining basal metabolism levels. This study also focused on the mutants with a z-score of -1.5 or below, representing strains with deficiencies along the ILI formation pathway. It would however be of great interest to focus on the opposite end of the spectrum and characterize the mutants that were ILI rich. The examination of these mutants could elucidate proteins essential to the maintenance or utilization of ILI. While these may most likely be TAG hydrolases or proteins involved in a response pathway triggered by a necessity to utilize ILI, it nevertheless would be of great value to follow up on these genes to see the other face of the ILI pathway coin.

Through this study we were able to observe consequences of ILI loss on bacteria growth in axenic culture as well as in pathogenesis. The growth curves of the mutant strains compared to WT *M. marinum* showed a delay into growth phase by the strains lacking lipid bodies. The bacterial doubling time of the strains however normalized to WT rates after 24 hours, a time which we have previously shown to be a state of ILI depletion in WT *M. marinum*. This developmental delay suggests ILI could play a role in the generation of bacterial mass, as indicated by the initial discrepancy in bacterial growth when the WT strain had ILI followed by relatively similar growth rates between all strains once WT *M. marinum* was in an ILI deplete state. Indeed, TAGs are a large source of energy estimated to store six times more energy than hydrated glycogen [211]. These energy depots are hydrolyzed into free fatty acids, ready for β-oxidation to fuel growth. The media replenishment experiment provided some evidence to this theory, though a lack of a *mce1* mutant at the time of the assay makes it difficult to parse the impact of ILI versus the impact of fresh nutrients on the growth of bacteria. Nevertheless, the shared growth delay exhibited by the remaining ILI defective mutants proves promising and requires further investigation. Our study also adds mounting evidence to the role of ILI in virulence. Previous works have shown that TAG or ILI accumulation is critical for successful pathogenesis of many *Mycobacteria*, presented by studies on *mce1* mutants in Mtb as well as on lipid rich versus lipid poor *M. abscessus* in zebrafish [71], [130]. Here we show that ILI deficient strains were attenuated to varying degrees in BMDMs. Collectively, our data presents 4 genes implicated in marked reduction of ILI formation in *M. marinum* grown in broth and in BMDM. Of note, due to time constraints we were unable to ascertain if complementation of the genes rescued the attenuations displayed by the ILI defective mutant strains and thus cannot clearly link virulence with a proper ILI formation program. However, our data does provide indirect evidence highlighting the importance of ILI in pathogenesis. The attenuation displayed by our 4 mutants, as well the *mce1E* mutant attenuation we

see in our hands, corroborate findings from previous labs that *mce1* is important for virulence [71], [157], [206]. Together, these data suggest that functional ILI biogenesis and homeostasis are critical to *M. marinum* and Mtb pathogenesis. Comprehensive characterization of the genes identified in our screen will reveal the mechanistic role that they play in ILI formation and will also prove beneficial as alternative models to study ILI deficiency and comprehend the role that ILI play in cellular development and pathogenesis. Greater understanding of ILI biogenesis will undoubtedly pave the way for combatting NRP Mtb and quelling the persistence and global spread of TB.

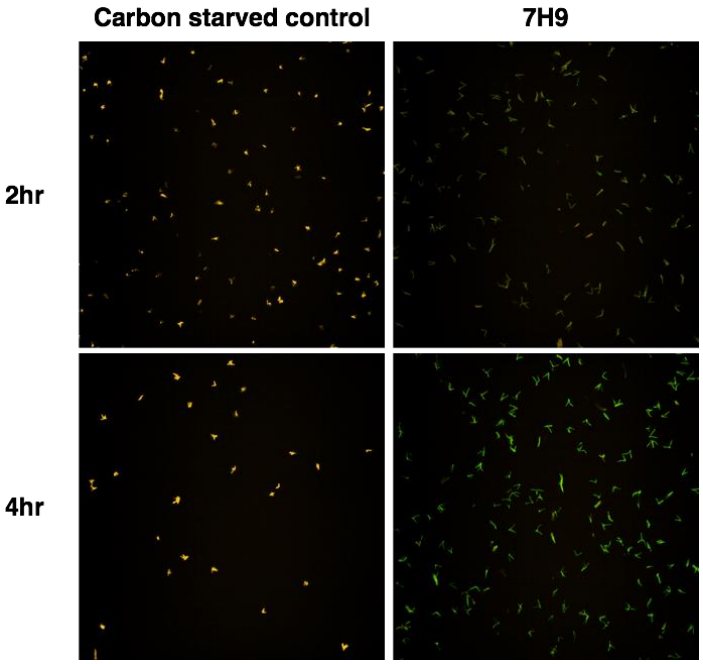

Figure 1. *M. marinum* readily uptakes BODIPY FL C_{16} when cultured in 7H9 media. Confocal images of WT mCherry fluorescent *M. marinum* cultured in Minimal Media (left) or 7H9 Media (right) 2 and 4 hours post pulse with BODIPY FL C_{16}. Images were taken at 63x.

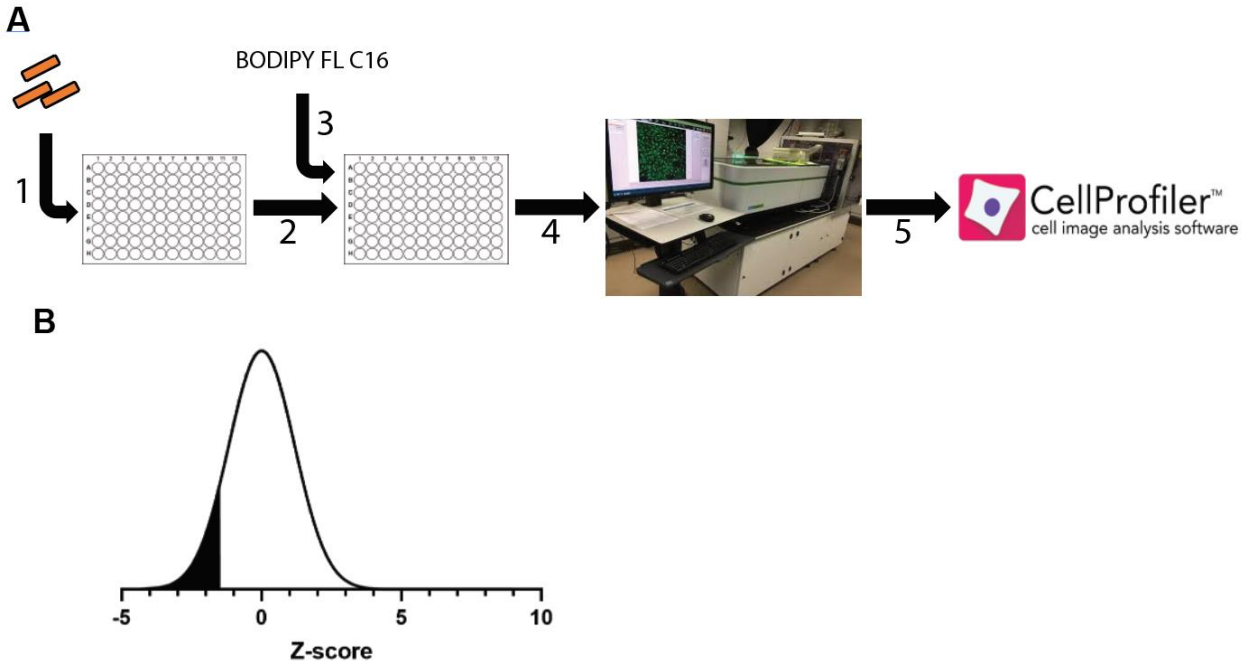

Figure 2. Primary screen of 5500 *M. marinum* mutants identifies 100 genes involved in incorporation of BODIPY FL C_{16} into ILI. (A) Schematic of primary screen. Mutant *M. marinum* are seeded from an arrayed transposon mutagenesis library and WT *M. marinum* into 96-well v-bottom plates with 7H9 media [1]. Strains are cultured for 2 days [2] and pulsed for 4 hours with 5 µM BODIPY FL C_{16} [3], and subsequently fixed with 10% formalin. Fixed samples are washed and transferred into imaging plates for immediate imaging on a high-throughput confocal microscope [4]. Resulting images are analyzed on CellProfiler [5]. (B) Z-score distribution of all mutant plates. A composite z-score threshold of -1.5 was applied to triage candidate mutants and select for highly ILI-deficient mutant strains.

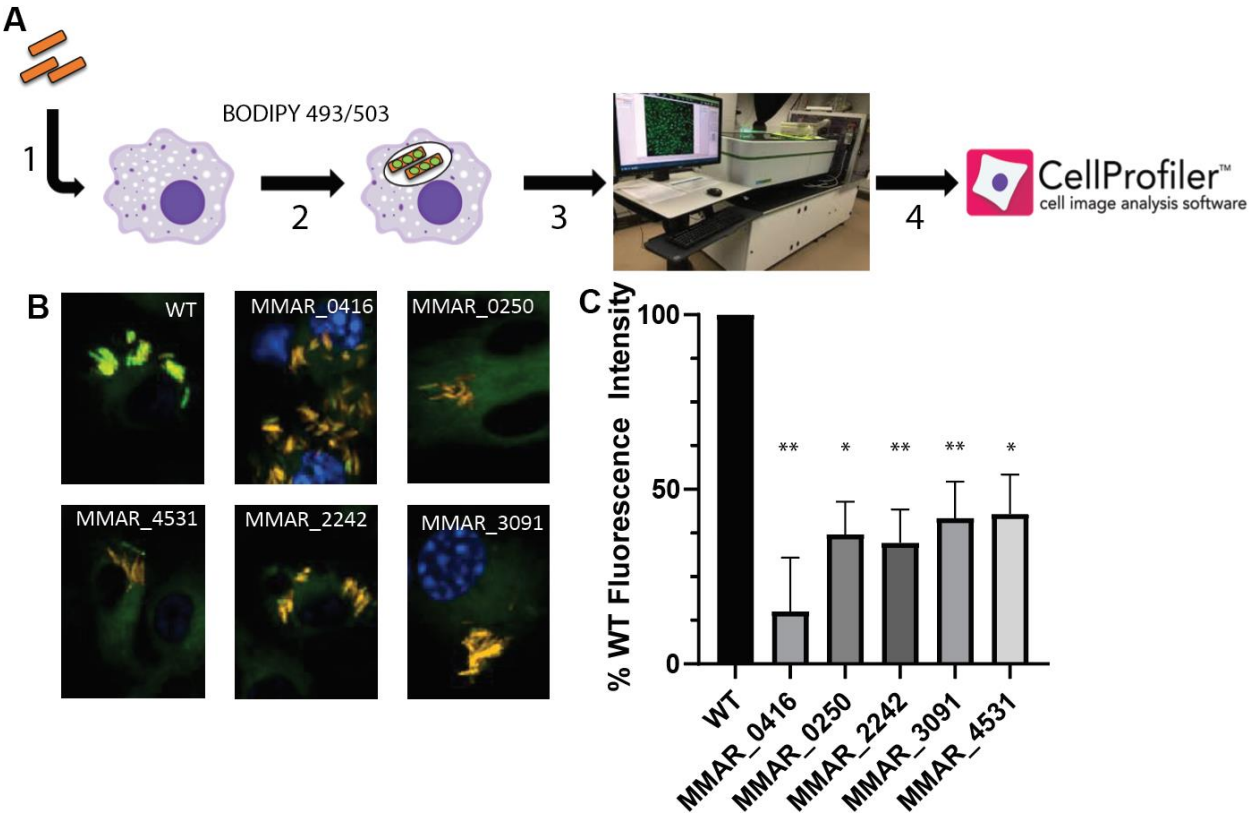

Figure 3. Secondary screen in C57BL/6 bone marrow derived macrophages identifies five *M. marinum* mutants defective in ILI formation. (A) *M. marinum* mutants identified in the primary screen were grown to mid-phase and used to infect C57BL/6 BMDM [1]. At various time points samples were fixed with 10% formalin and stained with 5 µM BODIPY 493/503 for visualization of neutral lipids [2]. Samples were immediately imaged on a high-throughput confocal microscope [3]. Images were quantified using CellProfiler [4]. (B) Confocal images of the B6 macrophages infected with the identified mCherry fluorescent *M. marinum* strains. Samples were stained with DAPI and BODIPY 493/503 post fixation and imaged at 63x. (C) Quantification of integrated BODIPY 493/503 signal was first normalized to mCherry signal and then normalized to WT intensity per experiment. Data are means $\pm$ SD (N=3) *p<0.05,**p<0.01 (Mann-Whitney test comparing WT to each mutant)

MMAR Locus	Gene Name/Function	Rv ID
MMAR_0250	Conserved hypothetical protein	NH
MMAR_0416	MCE-family lipoprotein LprK (MCE-family lipoprotein Mce1E)	Rv0173
MMAR_2242	4-aminobutyrate aminotransferase GabT_1	NH
MMAR_3091	ATPase	Rv2215c
MMAR_4531	conserved hypothetical protein	Rv0976c

Table 1. *M. marinum* ILI deficient mutants. Compiled list of the five highly ILI deficient *M. marinum* mutants identified from primary screen in broth and secondary screen in macrophage infections. MMAR Locus indicates the gene disrupted by transposon insertion. Rv ID indicates the homologous gene in Mtb strain H37Rv. “NH” denotes genes with no direct homology to H37Rv.

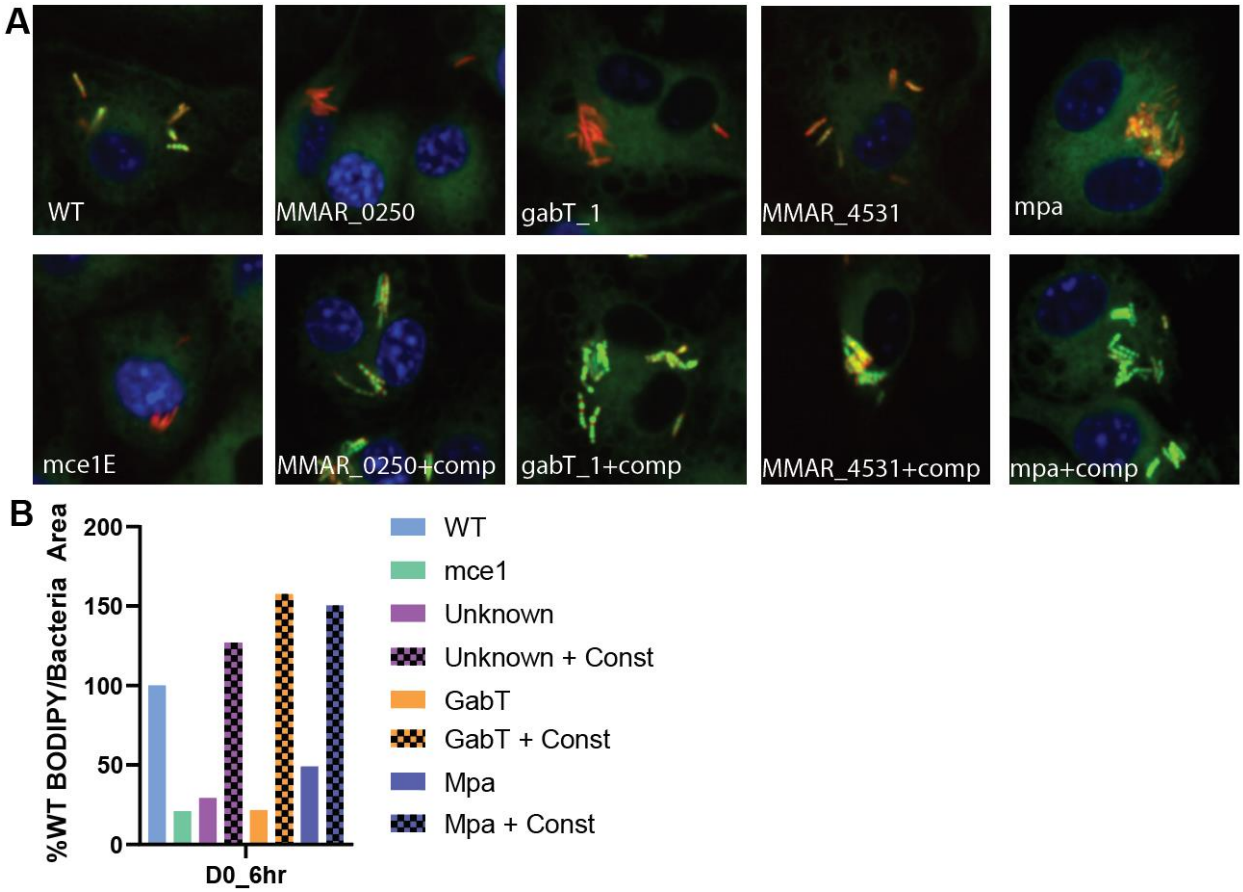

Figure 4. Complementation of mutant *M. marinum* strains. (A) *M. marinum* mutants and strains complemented with the native gene expressed under the constitutive promoter GroEL2 via pMV306zeo were used to infect B6 BMDM at an MOI of 1. Samples were fixed 6 hours post infection and stained with DAPI and BODIPY 493/503. Images were captured at 63x. (B) Quantification of integrated BODIPY 493/503 signal was first normalized to mCherry signal and then normalized to WT intensity (n=1).

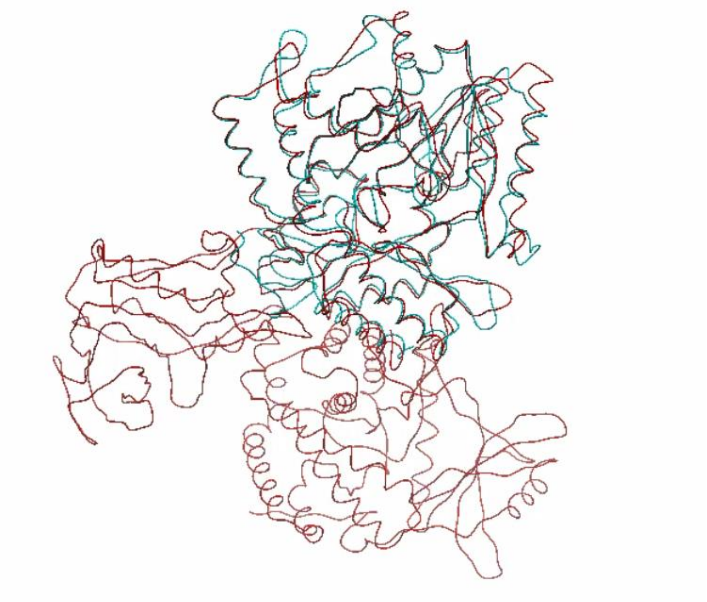

Figure 5. Predicted structure of MMAR_2242 shares some structural similarities to Rv2589. Protein structures of MMAR_2242/GabT_1 (red) and Rv2589/GabT (blue) were predicted using AlphaFold and overlayed to display structural homology.

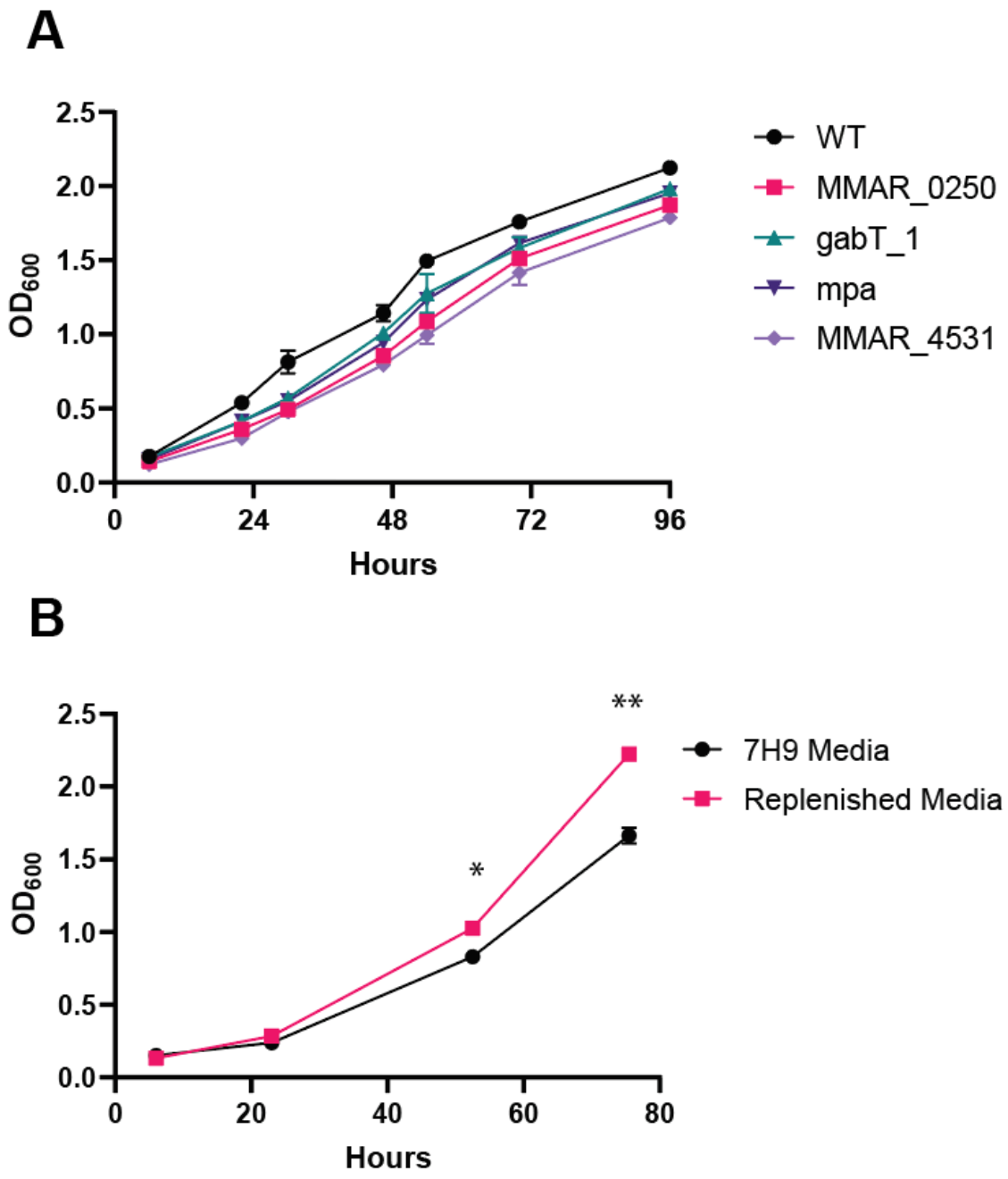

Figure 6. ILI Mutants demonstrate slight growth defect. (A) WT and mutant strains were cultured in 30 mL Nalgene inkwells with 10 mL 7H9 media. OD_{600} measurements were taken at the indicated time points. Data are means ± SD (n=2) (B) WT *M. marinum* was cultured in 7H9 media and back diluted to cultures of OD 0.05. Cultures were either left to grow in their initial 7H9 media or were replenished with fresh media. Data are means ± SD (n=2) *p<0.05,**p<0.01 (student t-test comparing 7H9 to Replenished Media).

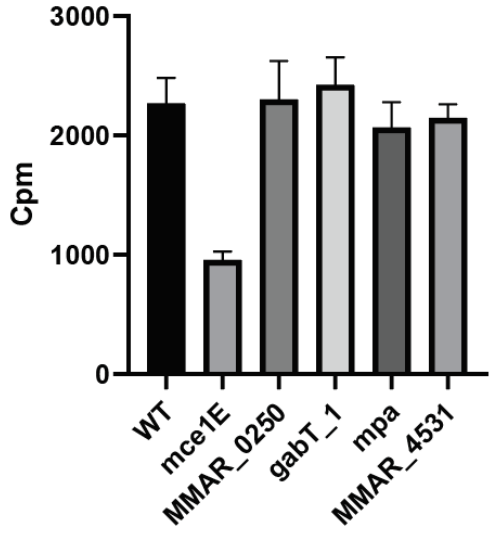

Figure 7. ILI deficiency of identified mutant strains is not due to impaired fatty acid import. WT and ILI defective mutant *M. marinum* strains were cultured with ^{14}C oleic acid. After culture for 4 hours samples were fixed and counts per minute (cpm) were quantified on a scintillation counter to determine fatty acid import capabilities. Data are means $\pm$ SD (n=2).

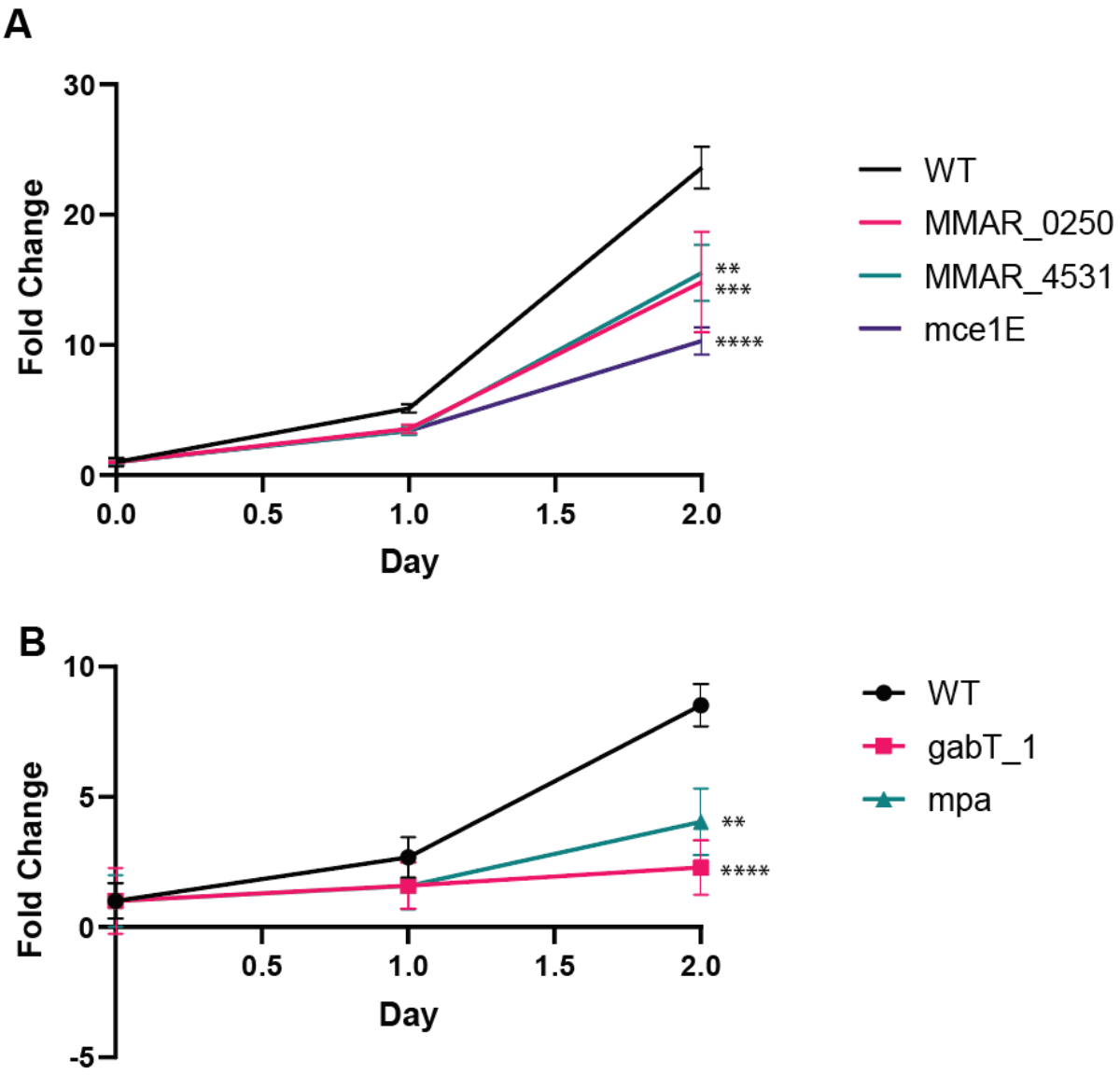

Figure 8. ILI deficient *M. marinum* strains are attenuated in resting BMDM. (A) BMDM were infected with WT, *MMAR_0250, MMAR_4531,* and *mce1E* mutant *M. marinum* strains at an MOI of 1. At each timepoint samples were taken for CFU and plated on 7H9 agar plates. Fold change in CFU for each strain was calculated with respect to D0 CFU. Data are fold changes ± SD (N=4) *p<0.05,**p<0.01, ***p<0.001, ****p<0.0001 (student t-test comparing WT to each mutant) (B) BMDM were infected with WT, *gabT_1,* and *mpa* mutant *M. marinum* strains at an MOI of 1. At each timepoint samples were fixed and imaged on a confocal microscope at 63x. Bacteria area was quantified using mCherry area. Fold change in CFU for each strain was calculated with respect to D0 mCherry area. Data are fold changes ± SD (N=4) *p<0.05,**p<0.01, ***p<0.001, ****p<0.0001 (student t-test comparing WT to each mutant)

Chapter 4: Conclusions and future perspectives

Despite the decades of groundbreaking and revolutionary research on Mtb, the understanding of Mtb pathogenesis and NRP in LTBI has evaded researchers, leading TB to continue to be a global plague. Substantial work has been done since the mid-20th century to uncover the intricacies behind LTBI and sustained Mtb viability. The discovery of the unique co-catabolism of multiple carbon sources by Mtb, its preferential usage of fatty acids *in vivo*, and the metabolic reprogramming to NRP have all expedited monumental advancement in the understanding of Mtb metabolism during infection. Through these works it is widely recognized that a critical component of Mtb pathogenesis in LTBI is the lipidomic remodeling of the bacteria and the marked accumulation of ILI in the bacilli. Indeed, a sustained consensus in the field for many years has been that ILI are a hallmark of NRP. Yet a few lines of evidence have suggested otherwise. Select clinical Mtb lineages have been shown to accumulate TAG in axenic culture, and Mtb has been shown to form ILI in resting macrophages [169]. Here, I demonstrated that *M. marinum* and clinical Mtb strains form ILI independent of NRP inducing states, challenging a long standing belief that ILI are formed as a consequence of a hypoxia driven *dosR* mediated transition to NRP. Furthermore, I identified four novel genes involved in the ILI formation pathway to serve as model ILI knockout strains to understand the role of ILI in mycobacterial pathogenesis.

Intracellular lipid inclusion formation in mycobacteria is a dynamic process associated with replication. The DosR response to hypoxia initiates the metabolic transition from active growth to NRP. The dormancy regulon triggers the expression of TAG synthase *tgs1* and the consequential accumulation of TAGs into ILI. This shunting of carbon sources from the TCA cycle to TAGs results in a decelerating metabolism and a state of dormancy. Our work surprisingly showed evidence that NRP and *dosR* expression are not required for ILI formation, and that ILI formation is associated with states of active replication in *M. marinum* and clinical Mtb isolates. We carefully proved through microscopy, biochemical, and genetic assays that actively replicating *M. marinum* cultured in axenic broth in the absence of preconceived environmental stimuli required for ILI formation were still able to form ILI. This finding was translated to clinical Mtb isolates spanning L1, L2, and L4 strains. Interestingly, when the previously identified external stressors were tested on *M. marinum*, we observed that hypoxia and NO stress are drivers of ILI formation conserved across mycobacteria, while ILI formation in a low nitrogen to carbon ratio environment may be a trait unique to *M. smegmatis* or *M. abscessus*. Indeed, while these two NTMs, as well as some other bacteria such as *R. opacus*, form ILI in nitrogen limited conditions, these conditions have yet to be tested on Mtb strains, making it unclear whether nitrogen deprivation induced ILI formation is a trait shared by a majority of mycobacteria. Nevertheless, the ability of *M. marinum* and Mtb to form ILI while replicating and then deplete them, as well as the varied response to external stressors, leads to questions of what role ILI play in the life cycle of pathogenesis. In depth speculation on this matter will be discussed later in this chapter, but it this finding led us to question if a stress response was even required for ILI formation. If bacteria were able to form ILI in normoxia, and if nitrogen limitation did not seem to impact *M. marinum*, was it possible that the ILI pathway was

distinct from the dormancy regulon? The RNASeq allowed us to probe the transcriptional differences between ILI producing and ILI barren Mtb strains. Prior works had reported the upregulation of the DosR regulon in L2 strains. As expected, many genes involved in the devR/dosR regulon were upregulated in our RNASeq data, with approximately 30% of the devR/dosR regulon significantly upregulated and another 30% upregulated albeit not significantly. Other targets with a high false discovery rate include *Rv2660c* and *Rv2661c*. Yet to be characterized, these hypothetical proteins have been shown to be significantly upregulated in a simultaneous nutrient starvation and oxygen depletion model [210]. Given that these stressors have been shown in the past to induce ILI in certain mycobacteria, it is possible that these unannotated genes are in fact ILI associated genes. Among the significantly differently expressed genes were a series of lipases. *LipV* and *lipQ* were upregulated, while *lipC, lipX,* and *lipF* were all downregulated. *Fas,* a fatty acid synthase involved in the biosynthesis of mycolic acids, was also downregulated. Other significant genes include a plethora of transmembrane or membrane associated proteins encoding genes, including *Rv1733c, Rv1735c, Rv1739c, Rv2620c, Rv3238c, Rv3239c, Rv3277, Rv3278c, Rv3335c,* and *Rv3395A*. ILI are thought to form from the inner leaflet of the lipid bilayer. Naturally, it is believed that proteins involved in ILI formation are transmembrane or membrane associated in nature. Furthermore, ILI have been shown to be a site of protein sequestration, with many ILI associated proteins [208]. These ILI associated proteins share an amphipathic helix domain that mediates protein binding to a phospholipid monolayer. Further investigation into the predicted structural domains of these and other proteins encoded by genes identified as differentially expressed in our RNA Seq may prove fruitful to the discovery of proteins involved in ILI formation. As mentioned in chapter 2, genes encoding the MmpL/S4 complex were differentially expressed in the L2 strain, as well as other *mmpL.* MmpL proteins are known for their role in regulating and stabilizing the cellular envelope [209]. In eukaryotic cells, phospholipid membrane composition has been implicated to be a driving force of lipid droplet budding [91]–[94], [187]. It would be interesting to investigate if the differential expression of the lipid homeostasis genes and *mmpL* genes led to an altered membrane mosaic in L2 strains, facilitating ILI synthesis. The differences in ILI formation between the L1 and L2 strain led us to question if there was a link between ILI formation and Mtb lineages. A screen of 60 clinical isolates demonstrated an inter and intra lineage variance in ILI formation. When we probed ILI high and ILI low isolates for *dosR* expression, we made the shocking revelation that *dosR* expression did not seem to correlate with ILI signal. While some ILI high clinical isolates had an elevated *dosR* transcript as expected, there were some ILI low isolates that also had high *dosR* expression. Even more startling, select ILI high clinical isolates had completely muted *dosR* transcription. Altogether, our findings challenge a long-held belief in the field and decouple ILI formation from NRP and *dosR* expression. Further work is being done on the clinical isolates to utilize this large dataset to potentially identify SNPs enriched for an ILI high phenotype.

Identification of novel genes involved in ILI biogenesis. As previously mentioned, studies in eukaryotic organisms have expanded the role of lipid bodies, with some works in prokaryotic cells suggesting a ILI were similarly multifunctional. To understand the role of ILI in mycobacteria, we first needed to establish a working model to study ILI

deficiency. While previous works have studied the impact of *mce1* and *tgs1* mutants on ILI formation, these mutants have an added defect: a disruption of the central carbon metabolism [189]. The loss of Mce1 or Tgs1 directly results in a loss of fatty acid import and TAG accumulation. Such a denial of a critical energy source integral for a functional central metabolism may have grand consequences beyond those associated with ILI loss, making it difficult to discriminate whether ILI loss or a dysfunctional metabolism is responsible for the attenuation displayed by the mutant bacteria. Hence, we sought to develop a screen in an *M. marinum* transposon mutagenesis library to identify genes involved in ILI formation that do not impact TAG accumulation or fatty acid import. By utilizing a high throughput confocal microscope, we were able to screen over 5500 mutants and found approximately 100 candidate genes. From there, a secondary screen in macrophages allowed us to prioritize mutants that were attenuated in a more biologically relevant setting. In a similar approach, we again screened the 100 candidate mutants through BMDMs and stained for neutral lipid accumulation by BODIPY 493/503 post staining, ultimately leading us to the identification of *MMAR_0250, gabT_1, mpa,* and *MMAR_4531* as genes involved in ILI formation. Due to the poor annotation of the *M. marinum* genome, the function of a majority of these genes is unknown. To start, *MMAR_0250* is unique to *M. marinum* with no direct homologs in other species. Is this gene important to ILI formation specifically in *M. marinum*? Are there any links to the pathogenesis of *M. marinum* and its alternating environments of cold-blooded organisms and water? Further investigation of this gene could provide clues to answering these questions. *GabT_1*, while having no direct homology to Mtb, is predicted to encode a 4-aminobutyrate aminotransferase GabT. GabT is a critical member of the GABA shunt in the TCA cycle, and Mtb is known to encode this protein as well, though by a different gene. When structural alignment of the predicted proteins was performed, we saw that the Mtb GabT aligned very well with the *M. marinum* GabT_1. GabT_1 however seems to be much larger with extraneous protein architecture. Does *gabT_1* truly encode a 4-aminobutyrate aminotransferase? Are the non-aligned superfluous regions superficial or might they be responsible for proper ILI formation? It would be interesting to utilize radiolabeled carbon-based metabolomics as well as targeted amino acid mutations to answer these questions and uncover the role of *gabT_1. Mpa* was a particularly surprising hit given that this gene has been well characterized in Mtb as a proteasome associated ATPase involved in targeted pupylation-dependent protein degradation in the bacteria [212]. While its direct involvement in the biogenesis of ILI seems unlikely, it is certainly plausible that Mpa degrades ILI inhibitory or regulatory proteins. The ILI deficient characteristics of the *mpa* mutant could be explained by the lack of Mpa leading to excess accumulation of ILI utilization proteins, such as TAG hydrolases, or negative regulators of ILI formation such as environmental response proteins. Which target proteins does Mpa degrade to cause an imbalance in ILI aggregation? Thorough scrutiny of pupylated proteins and specific mutations in these proteins is required to answer this question. Finally, *MMAR_4531*. The function of this gene is unknown, though it does have a homolog in Mtb, *Rv0976c*. The only known characteristic of this gene is that its encoded protein contains an acyclic terpene utilization domain AtuA. The acyclic terpene utilization pathway has been studied in *P. citronellolis,* a bacterium uniquely able to be cultured on acyclic terpenes as a sole carbon source. While the links to acyclic terpenes in

mycobacteria have yet to be understood, further characterization of this gene will be required to discover if the AtuA domain is critical to ILI inception. While we are currently unsure of the explicit involvement of these genes along the ILI formation pathway, we were able to confirm that they do not impact the import of long chain fatty acids. We then sought to utilize these mutants as models of ILI loss. Due to time limitations, we were only able to grasp a surface level understanding of the impact of ILI formation on the bacteria. Nevertheless, we were able to ascertain that impacted ILI formation led to an initial delay in growth as well as attenuation in macrophages. Further characterization of the genes' influences on ILI formation and application of these mutants to study the role of ILI will provide lucrative knowledge on all facets of ILI in mycobacteria.

Remaining questions and future perspectives

As alluded to several times throughout this work there remains much to understand about ILI in Mtb pathogenesis. First and foremost, what proteins constitute the machinery that drives ILI formation in *Mycobacteria*? Work done in eukaryotic cells has established a general understanding of how lipid droplets are formed in eukaryotic cells. Briefly, synthesized TAGs accumulate between the leaflets of the ER bilayer. While it is unknown whether the composition of the phospholipid membrane mosaic alone is sufficient to lead to lipid droplet budding, it has been documented that a few proteins, namely FIT proteins, seipins, and perilipins, play a role in facilitating lipid droplet budding or homeostasis. Unfortunately, little is known about the similarities or differences between the eukaryotic and prokaryotic lipid droplet formation process. In Mtb, the Mce1-LucA complex has been demonstrated to be required for the import of C_{16} and C_{18} fatty acids. This complex consists of integral membrane permease subunits YrbE1A and YrbE1B, Mce1A-F, Mam1A-D and LucA [71], [72]. It has been theorized that these proteins together form a multimeric structure that spans from the cytoplasmic membrane to the mycolic acids, though structural data has yet to be published to confirm the localization and size of this complex [52]. Mper1, a protein with low structural homology to mammalian perilipin, has also been identified as associated with ILI homeostasis. Interestingly, the data suggests it may have a role in fatty acid import or shuttling, with *mper1* mutant strains exhibiting a deficiency in ^{14}C-oleic acid incorporation into TAG and total ^{14}C-oleic acid import. Nonetheless, FIT and seipin-like proteins have yet to be identified in prokaryotes. The lack of known proteins directly contributing to ILI formation led to a lack of reliable ILI deficient models to study the role of ILI. While *tgs* or *mce1* mutant strains do lead to a depletion of ILI and attenuation in virulence, it is unknown whether the phenotype of the bacteria is a consequence of ILI loss or a consequence of a dysfunctional metabolism as a result of fatty acid and TAG devoid bacteria. The discovery of a gene that directly facilitates the physical manifestation of ILI and leaves TAG abundance relatively untouched would, if it exists, lead to rapid advancements in the understanding of the role that ILI play.

Our work in Chapter 2 illustrates a surprising discovery that *M. marinum*, distinct from other NTM and lab strains of Mtb, forms ILI while actively replicating independent of state of NRP or environmental stressors such as hypoxia. Even more interestingly, *M.*

marinum forms ILI and quickly depletes them, only forming ILI when fresh media or exogenous fatty acids are introduced to the system. These findings raise an important question: what purpose do ILI serve in *M. marinum*? The consensus in the field for years has been that ILI are formed as a means of slowing metabolism by shunting resources away from the TCA cycle and into fatty acid storage when faced with stressors [78], [124], [125], [189]. Yet some indirect lines of evidence have suggested that this may not be the whole story. Work in our lab has shown that Mtb in resting macrophages, and not IFN-γ activated macrophages, forms ILI. The mechanisms behind how IFN-γ activated macrophages inhibit ILI formation in Mtb is unknown, yet it is perplexing that the relatively stress-free environment of a resting macrophage would induce ILI formation, compared to the much more harsh environment of an activated macrophage [169]. Furthermore, L2 and select other Mtb clinical isolate strains have been shown to accumulate TAG and form ILI in broth [131], [185]. Yet the import and assimilation of exogenous free fatty acid into TAG is an energetically costly process—it is difficult to imagine the benefit of undergoing such a process when the alternative of simply processing bountiful sugar-based carbon sources through glycolysis and the TCA cycle, or even the immediate oxidization of free fatty acids to yield energy, is much more efficient and direct. This line of logic implies a role that ILI play beyond storing energy as, to reiterate, what would be the point of synthesizing TAG if only to immediately hydrolyze them into the fatty acid initially used to synthesize them? There are a few speculative thoughts on why *M. marinum* makes ILI while replicating.

First and foremost, it must be addressed that ILI in *M. marinum* still play a part as deposits of energy. ILI deficient mutant *M. marinum* experienced a delay in growth compared to the ILI bearing WT strain, suggesting the role of ILI as an energy deposit for cellular growth and biomass accumulation. More speculative ideas include the notion that the bacteria are constantly in a preparatory state: if there are sufficient means and available fatty acids to make ILI, they will be made. *M. marinum* as previously stated is a waterborne pathogen. While it optimally grows at 30°C, it must be ready to endure rapid changes to its environment, whether it be due to the nature of their cold-blooded hosts swimming between different underwater climates or being swept by the currents across a range of nautical temperatures. This theory is supported by ILI data of Mtb in resting, and not in activated, macrophages. It is conceivable that, as a human pathogen, Mtb will first encounter a relatively non-hostile host environment such as in resting alveolar macrophages. In this stable, lipid rich environment, Mtb would be able to build up ILI and prepare for defense against the onslaught of host immune factors by T cell activated macrophages following the onset of adaptive immunity. Another speculation regarding the role of ILI is that it serves as a cytosolic molecular concentrator. ILI in prokaryotes are relatively gargantuan and can reach sizes of 400 nm, spanning the width of a *R. opacus* bacilli [117]. Such colossal structures would exclude proteins and non-hydrophobic molecules, allowing for immensely concentrated regions of said molecules in the cytosol. ILI could thus play a role in modulating and regulating transcriptional processes dependent on threshold concentrations of critical molecules. ILI may also serve as a sink for cytotoxic fatty acids. Work in eukaryotic cells has shown that excess accumulation of free fatty acids is lipotoxic and is mitigated by assimilation into neutral lipids such as TAGs [210]. In a similar line of thinking it has been proposed

that fatty acid metabolism counteracts the accumulation of cholesterol and methylcitrate cycle derived toxic molecules by rerouting the flux of these molecules into less toxic neutral molecules [52]. It is possible that ILI may also play a role in signaling. In eukaryotic cells it has been demonstrated lipid droplets are a hub for signaling molecules [161], [211]. For instance, eicosanoids are lipid-based signaling molecules involved in the regulation of pro-inflammatory responses by host cells [212]. By acting as a site for eicosanoid synthesis and assemblage, lipid droplets have been recognized as de facto mediators of immune response [161], [213]. It was also been demonstrated in prokaryotes that amphiphilic lipids can be used as signaling molecules, specifically in the context of quorum sensing [214]. While there is yet to be clear evidence of quorum sensing in mycobacteria, there are a few indirect lines of evidence reviewed elsewhere [215]. Although further investigation into mycobacterial quorum sensing and the signaling molecules involved is necessary before any links with ILI can be established, it is interesting to speculate whether the ILI status of the bacteria is linked to Mtb resuscitation out of dormancy upon reactivation of TB out of LTBI. Finally, ILI in mycobacteria may be involved in protection from genotoxic stress. Work in *R. jostii* has shown that ILI localization to DNA via the intermediary protein MLDS led to increased protection from genotoxic stress. Curiously, MLDS shared sequence similarities to histone like protein Hlp in mycobacteria [120]. It would be interesting to investigate if Hlp shares a similar role to MLDS and if ILI in mycobacteria likewise play a part in protecting the bacilli from DNA damage. Mtb is often subjected to reactive oxygen and reactive nitrogen species *in vivo*, as well as searing chemical attacks from antitubercular drugs; ILI may play a role in protecting the bacteria from these external pressures. It is exciting to consider the many functions ILI play in the mycobacterial life cycle.

Lipid bodies have long been dismissed as a simple repository of energy, inert and nonreactive until the stored lipids need to be hydrolyzed. Work on eukaryotic organisms has defied this belief and pushed for the establishment of lipid droplet as multifunctional organelles [106], [111], [112], [116], [211], [216]. While work in the prokaryotic field has yet to define such diverse roles for ILI, there nevertheless is some mounting evidence that prokaryotic ILI also have function beyond energy compartmentalization [119], [120], [130]. The work outlined in this dissertation contributes to our understanding of lipid droplets by identifying a direct link between ILI formation and actively replicating *M. marinum*, establishing *M. marinum* as a highly relevant organism to study of ILI in clinical Mtb isolates. Indeed, our work translated to clinical isolates of Mtb and allowed us to examine the variance in ILI formation within and among lineages of Mtb, as well as allowed us to identify key transcriptional differences that could explain how ILI are formed. We further were able to uncouple NRP and *dosR* expression from ILI formation, challenging a prevailing notion in the field. In an orthogonal approach, we also identified genes that led to significant ILI-deficient *M. marinum* mutants, providing optimistic models to study the role of ILI. Together, these findings will prove to be promising in the discovery of the key players in the ILI formation pathway as well as uncovering why ILI are formed in replicating bacteria. A greater understanding of all facets surrounding ILI will undoubtedly be critical in identifying candidate proteins for molecular inhibition of ILI and will open new avenues for therapeutic approaches to combat the global TB epidemic.

References

[1] E. Tortoli, “Microbiological features and clinical relevance of new species of the genus Mycobacterium,” *Clin. Microbiol. Rev.*, vol. 27, no. 4, pp. 727–752, Oct. 2014.

[2] E. W. Tiemersma, M. J. van der Werf, M. W. Borgdorff, B. G. Williams, and N. J. D. Nagelkerke, “Natural history of tuberculosis: duration and fatality of untreated pulmonary tuberculosis in HIV negative patients: a systematic review,” *PLoS One*, vol. 6, no. 4, p. e17601, Apr. 2011.

[3] “WHO | Global Tuberculosis Report.” 2022.

[4] A. Calmette and C. Guérin, “Recherches expérimentales sur la défense de l’organisme contre l’infection tuberculeuse,” *Ann. Inst. Pasteur* , 1911.

[5] A. Calmette and C. Guérin, “Nouvelles recherches expérimentales sur la vaccination des bovidés contre la tuberculose,” *Ann. Inst. Pasteur* , 1920.

[6] M. S. Setia, C. Steinmaus, C. S. Ho, and G. W. Rutherford, “The role of BCG in prevention of leprosy: a meta-analysis,” *Lancet Infect. Dis.*, vol. 6, no. 3, pp. 162–170, Mar. 2006.

[7] E. Nemes *et al.*, “Prevention of M. tuberculosis Infection with H4:IC31 Vaccine or BCG Revaccination,” *N. Engl. J. Med.*, vol. 379, no. 2, pp. 138–149, Jul. 2018.

[8] B. B. Trunz, P. Fine, and C. Dye, “Effect of BCG vaccination on childhood tuberculous meningitis and miliary tuberculosis worldwide: a meta-analysis and assessment of cost-effectiveness,” *Lancet*, vol. 367, no. 9517, pp. 1173–1180, Apr. 2006.

[9] G. A. Coldwitz *et al.*, “The efficacy of bacillus Calmette-Guerin vaccination of newborns and infants in the prevention of tuberculosis: meta-analyses of the published literature. PEDIATRICS (ISSN 0031 4005). Copyright© 1995 by the American Academy of Pediatrics. 1995; 96 (1): 29-35.” .

[10] T. Cho, C. Khatchadourian, H. Nguyen, Y. Dara, S. Jung, and V. Venketaraman, “A review of the BCG vaccine and other approaches toward tuberculosis eradication,” *Hum. Vaccin. Immunother.*, vol. 17, no. 8, pp. 2454–2470, Aug. 2021.

[11] V. Tran, J. Liu, and M. A. Behr, “BCG Vaccines,” *Microbiol Spectr*, vol. 2, no. 1, pp. MGM2-0028–2013, Feb. 2014.

[12] J. A. Philips and J. D. Ernst, “Tuberculosis pathogenesis and immunity,” *Annu. Rev. Pathol.*, vol. 7, pp. 353–384, 2012.

[13] I. Comas *et al.*, “Out-of-Africa migration and Neolithic coexpansion of Mycobacterium tuberculosis with modern humans,” *Nat. Genet.*, vol. 45, no. 10, pp. 1176–1182, Oct. 2013.

[14] D. Brites and S. Gagneux, “Co-evolution of Mycobacterium tuberculosis and Homo sapiens,” *Immunol. Rev.*, vol. 264, no. 1, pp. 6–24, Mar. 2015.

[15] R. S. Flannagan, G. Cosío, and S. Grinstein, “Antimicrobial mechanisms of phagocytes and bacterial evasion strategies,” *Nat. Rev. Microbiol.*, vol. 7, no. 5, pp. 355–366, May 2009.

[16] J. M. Kinchen and K. S. Ravichandran, “Phagosome maturation: going through the acid test,” *Nat. Rev. Mol. Cell Biol.*, vol. 9, no. 10, pp. 781–795, Oct. 2008.

[17] I. Vergne, R. A. Fratti, P. J. Hill, J. Chua, J. Belisle, and V. Deretic, “Mycobacterium tuberculosis phagosome maturation arrest: mycobacterial phosphatidylinositol

analog phosphatidylinositol mannoside stimulates early endosomal fusion," *Mol. Biol. Cell*, vol. 15, no. 2, pp. 751–760, Feb. 2004.
[18] S. Sturgill-Koszycki *et al.*, "Lack of acidification in Mycobacterium phagosomes produced by exclusion of the vesicular proton-ATPase," *Science*, vol. 263, no. 5147, pp. 678–681, Feb. 1994.
[19] K. E. Zulauf, J. T. Sullivan, and M. Braunstein, "The SecA2 pathway of Mycobacterium tuberculosis exports effectors that work in concert to arrest phagosome and autophagosome maturation," *PLoS Pathog.*, vol. 14, no. 4, p. e1007011, Apr. 2018.
[20] S. A. Stanley, S. Raghavan, W. W. Hwang, and J. S. Cox, "Acute infection and macrophage subversion by Mycobacterium tuberculosis require a specialized secretion system," *Proc. Natl. Acad. Sci. U. S. A.*, vol. 100, no. 22, pp. 13001–13006, Oct. 2003.
[21] J. A. MacGurn and J. S. Cox, "A genetic screen for Mycobacterium tuberculosis mutants defective for phagosome maturation arrest identifies components of the ESX-1 secretion system," *Infect. Immun.*, vol. 75, no. 6, pp. 2668–2678, Jun. 2007.
[22] J. Augenstreich *et al.*, "ESX-1 and phthiocerol dimycocerosates of Mycobacterium tuberculosis act in concert to cause phagosomal rupture and host cell apoptosis," *Cell. Microbiol.*, vol. 19, no. 7, Jul. 2017.
[23] D. Houben *et al.*, "ESX-1-mediated translocation to the cytosol controls virulence of mycobacteria," *Cell. Microbiol.*, vol. 14, no. 8, pp. 1287–1298, Aug. 2012.
[24] N. van der Wel *et al.*, "M. tuberculosis and M. leprae translocate from the phagolysosome to the cytosol in myeloid cells," *Cell*, vol. 129, no. 7, pp. 1287–1298, Jun. 2007.
[25] R. Simeone *et al.*, "Phagosomal rupture by Mycobacterium tuberculosis results in toxicity and host cell death," *PLoS Pathog.*, vol. 8, no. 2, p. e1002507, Feb. 2012.
[26] L. M. Stamm *et al.*, "Mycobacterium marinum escapes from phagosomes and is propelled by actin-based motility," *J. Exp. Med.*, vol. 198, no. 9, pp. 1361–1368, Nov. 2003.
[27] E. Guirado and L. S. Schlesinger, "Modeling the Mycobacterium tuberculosis Granuloma - the Critical Battlefield in Host Immunity and Disease," *Front. Immunol.*, vol. 4, p. 98, Apr. 2013.
[28] M. Belton *et al.*, "Hypoxia and tissue destruction in pulmonary TB," *Thorax*, vol. 71, no. 12, pp. 1145–1153, Dec. 2016.
[29] M. M. Ravesloot-Chávez, E. Van Dis, and S. A. Stanley, "The Innate Immune Response to Mycobacterium tuberculosis Infection," *Annu. Rev. Immunol.*, vol. 39, pp. 611–637, Apr. 2021.
[30] A. Cohen, V. D. Mathiasen, T. Schön, and C. Wejse, "The global prevalence of latent tuberculosis: a systematic review and meta-analysis," *Eur. Respir. J.*, vol. 54, no. 3, Sep. 2019.
[31] R. M. G. J. Houben and P. J. Dodd, "The Global Burden of Latent Tuberculosis Infection: A Re-estimation Using Mathematical Modelling," *PLoS Med.*, vol. 13, no. 10, p. e1002152, Oct. 2016.
[32] G. Canetti, *The Tubercle Bacillus in the Pulmonary Lesion of Man: Histobacteriology and Its Bearing on the Therapy of Pulmonary Tuberculosis*. Springer Publishing Company, 1955.

[33] E. M. Medlar, S. Bernstein, and D. M. Steward, “A bacteriologic study of resected tuberculous lesions,” *Am. Rev. Tuberc.*, vol. 66, no. 1, pp. 36–43, Jul. 1952.
[34] F. Beck and D. Yegian, “A study of the tubercle bacillus in resected pulmonary lesions,” *Am. Rev. Tuberc.*, vol. 66, no. 1, pp. 44–51, Jul. 1952.
[35] L. G. Wayne, “Dynamics of submerged growth of Mycobacterium tuberculosis under aerobic and microaerophilic conditions,” *Am. Rev. Respir. Dis.*, vol. 114, no. 4, pp. 807–811, Oct. 1976.
[36] L. G. Wayne and L. G. Hayes, “An in vitro model for sequential study of shiftdown of Mycobacterium tuberculosis through two stages of nonreplicating persistence,” *Infect. Immun.*, vol. 64, no. 6, pp. 2062–2069, Jun. 1996.
[37] A. A. Velayati *et al.*, “Sequential adaptation in latent tuberculosis bacilli: observation by atomic force microscopy (AFM),” *Int. J. Clin. Exp. Med.*, vol. 4, no. 3, pp. 193–199, Sep. 2011.
[38] E. Iona, F. Giannoni, M. Pardini, L. Brunori, G. Orefici, and L. Fattorini, “Metronidazole plus rifampin sterilizes long-term dormant Mycobacterium tuberculosis,” *Antimicrob. Agents Chemother.*, vol. 51, no. 4, pp. 1537–1540, Apr. 2007.
[39] M. O. Shleeva, Y. K. Kudykina, G. N. Vostroknutova, N. E. Suzina, A. L. Mulyukin, and A. S. Kaprelyants, “Dormant ovoid cells of Mycobacterium tuberculosis are formed in response to gradual external acidification,” *Tuberculosis* , vol. 91, no. 2, pp. 146–154, Mar. 2011.
[40] R. J. H. Hammond, V. O. Baron, K. Oravcova, S. Lipworth, and S. H. Gillespie, “Phenotypic resistance in mycobacteria: is it because I am old or fat that I resist you?,” *J. Antimicrob. Chemother.*, vol. 70, no. 10, pp. 2823–2827, Jul. 2015.
[41] A. A. Velayati *et al.*, “Differences in cell wall thickness between resistant and nonresistant strains of Mycobacterium tuberculosis: using transmission electron microscopy,” *Chemotherapy*, vol. 55, no. 5, pp. 303–307, Jun. 2009.
[42] K. Jakkala and P. Ajitkumar, “Hypoxic Non-replicating Persistent Mycobacterium tuberculosis Develops Thickened Outer Layer That Helps in Restricting Rifampicin Entry,” *Front. Microbiol.*, vol. 10, p. 2339, Oct. 2019.
[43] J. Bacon *et al.*, “Non-replicating Mycobacterium tuberculosis elicits a reduced infectivity profile with corresponding modifications to the cell wall and extracellular matrix,” *PLoS One*, vol. 9, no. 2, p. e87329, Feb. 2014.
[44] K. Y. Rhee *et al.*, “Central carbon metabolism in Mycobacterium tuberculosis: an unexpected frontier,” *Trends Microbiol.*, vol. 19, no. 7, pp. 307–314, Jul. 2011.
[45] J. Monod, “THE GROWTH OF BACTERIAL CULTURES,” *Annu. Rev. Microbiol.*, vol. 3, no. 1, pp. 371–394, Oct. 1949.
[46] D. Chu and D. J. Barnes, “The lag-phase during diauxic growth is a trade-off between fast adaptation and high growth rate,” *Sci. Rep.*, vol. 6, p. 25191, Apr. 2016.
[47] L. P. S. de Carvalho, S. M. Fischer, J. Marrero, C. Nathan, S. Ehrt, and K. Y. Rhee, “Metabolomics of Mycobacterium tuberculosis reveals compartmentalized co-catabolism of carbon substrates,” *Chem. Biol.*, vol. 17, no. 10, pp. 1122–1131, Oct. 2010.
[48] D. F. Warner, “Mycobacterium tuberculosis metabolism,” *Cold Spring Harb. Perspect. Med.*, vol. 5, no. 4, Dec. 2014.

[49] K. Borah *et al.*, “Metabolic fluxes for nutritional flexibility of Mycobacterium tuberculosis,” *Mol. Syst. Biol.*, vol. 17, no. 5, p. e10280, May 2021.
[50] T. Noy *et al.*, “Central Role of Pyruvate Kinase in Carbon Co-catabolism of Mycobacterium tuberculosis,” *J. Biol. Chem.*, vol. 291, no. 13, pp. 7060–7069, Mar. 2016.
[51] S. Ehrt and K. Rhee, “Mycobacterium tuberculosis metabolism and host interaction: mysteries and paradoxes,” *Curr. Top. Microbiol. Immunol.*, vol. 374, pp. 163–188, 2013.
[52] K. M. Wilburn, R. A. Fieweger, and B. C. VanderVen, “Cholesterol and fatty acids grease the wheels of Mycobacterium tuberculosis pathogenesis,” *Pathog. Dis.*, vol. 76, no. 2, Mar. 2018.
[53] L. Shi *et al.*, “Carbon flux rerouting during Mycobacterium tuberculosis growth arrest,” *Mol. Microbiol.*, vol. 99, no. 6, p. 1179, Mar. 2016.
[54] J. Marrero, K. Y. Rhee, D. Schnappinger, K. Pethe, and S. Ehrt, “Gluconeogenic carbon flow of tricarboxylic acid cycle intermediates is critical for Mycobacterium tuberculosis to establish and maintain infection,” *Proc. Natl. Acad. Sci. U. S. A.*, vol. 107, no. 21, pp. 9819–9824, May 2010.
[55] E. J. Muñoz-Elías, A. M. Upton, J. Cherian, and J. D. McKinney, “Role of the methylcitrate cycle in Mycobacterium tuberculosis metabolism, intracellular growth, and virulence,” *Mol. Microbiol.*, vol. 60, no. 5, pp. 1109–1122, Jun. 2006.
[56] R. Van der Geize *et al.*, “A gene cluster encoding cholesterol catabolism in a soil actinomycete provides insight into Mycobacterium tuberculosis survival in macrophages,” *Proc. Natl. Acad. Sci. U. S. A.*, vol. 104, no. 6, pp. 1947–1952, Feb. 2007.
[57] E. J. Muñoz-Elías and J. D. McKinney, “Mycobacterium tuberculosis isocitrate lyases 1 and 2 are jointly required for in vivo growth and virulence,” *Nat. Med.*, vol. 11, no. 6, pp. 638–644, Jun. 2005.
[58] J. D. McKinney *et al.*, “Persistence of Mycobacterium tuberculosis in macrophages and mice requires the glyoxylate shunt enzyme isocitrate lyase,” *Nature*, vol. 406, no. 6797, pp. 735–738, Aug. 2000.
[59] H. Bloch and W. Segal, “Biochemical differentiation of Mycobacterium tuberculosis grown in vivo and in vitro,” *J. Bacteriol.*, vol. 72, no. 2, pp. 132–141, Aug. 1956.
[60] S. T. Cole *et al.*, “Deciphering the biology of Mycobacterium tuberculosis from the complete genome sequence,” *Nature*, vol. 393, no. 6685, pp. 537–544, Jun. 1998.
[61] R. M. Macnab, “Escherichia coli and Salmonella: cellular and molecular biology,” *Flagella and Motility*, 1996.
[62] P. Fontán, V. Aris, S. Ghanny, P. Soteropoulos, and I. Smith, “Global transcriptional profile of Mycobacterium tuberculosis during THP-1 human macrophage infection,” *Infect. Immun.*, vol. 76, no. 2, pp. 717–725, Feb. 2008.
[63] H. Rachman *et al.*, “Unique transcriptome signature of Mycobacterium tuberculosis in pulmonary tuberculosis,” *Infect. Immun.*, vol. 74, no. 2, pp. 1233–1242, Feb. 2006.
[64] K. H. Rohde, R. B. Abramovitch, and D. G. Russell, “Mycobacterium tuberculosis invasion of macrophages: linking bacterial gene expression to environmental cues,” *Cell Host Microbe*, vol. 2, no. 5, pp. 352–364, Nov. 2007.

[65] K. H. Rohde, D. F. T. Veiga, S. Caldwell, G. Balázsi, and D. G. Russell, “Linking the transcriptional profiles and the physiological states of Mycobacterium tuberculosis during an extended intracellular infection,” *PLoS Pathog.*, vol. 8, no. 6, p. e1002769, Jun. 2012.
[66] L. Tailleux *et al.*, “Probing host pathogen cross-talk by transcriptional profiling of both Mycobacterium tuberculosis and infected human dendritic cells and macrophages,” *PLoS One*, vol. 3, no. 1, p. e1403, Jan. 2008.
[67] E. Dubnau, J. Chan, V. P. Mohan, and I. Smith, “responses of mycobacterium tuberculosis to growth in the mouse lung,” *Infect. Immun.*, vol. 73, no. 6, pp. 3754–3757, Jun. 2005.
[68] D. Schnappinger *et al.*, “Transcriptional Adaptation of Mycobacterium tuberculosis within Macrophages: Insights into the Phagosomal Environment,” *J. Exp. Med.*, vol. 198, no. 5, pp. 693–704, Sep. 2003.
[69] M. Jackson, “The mycobacterial cell envelope-lipids,” *Cold Spring Harb. Perspect. Med.*, vol. 4, no. 10, Aug. 2014.
[70] M. Jankute, J. A. G. Cox, J. Harrison, and G. S. Besra, “Assembly of the Mycobacterial Cell Wall,” *Annu. Rev. Microbiol.*, vol. 69, pp. 405–423, 2015.
[71] E. V. Nazarova *et al.*, “Rv3723/LucA coordinates fatty acid and cholesterol uptake in Mycobacterium tuberculosis,” *Elife*, vol. 6, Jun. 2017.
[72] E. V. Nazarova, C. R. Montague, L. Huang, T. La, D. Russell, and B. C. VanderVen, “The genetic requirements of fatty acid import by Mycobacterium tuberculosis within macrophages,” *Elife*, vol. 8, Feb. 2019.
[73] J. T. Talley and S. S. Mohiuddin, *Biochemistry, Fatty Acid Oxidation*. StatPearls Publishing, 2023.
[74] K. Takayama, C. Wang, and G. S. Besra, “Pathway to synthesis and processing of mycolic acids in Mycobacterium tuberculosis,” *Clin. Microbiol. Rev.*, vol. 18, no. 1, pp. 81–101, Jan. 2005.
[75] H. Marrakchi, M.-A. Lanéelle, and M. Daffé, “Mycolic Acids: Structures, Biosynthesis, and Beyond,” *Chem. Biol.*, vol. 21, no. 1, pp. 67–85, Jan. 2014.
[76] J. Daniel *et al.*, “Induction of a novel class of diacylglycerol acyltransferases and triacylglycerol accumulation in Mycobacterium tuberculosis as it goes into a dormancy-like state in culture,” *J. Bacteriol.*, vol. 186, no. 15, pp. 5017–5030, Aug. 2004.
[77] R. K. Maurya, S. Bharti, and M. Y. Krishnan, “Triacylglycerols: Fuelling the Hibernating Mycobacterium tuberculosis,” *Front. Cell. Infect. Microbiol.*, vol. 8, p. 450, 2018.
[78] N. J. Garton, H. Christensen, D. E. Minnikin, R. A. Adegbola, and M. R. Barer, “Intracellular lipophilic inclusions of mycobacteria in vitro and in sputum,” *Microbiology*, vol. 148, no. Pt 10, pp. 2951–2958, Oct. 2002.
[79] H. Christensen, N. J. Garton, R. W. Horobin, D. E. Minnikin, and M. R. Barer, “Lipid domains of mycobacteria studied with fluorescent molecular probes,” *Mol. Microbiol.*, vol. 31, no. 5, pp. 1561–1572, Mar. 1999.
[80] R. Bansal-Mutalik and H. Nikaido, “Mycobacterial outer membrane is a lipid bilayer and the inner membrane is unusually rich in diacyl phosphatidylinositol dimannosides,” *Proc. Natl. Acad. Sci. U. S. A.*, vol. 111, no. 13, pp. 4958–4963, Apr. 2014.

[81] A. Ortalo-Magné *et al.*, “Identification of the surface-exposed lipids on the cell envelopes of Mycobacterium tuberculosis and other mycobacterial species,” *J. Bacteriol.*, vol. 178, no. 2, pp. 456–461, Jan. 1996.
[82] C. Zhang and P. Liu, “The lipid droplet: A conserved cellular organelle,” *Protein Cell*, vol. 8, no. 11, pp. 796–800, Nov. 2017.
[83] R. V. Farese Jr and T. C. Walther, “Lipid droplets finally get a little R-E-S-P-E-C-T,” *Cell*, vol. 139, no. 5, pp. 855–860, Nov. 2009.
[84] J. A. Olzmann and P. Carvalho, “Dynamics and functions of lipid droplets,” *Nat. Rev. Mol. Cell Biol.*, vol. 20, no. 3, pp. 137–155, Mar. 2019.
[85] M. Wältermann and A. Steinbüchel, “Neutral lipid bodies in prokaryotes: recent insights into structure, formation, and relationship to eukaryotic lipid depots,” *J. Bacteriol.*, vol. 187, no. 11, pp. 3607–3619, Jun. 2005.
[86] D. J. Murphy, “The dynamic roles of intracellular lipid droplets: from archaea to mammals,” *Protoplasma*, vol. 249, no. 3, pp. 541–585, Jul. 2012.
[87] K. Tauchi-Sato, S. Ozeki, T. Houjou, R. Taguchi, and T. Fujimoto, “The Surface of Lipid Droplets Is a Phospholipid Monolayer with a Unique Fatty Acid Composition*,” *J. Biol. Chem.*, vol. 277, no. 46, pp. 44507–44512, Nov. 2002.
[88] H. Khandelia, L. Duelund, K. I. Pakkanen, and J. H. Ipsen, “Triglyceride blisters in lipid bilayers: implications for lipid droplet biogenesis and the mobile lipid signal in cancer cell membranes,” *PLoS One*, vol. 5, no. 9, p. e12811, Sep. 2010.
[89] L. Duelund *et al.*, “Composition, structure and properties of POPC–triolein mixtures. Evidence of triglyceride domains in phospholipid bilayers,” *Biochimica et Biophysica Acta (BBA) - Biomembranes*, vol. 1828, no. 8, pp. 1909–1917, Aug. 2013.
[90] A. R. Thiam and L. Forêt, “The physics of lipid droplet nucleation, growth and budding,” *Biochim. Biophys. Acta*, vol. 1861, no. 8 Pt A, pp. 715–722, Aug. 2016.
[91] O. Adeyo *et al.*, “The yeast lipin orthologue Pah1p is important for biogenesis of lipid droplets,” *J. Cell Biol.*, vol. 192, no. 6, pp. 1043–1055, Mar. 2011.
[92] W. Fei *et al.*, “A Role for Phosphatidic Acid in the Formation of ‘Supersized’ Lipid Droplets,” *PLoS Genet.*, vol. 7, no. 7, p. e1002201, Jul. 2011.
[93] J. R. Skinner *et al.*, “Diacylglycerol enrichment of endoplasmic reticulum or lipid droplets recruits perilipin 3/TIP47 during lipid storage and mobilization,” *J. Biol. Chem.*, vol. 284, no. 45, pp. 30941–30948, Nov. 2009.
[94] K. Ben M’barek, D. Ajjaji, A. Chorlay, S. Vanni, L. Forêt, and A. R. Thiam, “ER Membrane Phospholipids and Surface Tension Control Cellular Lipid Droplet Formation,” *Dev. Cell*, vol. 41, no. 6, pp. 591-604.e7, Jun. 2017.
[95] B. Kadereit *et al.*, “Evolutionarily conserved gene family important for fat storage,” *Proc. Natl. Acad. Sci. U. S. A.*, vol. 105, no. 1, pp. 94–99, Jan. 2008.
[96] W. Fei *et al.*, “Fld1p, a functional homologue of human seipin, regulates the size of lipid droplets in yeast,” *J. Cell Biol.*, vol. 180, no. 3, pp. 473–482, Feb. 2008.
[97] H. Wang *et al.*, “Seipin is required for converting nascent to mature lipid droplets,” *Elife*, vol. 5, Aug. 2016.
[98] Q. Gao *et al.*, “Pet10p is a yeast perilipin that stabilizes lipid droplets and promotes their assembly,” *J. Cell Biol.*, vol. 216, no. 10, pp. 3199–3217, Oct. 2017.
[99] V. Choudhary, N. Ojha, A. Golden, and W. A. Prinz, “A conserved family of proteins facilitates nascent lipid droplet budding from the ER,” *J. Cell Biol.*, vol. 211, no. 2, pp. 261–271, Oct. 2015.

[100] W. A. Prinz, “Bridging the gap: membrane contact sites in signaling, metabolism, and organelle dynamics,” *J. Cell Biol.*, vol. 205, no. 6, pp. 759–769, Jun. 2014.
[101] A. M. Valm *et al.*, “Applying systems-level spectral imaging and analysis to reveal the organelle interactome,” *Nature*, vol. 546, no. 7656, pp. 162–167, Jun. 2017.
[102] E. Currie *et al.*, “High confidence proteomic analysis of yeast LDs identifies additional droplet proteins and reveals connections to dolichol synthesis and sterol acetylation,” *J. Lipid Res.*, vol. 55, no. 7, pp. 1465–1477, Jul. 2014.
[103] K. Bersuker *et al.*, “A Proximity Labeling Strategy Provides Insights into the Composition and Dynamics of Lipid Droplet Proteomes,” *Dev. Cell*, vol. 44, no. 1, pp. 97-112.e7, Jan. 2018.
[104] C. Moessinger, L. Kuerschner, J. Spandl, A. Shevchenko, and C. Thiele, “Human lysophosphatidylcholine acyltransferases 1 and 2 are located in lipid droplets where they catalyze the formation of phosphatidylcholine,” *J. Biol. Chem.*, vol. 286, no. 24, pp. 21330–21339, Jun. 2011.
[105] C. Chitraju *et al.*, “Triglyceride Synthesis by DGAT1 Protects Adipocytes from Lipid-Induced ER Stress during Lipolysis,” *Cell Metab.*, vol. 26, no. 2, pp. 407-418.e3, Aug. 2017.
[106] T. B. Nguyen *et al.*, “DGAT1-Dependent Lipid Droplet Biogenesis Protects Mitochondrial Function during Starvation-Induced Autophagy,” *Dev. Cell*, vol. 42, no. 1, pp. 9-21.e5, Jul. 2017.
[107] M. A. Schmidt and E. M. Herman, “Suppression of soybean oleosin produces micro-oil bodies that aggregate into oil body/ER complexes,” *Mol. Plant*, vol. 1, no. 6, pp. 910–924, Nov. 2008.
[108] R. C. N. Melo, H. D’Avila, D. L. Fabrino, P. E. Almeida, and P. T. Bozza, “Macrophage lipid body induction by Chagas disease in vivo: putative intracellular domains for eicosanoid formation during infection,” *Tissue Cell*, vol. 35, no. 1, pp. 59–67, Feb. 2003.
[109] C. Bandeira-Melo, M. Phoofolo, and P. F. Weller, “Extranuclear Lipid Bodies, Elicited by CCR3-mediated Signaling Pathways, Are the Sites of Chemokine-enhanced Leukotriene C4 Production in Eosinophils and Basophils *,” *J. Biol. Chem.*, vol. 276, no. 25, pp. 22779–22787, Jun. 2001.
[110] P. Pacheco *et al.*, “Lipopolysaccharide-induced leukocyte lipid body formation in vivo: innate immunity elicited intracellular Loci involved in eicosanoid metabolism,” *J. Immunol.*, vol. 169, no. 11, pp. 6498–6506, Dec. 2002.
[111] S. Cermelli, Y. Guo, S. P. Gross, and M. A. Welte, “The lipid-droplet proteome reveals that droplets are a protein-storage depot,” *Curr. Biol.*, vol. 16, no. 18, pp. 1783–1795, Sep. 2006.
[112] K. J. Helbig *et al.*, “The antiviral protein viperin inhibits hepatitis C virus replication via interaction with nonstructural protein 5A,” *Hepatology*, vol. 54, no. 5, pp. 1506–1517, Nov. 2011.
[113] E. R. Hinson and P. Cresswell, “The antiviral protein, viperin, localizes to lipid droplets via its N-terminal amphipathic α-helix,” *Proceedings of the National Academy of Sciences*, vol. 106, no. 48, pp. 20452–20457, 2009.
[114] S. Virtue and A. Vidal-Puig, “Adipose tissue expandability, lipotoxicity and the Metabolic Syndrome--an allostatic perspective,” *Biochim. Biophys. Acta*, vol. 1801, no. 3, pp. 338–349, Mar. 2010.

[115] N. Krahmer, R. V. Farese Jr, and T. C. Walther, “Balancing the fat: lipid droplets and human disease,” *EMBO Mol. Med.*, vol. 5, no. 7, pp. 973–983, Jul. 2013.
[116] J. M. Inloes *et al.*, “The hereditary spastic paraplegia-related enzyme DDHD2 is a principal brain triglyceride lipase,” *Proc. Natl. Acad. Sci. U. S. A.*, vol. 111, no. 41, pp. 14924–14929, Oct. 2014.
[117] M. Wältermann *et al.*, “Mechanism of lipid-body formation in prokaryotes: how bacteria fatten up,” *Mol. Microbiol.*, vol. 55, no. 3, pp. 750–763, Feb. 2005.
[118] D. P. MacEachran, M. E. Prophete, and A. J. Sinskey, “The Rhodococcus opacus PD630 heparin-binding hemagglutinin homolog TadA mediates lipid body formation,” *Appl. Environ. Microbiol.*, vol. 76, no. 21, pp. 7217–7225, Nov. 2010.
[119] H. M. Alvarez, M. F. Souto, A. Viale, and O. H. Pucci, “Biosynthesis of fatty acids and triacylglycerols by 2,6,10,14-tetramethyl pentadecane-grown cells of Nocardia globerula 432,” *FEMS Microbiol. Lett.*, vol. 200, no. 2, pp. 195–200, Jun. 2001.
[120] C. Zhang *et al.*, “Bacterial lipid droplets bind to DNA via an intermediary protein that enhances survival under stress,” *Nat. Commun.*, vol. 8, p. 15979, Jul. 2017.
[121] K. L. Burdon, “Fatty Material in Bacteria and Fungi Revealed by Staining Dried, Fixed Slide Preparations,” *J. Bacteriol.*, vol. 52, no. 6, pp. 665–678, Dec. 1946.
[122] Burdon Kenneth L., “Disparity in Appearance of True Hansen’s Bacilli and Cultured ”Leprosy Bacilli” When Stained for Fat,” *J. Bacteriol.*, vol. 52, no. 6, pp. 679–680, Dec. 1946.
[123] H. L. Sheehan and F. Whitwell, “The staining of tubercle bacilli with Sudan black B,” *J. Pathol. Bacteriol.*, vol. 61, no. 2, pp. 269–71, pl, Apr. 1949.
[124] N. J. Garton *et al.*, “Cytological and transcript analyses reveal fat and lazy persister-like bacilli in tuberculous sputum,” *PLoS Med.*, vol. 5, no. 4, p. e75, Apr. 2008.
[125] I. Mallick *et al.*, “Intrabacterial lipid inclusions in mycobacteria: unexpected key players in survival and pathogenesis?,” *FEMS Microbiol. Rev.*, vol. 45, no. 6, Nov. 2021.
[126] T. Iuvone, R. Carnuccio, and M. Di Rosa, “Modulation of granuloma formation by endogenous nitric oxide,” *Eur. J. Pharmacol.*, vol. 265, no. 1–2, pp. 89–92, Nov. 1994.
[127] H.-D. Park *et al.*, “Rv3133c/dosR is a transcription factor that mediates the hypoxic response of Mycobacterium tuberculosis,” *Mol. Microbiol.*, vol. 48, no. 3, pp. 833–843, May 2003.
[128] S. Huang, W. Zhou, W. Tang, Y. Zhang, Y. Hu, and S. Chen, “Genome-scale analyses of transcriptional start sites in Mycobacterium marinum under normoxic and hypoxic conditions,” *BMC Genomics*, vol. 22, no. 1, p. 235, Apr. 2021.
[129] T. D. Sirakova *et al.*, “Identification of a diacylglycerol acyltransferase gene involved in accumulation of triacylglycerol in Mycobacterium tuberculosis under stress,” *Microbiology*, vol. 152, no. Pt 9, pp. 2717–2725, Sep. 2006.
[130] P. Santucci *et al.*, “Nitrogen deprivation induces triacylglycerol accumulation, drug tolerance and hypervirulence in mycobacteria,” *Sci. Rep.*, vol. 9, no. 1, p. 8667, Jun. 2019.
[131] S. Vijay *et al.*, “Ultrastructural Analysis of Cell Envelope and Accumulation of Lipid Inclusions in Clinical Mycobacterium tuberculosis Isolates from Sputum, Oxidative Stress, and Iron Deficiency,” *Front. Microbiol.*, vol. 8, p. 2681, 2017.

[132] H. Ohno *et al.*, “The effects of reactive nitrogen intermediates on gene expression in Mycobacterium tuberculosis,” *Cell. Microbiol.*, vol. 5, no. 9, pp. 637–648, Sep. 2003.
[133] M. I. Voskuil *et al.*, “Inhibition of respiration by nitric oxide induces a Mycobacterium tuberculosis dormancy program,” *J. Exp. Med.*, vol. 198, no. 5, pp. 705–713, Sep. 2003.
[134] D. Raze *et al.*, “Heparin-Binding Hemagglutinin Adhesin (HBHA) Is Involved in Intracytosolic Lipid Inclusions Formation in Mycobacteria,” *Front. Microbiol.*, vol. 9, p. 2258, Sep. 2018.
[135] J. Daniel, N. Kapoor, T. Sirakova, R. Sinha, and P. Kolattukudy, “The perilipin-like PPE15 protein in Mycobacterium tuberculosis is required for triacylglycerol accumulation under dormancy-inducing conditions,” *Mol. Microbiol.*, vol. 101, no. 5, pp. 784–794, Sep. 2016.
[136] R. M. Armstrong, D. C. Carter, S. N. Atkinson, S. S. Terhune, and T. C. Zahrt, “Association of Mycobacterium Proteins with Lipid Droplets,” *J. Bacteriol.*, vol. 200, no. 16, Aug. 2018.
[137] B. W. James, A. Williams, and P. D. Marsh, “The physiology and pathogenicity of Mycobacterium tuberculosis grown under controlled conditions in a defined medium,” *J. Appl. Microbiol.*, vol. 88, no. 4, pp. 669–677, Apr. 2000.
[138] W. D. Travis, L. B. Travis, G. D. Roberts, D. W. Su, and L. W. Weiland, “The histopathologic spectrum in Mycobacterium marinum infection,” *Arch. Pathol. Lab. Med.*, vol. 109, no. 12, pp. 1109–1113, Dec. 1985.
[139] J. Aronson, “Spontaneous Tuberculosis in Salt Water Fish,” *J. Infect. Dis.*, vol. 39, no. 4, pp. 315–320, 1926.
[140] S. Swift and H. Cohen, “Granulomas of the skin due to Mycobacterium balnei after abrasions from a fish tank,” *N. Engl. J. Med.*, vol. 267, pp. 1244–1246, Dec. 1962.
[141] H. F. Clark and C. C. Shepard, “EFFECT OF ENVIRONMENTAL TEMPERATURES ON INFECTION WITH MYCOBACTERIUM MARINUM (BALNEI) OF MICE AND A NUMBER OF POIKILOTHERMIC SPECIES,” *J. Bacteriol.*, vol. 86, no. 5, pp. 1057–1069, Nov. 1963.
[142] S. Kurokawa *et al.*, “Comparative genome analysis of fish and human isolates of Mycobacterium marinum,” *Mar. Biotechnol.* , vol. 15, no. 5, pp. 596–605, Oct. 2013.
[143] T. Rogall, J. Wolters, T. Flohr, and E. C. Böttger, “Towards a phylogeny and definition of species at the molecular level within the genus Mycobacterium,” *Int. J. Syst. Bacteriol.*, vol. 40, no. 4, pp. 323–330, Oct. 1990.
[144] T. Tønjum, D. B. Welty, E. Jantzen, and P. L. Small, “Differentiation of Mycobacterium ulcerans, M. marinum, and M. haemophilum: mapping of their relationships to M. tuberculosis by fatty acid profile analysis, DNA-DNA hybridization, and 16S rRNA gene sequence analysis,” *J. Clin. Microbiol.*, vol. 36, no. 4, pp. 918–925, Apr. 1998.
[145] J. M. Davis, H. Clay, J. L. Lewis, N. Ghori, P. Herbomel, and L. Ramakrishnan, “Real-time visualization of mycobacterium-macrophage interactions leading to initiation of granuloma formation in zebrafish embryos,” *Immunity*, vol. 17, no. 6, pp. 693–702, Dec. 2002.

[146] H. Myllymäki, C. A. Bäuerlein, and M. Rämet, “The Zebrafish Breathes New Life into the Study of Tuberculosis,” *Front. Immunol.*, vol. 7, p. 196, May 2016.
[147] C. Barisch, P. Paschke, M. Hagedorn, M. Maniak, and T. Soldati, “Lipid droplet dynamics at early stages of Mycobacterium marinum infection in Dictyostelium,” *Cell. Microbiol.*, vol. 17, no. 9, pp. 1332–1349, Sep. 2015.
[148] C. Barisch and T. Soldati, “Mycobacterium marinum Degrades Both Triacylglycerols and Phospholipids from Its Dictyostelium Host to Synthesise Its Own Triacylglycerols and Generate Lipid Inclusions,” *PLoS Pathog.*, vol. 13, no. 1, p. e1006095, Jan. 2017.
[149] M. Parikka *et al.*, “Mycobacterium marinum causes a latent infection that can be reactivated by gamma irradiation in adult zebrafish,” *PLoS Pathog.*, vol. 8, no. 9, p. e1002944, Sep. 2012.
[150] J. Jiang *et al.*, “Transcriptome Changes of Mycobacterium marinum in the Process of Resuscitation From Hypoxia-Induced Dormancy,” *Front. Genet.*, vol. 10, p. 1359, 2019.
[151] T. P. Stinear *et al.*, “Insights from the complete genome sequence of Mycobacterium marinum on the evolution of Mycobacterium tuberculosis,” *Genome Res.*, vol. 18, no. 5, pp. 729–741, May 2008.
[152] Q. Zhang *et al.*, “EsxA membrane-permeabilizing activity plays a key role in mycobacterial cytosolic translocation and virulence: effects of single-residue mutations at glutamine 5,” *Sci. Rep.*, vol. 6, p. 32618, Sep. 2016.
[153] M. Hagedorn, K. H. Rohde, D. G. Russell, and T. Soldati, “Infection by tubercular mycobacteria is spread by nonlytic ejection from their amoeba hosts,” *Science*, vol. 323, no. 5922, pp. 1729–1733, Mar. 2009.
[154] C. L. Cosma, D. R. Sherman, and L. Ramakrishnan, “The secret lives of the pathogenic mycobacteria,” *Annu. Rev. Microbiol.*, vol. 57, pp. 641–676, 2003.
[155] G. Gago, L. Diacovich, and H. Gramajo, “Lipid metabolism and its implication in mycobacteria-host interaction,” *Curr. Opin. Microbiol.*, vol. 41, pp. 36–42, Feb. 2018.
[156] D. G. Russell, P.-J. Cardona, M.-J. Kim, S. Allain, and F. Altare, “Foamy macrophages and the progression of the human tuberculosis granuloma,” *Nat. Immunol.*, vol. 10, no. 9, pp. 943–948, Sep. 2009.
[157] A. Gioffré *et al.*, “Mutation in mce operons attenuates Mycobacterium tuberculosis virulence,” *Microbes Infect.*, vol. 7, no. 3, pp. 325–334, Mar. 2005.
[158] I. Caire-Brändli *et al.*, “Reversible lipid accumulation and associated division arrest of Mycobacterium avium in lipoprotein-induced foamy macrophages may resemble key events during latency and reactivation of tuberculosis,” *Infect. Immun.*, vol. 82, no. 2, pp. 476–490, Feb. 2014.
[159] A. P. Velázquez, T. Tatsuta, R. Ghillebert, I. Drescher, and M. Graef, “Lipid droplet-mediated ER homeostasis regulates autophagy and cell survival during starvation,” *J. Cell Biol.*, vol. 212, no. 6, pp. 621–631, Mar. 2016.
[160] R. J. Schulze, A. Sathyanarayan, and D. G. Mashek, “Breaking fat: The regulation and mechanisms of lipophagy,” *Biochim. Biophys. Acta Mol. Cell Biol. Lipids*, vol. 1862, no. 10 Pt B, pp. 1178–1187, Oct. 2017.

[161] P. T. Bozza, I. Bakker-Abreu, R. A. Navarro-Xavier, and C. Bandeira-Melo, “Lipid body function in eicosanoid synthesis: an update,” *Prostaglandins Leukot. Essent. Fatty Acids*, vol. 85, no. 5, pp. 205–213, Nov. 2011.
[162] J. Quillaguamán, H. Guzmán, D. Van-Thuoc, and R. Hatti-Kaul, “Synthesis and production of polyhydroxyalkanoates by halophiles: current potential and future prospects,” *Appl. Microbiol. Biotechnol.*, vol. 85, no. 6, pp. 1687–1696, Feb. 2010.
[163] A. Steinbüchel and B. Füchtenbusch, “Bacterial and other biological systems for polyester production,” *Trends Biotechnol.*, vol. 16, no. 10, pp. 419–427, Oct. 1998.
[164] H. M. Alvarez and A. Steinbüchel, “Triacylglycerols in prokaryotic microorganisms,” *Appl. Microbiol. Biotechnol.*, vol. 60, no. 4, pp. 367–376, Dec. 2002.
[165] L. G. Wayne and C. D. Sohaskey, “Nonreplicating persistence of mycobacterium tuberculosis,” *Annu. Rev. Microbiol.*, vol. 55, pp. 139–163, 2001.
[166] L. E. Via *et al.*, “Tuberculous granulomas are hypoxic in guinea pigs, rabbits, and nonhuman primates,” *Infect. Immun.*, vol. 76, no. 6, pp. 2333–2340, Jun. 2008.
[167] K. L. Low *et al.*, “Triacylglycerol utilization is required for regrowth of in vitro hypoxic nonreplicating Mycobacterium bovis bacillus Calmette-Guerin,” *J. Bacteriol.*, vol. 191, no. 16, pp. 5037–5043, Aug. 2009.
[168] J. Daniel, H. Maamar, C. Deb, T. D. Sirakova, and P. E. Kolattukudy, “Mycobacterium tuberculosis uses host triacylglycerol to accumulate lipid droplets and acquires a dormancy-like phenotype in lipid-loaded macrophages,” *PLoS Pathog.*, vol. 7, no. 6, p. e1002093, Jun. 2011.
[169] M. Knight, J. Braverman, K. Asfaha, K. Gronert, and S. Stanley, “Lipid droplet formation in Mycobacterium tuberculosis infected macrophages requires IFN-γ/HIF-1α signaling and supports host defense,” *PLoS Pathog.*, vol. 14, no. 1, p. e1006874, Jan. 2018.
[170] J. Blanchette, M. Jaramillo, and M. Olivier, “Signalling events involved in interferon-gamma-inducible macrophage nitric oxide generation,” *Immunology*, vol. 108, no. 4, pp. 513–522, Apr. 2003.
[171] A. J. Martinot *et al.*, “Mycobacterial Metabolic Syndrome: LprG and Rv1410 Regulate Triacylglyceride Levels, Growth Rate and Virulence in Mycobacterium tuberculosis,” *PLoS Pathog.*, vol. 12, no. 1, p. e1005351, Jan. 2016.
[172] T. Parish, “Electroporation of Mycobacteria,” *Methods Mol. Biol.*, vol. 2314, pp. 273–284, 2021.
[173] K. H. Darwin, S. Ehrt, J.-C. Gutierrez-Ramos, N. Weich, and C. F. Nathan, “The proteasome of Mycobacterium tuberculosis is required for resistance to nitric oxide,” *Science*, vol. 302, no. 5652, pp. 1963–1966, Dec. 2003.
[174] L. L. Listenberger and D. A. Brown, “Fluorescent detection of lipid droplets and associated proteins,” *Curr. Protoc. Cell Biol.*, vol. Chapter 24, p. Unit 24.2, Jun. 2007.
[175] M. P. Weir, W. H. Langridge 3rd, and R. W. Walker, “Relationships between oleic acid uptake and lipid metabolism in Mycobacterium smegmatis,” *Am. Rev. Respir. Dis.*, vol. 106, no. 3, pp. 450–457, Sep. 1972.
[176] C. McCarthy, “Utilization of palmitic acid by Mycobacterium avium,” *Infect. Immun.*, vol. 4, no. 3, pp. 199–204, Sep. 1971.

[177] J. G. Rodríguez *et al.*, “Global adaptation to a lipid environment triggers the dormancy-related phenotype of Mycobacterium tuberculosis,” *MBio*, vol. 5, no. 3, pp. e01125-14, May 2014.
[178] N. Sukumar, S. Tan, B. B. Aldridge, and D. G. Russell, “Exploitation of Mycobacterium tuberculosis reporter strains to probe the impact of vaccination at sites of infection,” *PLoS Pathog.*, vol. 10, no. 9, p. e1004394, Sep. 2014.
[179] W. B. Schaefer and C. W. Lewis Jr, “Effect of oleic acid on growth and cell structure of mycobacteria,” *J. Bacteriol.*, vol. 90, no. 5, pp. 1438–1447, Nov. 1965.
[180] A. S. Greenberg, J. J. Egan, S. A. Wek, N. B. Garty, E. J. Blanchette-Mackie, and C. Londos, “Perilipin, a major hormonally regulated adipocyte-specific phosphoprotein associated with the periphery of lipid storage droplets,” *J. Biol. Chem.*, vol. 266, no. 17, pp. 11341–11346, Jun. 1991.
[181] L. E. Swaim, L. E. Connolly, H. E. Volkman, O. Humbert, D. E. Born, and L. Ramakrishnan, “Mycobacterium marinum infection of adult zebrafish causes caseating granulomatous tuberculosis and is moderated by adaptive immunity,” *Infect. Immun.*, vol. 74, no. 11, pp. 6108–6117, Nov. 2006.
[182] R. Heintzmann and T. Huser, “Super-Resolution Structured Illumination Microscopy,” *Chem. Rev.*, vol. 117, no. 23, pp. 13890–13908, Dec. 2017.
[183] N. Jacquier, V. Choudhary, M. Mari, A. Toulmay, F. Reggiori, and R. Schneiter, “Lipid droplets are functionally connected to the endoplasmic reticulum in Saccharomyces cerevisiae,” *J. Cell Sci.*, vol. 124, no. Pt 14, pp. 2424–2437, Jul. 2011.
[184] F. Wilfling *et al.*, “Triacylglycerol synthesis enzymes mediate lipid droplet growth by relocalizing from the ER to lipid droplets,” *Dev. Cell*, vol. 24, no. 4, pp. 384–399, Feb. 2013.
[185] M. B. Reed, S. Gagneux, K. Deriemer, P. M. Small, and C. E. Barry 3rd, “The W-Beijing lineage of Mycobacterium tuberculosis overproduces triglycerides and has the DosR dormancy regulon constitutively upregulated,” *J. Bacteriol.*, vol. 189, no. 7, pp. 2583–2589, Apr. 2007.
[186] P. Domenech *et al.*, “Unique Regulation of the DosR Regulon in the Beijing Lineage of Mycobacterium tuberculosis,” *J. Bacteriol.*, vol. 199, no. 2, Jan. 2017.
[187] V. Choudhary *et al.*, “Architecture of Lipid Droplets in Endoplasmic Reticulum Is Determined by Phospholipid Intrinsic Curvature,” *Curr. Biol.*, vol. 28, no. 6, pp. 915-926.e9, Mar. 2018.
[188] C. M. Sassetti and E. J. Rubin, “Genetic requirements for mycobacterial survival during infection,” *Proc. Natl. Acad. Sci. U. S. A.*, vol. 100, no. 22, pp. 12989–12994, Oct. 2003.
[189] S.-H. Baek, A. H. Li, and C. M. Sassetti, “Metabolic regulation of mycobacterial growth and antibiotic sensitivity,” *PLoS Biol.*, vol. 9, no. 5, p. e1001065, May 2011.
[190] A. Blumenthal, C. Trujillo, S. Ehrt, and D. Schnappinger, “Simultaneous analysis of multiple Mycobacterium tuberculosis knockdown mutants in vitro and in vivo,” *PLoS One*, vol. 5, no. 12, p. e15667, Dec. 2010.
[191] C. Deb *et al.*, “A novel in vitro multiple-stress dormancy model for Mycobacterium tuberculosis generates a lipid-loaded, drug-tolerant, dormant pathogen,” *PLoS One*, vol. 4, no. 6, p. e6077, Jun. 2009.

[192] O. Quehenberger, A. Armando, D. Dumlao, D. L. Stephens, and E. A. Dennis, “Lipidomics analysis of essential fatty acids in macrophages,” *Prostaglandins Leukot. Essent. Fatty Acids*, vol. 79, no. 3–5, pp. 123–129, Nov. 2008.
[193] N. S. Hill and M. D. Welch, “A glycine-rich PE_PGRS protein governs mycobacterial actin-based motility,” *Nat. Commun.*, vol. 13, no. 1, p. 3608, Jun. 2022.
[194] B. Qiu and M. C. Simon, “BODIPY 493/503 Staining of Neutral Lipid Droplets for Microscopy and Quantification by Flow Cytometry,” *Bio Protoc*, vol. 6, no. 17, Sep. 2016.
[195] M. I. Samanovic, H. Li, and K. H. Darwin, “The pup-proteasome system of Mycobacterium tuberculosis,” *Subcell. Biochem.*, vol. 66, pp. 267–295, 2013.
[196] A. Pavić *et al.*, “Functional Characterization of the γ-Aminobutyric Acid Transporter from Mycobacterium smegmatis MC2 155 Reveals Sodium-Driven GABA Transport,” *J. Bacteriol.*, vol. 203, no. 4, Jan. 2021.
[197] S. Michaeli and H. Fromm, “Closing the loop on the GABA shunt in plants: are GABA metabolism and signaling entwined?,” *Front. Plant Sci.*, vol. 6, p. 419, Jun. 2015.
[198] C. Feehily and K. A. G. Karatzas, “Role of glutamate metabolism in bacterial responses towards acid and other stresses,” *J. Appl. Microbiol.*, vol. 114, no. 1, pp. 11–24, Jan. 2013.
[199] R. A. Festa *et al.*, “Prokaryotic ubiquitin-like protein (Pup) proteome of Mycobacterium tuberculosis [corrected],” *PLoS One*, vol. 5, no. 1, p. e8589, Jan. 2010.
[200] C. Poulsen *et al.*, “Proteome-wide identification of mycobacterial pupylation targets,” *Mol. Syst. Biol.*, vol. 6, p. 386, Jul. 2010.
[201] J. Watrous *et al.*, “Expansion of the mycobacterial ‘PUPylome,’” *Mol. Biosyst.*, vol. 6, no. 2, pp. 376–385, Feb. 2010.
[202] F. Striebel, F. Imkamp, M. Sutter, M. Steiner, A. Mamedov, and E. Weber-Ban, “Bacterial ubiquitin-like modifier Pup is deamidated and conjugated to substrates by distinct but homologous enzymes,” *Nat. Struct. Mol. Biol.*, vol. 16, no. 6, pp. 647–651, Jun. 2009.
[203] C. M. Sassetti, D. H. Boyd, and E. J. Rubin, “Genes required for mycobacterial growth defined by high density mutagenesis,” *Mol. Microbiol.*, vol. 48, no. 1, pp. 77–84, Apr. 2003.
[204] K. Förster-Fromme and D. Jendrossek, “Identification and characterization of the acyclic terpene utilization gene cluster of Pseudomonas citronellolis,” *FEMS Microbiol. Lett.*, vol. 264, no. 2, pp. 220–225, Nov. 2006.
[205] T. Parbhoo, H. Schurz, J. M. Mouton, and S. L. Sampson, “Persistence of Mycobacterium tuberculosis in response to infection burden and host-induced stressors,” *Front. Cell. Infect. Microbiol.*, vol. 12, p. 981827, Dec. 2022.
[206] K. Y. Dunphy, R. H. Senaratne, M. Masuzawa, L. V. Kendall, and L. W. Riley, “Attenuation of Mycobacterium tuberculosis functionally disrupted in a fatty acyl-coenzyme A synthetase gene fadD5,” *J. Infect. Dis.*, vol. 201, no. 8, pp. 1232–1239, Apr. 2010.
[207] J. C. Betts, P. T. Lukey, L. C. Robb, R. A. McAdam, and K. Duncan, “Evaluation of a nutrient starvation model of Mycobacterium tuberculosis persistence by gene

and protein expression profiling," *Mol. Microbiol.*, vol. 43, no. 3, pp. 717–731, Feb. 2002.
[208] G. Melly and G. E. Purdy, "MmpL Proteins in Physiology and Pathogenesis of M. tuberculosis," *Microorganisms*, vol. 7, no. 3, Mar. 2019.
[209] A. A. H. Alhuwaider and D. A. Dougan, "AAA+ Machines of Protein Destruction in Mycobacteria," *Front Mol Biosci*, vol. 4, p. 49, Jul. 2017.
[210] L. L. Listenberger *et al.*, "Triglyceride accumulation protects against fatty acid-induced lipotoxicity," *Proc. Natl. Acad. Sci. U. S. A.*, vol. 100, no. 6, pp. 3077–3082, Mar. 2003.
[211] M. T. Accioly *et al.*, "Lipid bodies are reservoirs of cyclooxygenase-2 and sites of prostaglandin-E2 synthesis in colon cancer cells," *Cancer Res.*, vol. 68, no. 6, pp. 1732–1740, Mar. 2008.
[212] A. E. F. Sheppe and M. J. Edelmann, "Roles of Eicosanoids in Regulating Inflammation and Neutrophil Migration as an Innate Host Response to Bacterial Infections," *Infect. Immun.*, vol. 89, no. 8, p. e0009521, Jul. 2021.
[213] A. L. S. Cruz, E. de A. Barreto, N. P. B. Fazolini, J. P. B. Viola, and P. T. Bozza, "Lipid droplets: platforms with multiple functions in cancer hallmarks," *Cell Death Dis.*, vol. 11, no. 2, p. 105, Feb. 2020.
[214] M. Dow and L. M. Naughton, "Amphiphilic Lipids, Signaling Molecules, and Quorum Sensing," in *Cellular Ecophysiology of Microbe*, T. Krell, Ed. Cham: Springer International Publishing, 2017, pp. 1–19.
[215] D. Mallaiah and Pallaval Veera Bramhachari, "Quorum Sensing in Mycobacterium Tuberculosis: Its Role in Biofilms and Pathogenesis," in *Implication of Quorum Sensing System in Biofilm Formation and Virulence*, Pallaval Veera Bramhachari, Ed. Singapore: Springer Singapore, 2018, pp. 329–335.
[216] F. R. Maxfield and I. Tabas, "Role of cholesterol and lipid organization in disease," *Nature*, vol. 438, no. 7068, pp. 612–621, Dec. 2005.